

AMERICAN UNIVERSITY OF BEIRUT

ELECTROSPINNING OF NANOFIBERS:
BREATHABLE, WATERPROOF AND PROTECTIVE
ADVANCED TEXTILES.

by
FOUAD JR. NAAMAN MAKSOUD

A thesis
submitted in partial fulfillment of the requirements
for the degree of Master of Science
to the Department of Petroleum and Chemical Engineering
of the Faculty of Engineering and Architecture
at the American University of Beirut


Beirut, Lebanon
September 2016

AMERICAN UNIVERSITY OF BEIRUT

ELECTROSPINNING OF NANOFIBERS:
BREATHABLE, WATERPROOF AND PROTECTIVE ADVANCED TEXTILES.

by
FOUAD JR. NAAMAN MAKSOUUD

Approved by:



Prof. Ali Tehrani, Assistant Professor

Advisor

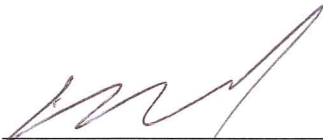
Department of Petroleum and Chemical Engineering



Prof. Nesreen Ghaddar, Professor

Member of Committee

Department of Mechanical Engineering



Prof. Kamel Abo Ghali, Professor, Chairman

Member of Committee

Department of Mechanical Engineering

Date of thesis/dissertation defense: September 7, 2016

AMERICAN UNIVERSITY OF BEIRUT

THESIS RELEASE FORM

Student Name: _____
Last First Middle

Master's Thesis Master's Project Doctoral Dissertation

I authorize the American University of Beirut to: (a) reproduce hard or electronic copies of my thesis, dissertation, or project; (b) include such copies in the archives and digital repositories of the University; and (c) make freely available such copies to third parties for research or educational purposes.

I authorize the American University of Beirut, to: (a) reproduce hard or electronic copies of it; (b) include such copies in the archives and digital repositories of the University; and (c) make freely available such copies to third parties for research or educational purposes after:

One ---- year from the date of submission of my thesis, dissertation, or project.

Two ---- years from the date of submission of my thesis, dissertation, or project.

Three ---- years from the date of submission of my thesis, dissertation, or project.

Signature

Date

ACKNOWLEDGEMENTS

When I set out to write my master's degree dissertation, I knew the work was going to be unlike anything I'd done before. But I never guessed how many people would guide me along the way. Every author says his or her book would not have been possible without assistance. In my case, it's true.

First and foremost, I would like to express my sincere gratitude to Prof. Ali Tehrani for both mentorship and friendship during my graduate studies at AUB. Without his guidance and persistent help this dissertation would not have been possible. I am indebted to Prof. Nesreen Ghaddar, who has been a constant source of encouragement and enthusiasm.

I wish to thank Prof. Kamel Abo Ghali for his support and unceasing help to make things possible.

My advisors gave me the opportunity to develop own individuality, independent thinking and self-sufficiency by being allowed to work with such independence.

I am very grateful to all the people I have met along the way and have contributed to the development of my research, in particular Eng. Sary Fayyad, Eng. Mouhamad Lameh and Dr. Nagham Ismail.

I have built the "AT711 β Industrial electrospinner" from scratch during my M.Sc. project from my own budget. Yet, I believe this machine owes its existence to the help, support and inspiration of Eng. Ziad Eid, Chairman Mohamad Ahmad, Eng. Rita Khalil, Mr. Joseph Nassif, Eng. Ghassan Deeb, Eng. Khaled Joujou, Dr. Youssef Mouneimne, Eng. Joan Younes, Mrs. Rania Shatila Mrs. Samar Khalil, Mr. Talal Abou Mjahed, Mr. Hicham Ghalayini, Mr. Maher Banna, Mr. Danny Ghattas, Eng. Christian Mezhir, Eng. Juliana Maksoud, Eng. Toufik Khoury, Eng. Hadi Kabbani, Eng. Nicolas Abdelkarim, Eng. Ayman Hijazi, MD. Hisham Bahmad and MD. Mohamad Kassab.

Finally, and most importantly, I would like to express my deepest gratitude to my Fiancée Samar. Her support, inspiration, creativeness and unwavering love were undeniably the bedrock upon which the past six years of my life have been built. My warm appreciation goes to my mother Vida who taught me how to write my first letters, I wrote this dissertation for her. To my father and dearest friend Naaman, the man who shaped me. To my sisters, Cynthia and Chloé, their faith allowed me to be as ambitious as I wanted. They all gave me strength and motivation to tackle all challenges head on.

AN ABSTRACT OF THE THESIS OF

Fouad Jr. Naaman Maksoud for Master of Science

Major: Chemical Engineering

Title: Electrospinning of Nanofibers: Breathable, Waterproof and Protective Advanced Textiles.

Electrospinning has been recognized as an efficient technique to produce polymeric nanofibers with diameter in the range of 100 nm to several microns. Considering electrospun webs' outstanding properties (i.e., high surface area and high porosity), it can be used in many different applications (e.g., membranes, filters, advanced composites, wound dressing, and waterproof breathable fabrics).

In this project, a large number of nanofibrous polyurethane (PU) webs were electrospun by changing different effective parameters (e.g., polymeric concentration, voltage, feed flow, etc.). The physical-chemical properties of the webs (i.e., fiber diameters, thickness, areal density, porosity, contact angle, waterproofness, air permeability, water vapor transmittance and aerosol filtration) were studied based on standard test methods. A commercially available waterproof breathable fabric (Tyvek PT31L0 from DuPont™) was used as a reference for benchmarking. The diameter of electrospun nanofibers at various conditions were in the range between 150 and 420 nm. The minimum fiber diameter of 150 nm was achieved from electrospinning of 10wt.% PU in DMF, at feed rate of 500 $\mu\text{l/h}$, voltage of 25 000V, and tip to collector distance of 15 cm. The longer time of electrospinning increased the thickness and reduced the porosity of the webs. By optimization of the electrospinning parameters, we were able to make a web with high level of waterproofness, high air permeability, and high water vapor transmittance. In addition, the optimized electrospun web showed very promising aerosol filtration efficiency with complete removal of particles larger than 0.5 μm and reducing the concentration of smaller particles by 94%.

The results of this study show the possibility of using electrospinning technique for transforming a cheap raw material (industrial grade PU) to nanofibrous web for advanced applications.

KEYWORDS

Electrospinning, Nanofibers, Electrospun, Breathable, Waterproof, Protective.

مستخلص رسالة

فؤاد جونيور نعمان مقصود لماجستير في الهندسة
الاختصاص: هندسة كيميائية

العنوان: النسيج الكهربائي لألياف النانو: أقمشة
وقائية, صالحة للتنفس ومضادة للماء

يعتبر النسيج الكهربائي تقنية فعالة جدا لإنتاج ألياف النانو البوليمرية بأقطار أقل من ٢٠٠ نانومتر. إن الشبكة المحبوكة لديها العديد من الخصائص المتميزة مثل المساحة السطحية الكبيرة جدا بالنسبة إلى الحجم بالإضافة إلى المسامية العالية والمرونة في وظائف السطح كما الأداء الميكانيكي العالي (مثل الصلابة و قوة الشد). هذه الخصائص المتميزة تمكن ألياف النانو البوليمرية من أن تكون المرشح الأفضل لتطبيقات هامة لا تعد ولا تحصى, على سبيل المثال: الأغشية, الفلترات, المركبات المتقدمة, الضماضات الطبية والأقمشة الصالحة للتنفس والمضادة للماء.

نظام الملابس الوقائي التقليدي يعرض الشخص إلى حرارة جسده الداخلية لأنه يعوق إنتقال بخار الماء ويقلل التهوية. إن التكنولوجيا الحديثة للأقمشة المتنفسة تستند على الأغشية المغلفة أو المطلية وعادة ما تكون مصنوعة من مركب البولي تترافلوروايثيلين. من أهم سلبيات المنسوجات المتنفسة المتوفرة في الأسواق هو سعرها المرتفع, على سبيل المثال اقمشة غورتاكس, ايفانت ودوبون. الأغشية المصنوعة من ألياف النانو لديها القدرة على استبدال هذه المنسوجات.

في هذا المشروع, تمت دراسة مواضيع مقومات الماء وتقنية التنفس وأداء الحماية من مختلف النواحي الفيزيائية والكيميائية المعنية في تكنولوجيا النسيج الكهربائي على قطر الألياف المنتجة, السماكة كما المسامية المطلوبة لتأمين الراحة والحماية.

الكلمات المفاتيح

النسيج الكهربائي, ألياف النانو, الكهرونسيج, صالح للتنفس, مضاد للماء, وقائي.

NOMENCLATURE

| Symbol | Description | Unit |
|--|--|-----------------------|
| ρ | Density of the solution | (kg/m ³) |
| v | Velocity | (m/s) |
| Q | Volumetric mass flow rate | (m ³ /s) |
| p | Pressure | (Pa) |
| δ | Surface tension coefficient | (N/m) |
| g | Gravity | (m/s ²) |
| E | Electric field | (V/m) |
| I | Current | (A) |
| WVTR | water vapor transfer rate | (g/m ² .h) |
| G | weight | (g) |
| A | surface area | (m ²) |
| %wt | weight of the polymer per weight of solution | |
| $\rho_{solution}, \rho_{PU}, \rho_{DMF}$ | density of the solution, PU and DMF respectively | (Kg/m ³) |
| r_f | the expected mean radius of the collected fibers | nm |
| r_d | radius of the drum | cm |
| V_{DMF} | Volume of DMF | (m ³) |
| m_{PU} | Mass of PU | (g) |
| E_∞ | Constant electric field | (V/m) |
| PVDF | Polyvinylidene fluoride | |
| PTFE | Polytetrafluoroethylene | |
| PU | Polyurethane | |
| PAN | Polyacrylonitrile | |
| DMF | Dimethylformamide | |
| DMAC | Dimethylacetamide | |

CONTENTS

| | |
|--|------|
| ACKNOWLEDGEMENTS | v |
| ABSTRACT..... | vi |
| NOMENCLATURE | viii |
| ILLUSTRATIONS | xi |
| TABLES | xiii |
| Chapter | |
| 1.INTRODUCTION | 1 |
| 1.1 History | 4 |
| 2.THEORETICAL BACKGROUND..... | 7 |
| 2.1 Voltage..... | 7 |
| 2.2 Feed Rate | 9 |
| 2.3 Tip to Collector Distance..... | 9 |
| 2.4 Drum Speed | 10 |
| 2.5 Electrospinning Duration..... | 11 |
| 2.6 Substrate..... | 12 |
| 2.7 Limitations | 14 |
| 3.MATERIALS AND EQUIPMENT..... | 17 |
| 3.1 Solution Preparation | 17 |
| 3.1.1 Density | 17 |
| 3.1.2 Concentration..... | 17 |
| 3.1.3 Viscosity and Molecular Weight | 18 |
| 3.2 Electrospinning of Nanofibers | 20 |
| 4.EXPERIMENTAL..... | 21 |

| | |
|---|-----------|
| 4.1 Morphology | 21 |
| 4.1.1 Fibers diameter | 21 |
| 4.1.2 Areal Density | 21 |
| 4.1.3 Thickness | 21 |
| 4.1.4 Pore Size | 23 |
| 4.2 Evaluation of waterproofness | 25 |
| 4.2.1 HydroHead pressure test | 25 |
| 4.2.2 Contact Angle | 26 |
| 4.3 Breathability..... | 26 |
| 4.3.1 Air Permeability..... | 26 |
| 4.3.2 Water Vapor Transmission Rate..... | 27 |
| 4.4 Protection..... | 32 |
| 4.4.1 Aerosol Filtration..... | 32 |
| 5.RESULTS AND DISCUSSIONS..... | 38 |
| 5.1 Raw material specifications | 38 |
| 5.2 Electrospun Morphology | 44 |
| 5.3 Waterproofness | 57 |
| 5.4 Breathability..... | 61 |
| 5.5 Protection..... | 67 |
| 6.CONCLUSION | 74 |
| Future Prospective | 75 |
| 6.1 AT711 β Industrial electrospinner | 75 |
| APPENDIX..... | 76 |
| 1. Experimental Data | 76 |
| 2. Calculations | 81 |
| REFERENCES | 84 |

ILLUSTRATIONS

| Figure | Page |
|--|------|
| 1: SEM micrographs of waterproof – breathable (a) microporous membrane (Gortex™) (Hong et al., 2015). (b) electrospun polyurethane (PU) nanofiber web (Ding et al., 2009). | 2 |
| 2: Illustration of a composite waterproof and breathable fabrics with electrospun membrane. (Liang Chen, 2009) | 3 |
| 3: SEM images of the nanofibers at different applied voltages: (a) 12, (b) 15, (c) 20, and (d) 25 kV [3]. (Zhuo et al 2004) | 8 |
| 4: SEM Images for Nylon Mesh, a) Lower to c) higher magnification..... | 13 |
| 5: Mechanism of beads formation (Zhu et al., 2012)..... | 15 |
| 6: Electrospinning Process (Ismail et al., 2016) | 20 |
| 7: Brunswick thickness measuring tool | 22 |
| 8: Vertical sample holder for thickness analysis | 23 |
| 9: OCA15 Optical tensiometer | 26 |
| 10: Up-right Cup Method Setup Scheme..... | 28 |
| 11: Inverted Cup Method Setup Scheme | 29 |
| 12: Desiccant Method First Type Setup Scheme..... | 29 |
| 13: Desiccant Method Second Type Setup Scheme | 30 |
| 14: Assembly Steps for the Up-right Cup..... | 30 |
| 15: ASTM E96 distance..... | 30 |
| 16: Placement of Samples in Environmental Chamber | 31 |
| 17: Smaller Tunnel; Nano web Sample Holder (made in AUB shops) | 36 |
| 18: Aerosol Particle Schematic (not to scale)..... | 36 |
| 19: Aerosol Filtration Experimental Setup Scheme | 37 |
| 20: 3D Representation of the Experimental Setup (AutoCAD) | 37 |
| 21: Density vs. Wt% PU/DMF (Experimental and Theoretical) | 38 |
| 22: Evolution of fiber morphology with increasing concentration from a to h (Supaphol et al., 2005) | 39 |

| | |
|--|----|
| 23: Inherent Viscosity VS. Concentration | 42 |
| 24: SEM images of electrospun obtained at same conditions from different PU grades: a) TPUI-95, b) TPUA 760, c) TPUA-265 A, d) TPUI-E61D, e) TPUI-E80, f) TPUI-T95, g) RWTPUIG95, h) TPUI-H95..... | 44 |
| 25: SEM images of electrospun obtained at same conditions for different concentrations, | 45 |
| 26: Different examples of fibers morphology and degrees of beads formation a) full beads, b) Major beads, c) Minor beads d) No beads..... | 47 |
| 27: SEM micrographs from some of the samples prepared at various conditions. | 50 |
| 28: Variation of fiber diameter with the applied voltage at different tip to collector distances..... | 50 |
| 29: Relation between areal density and electrospinning time theoretically and experimentally | 53 |
| 30: Thickness results obtained by Brunswick film thickness measurement device in microns..... | 54 |
| 31: Pore size analysis results of different electrospun membranes obtained at different running times in comparison with Waterproof Breathable (WPB) textile, DuPont™ Tyvek, model PT31L0. | 56 |
| 32: Pore size distribution of 28hrs electrospun web | 56 |
| 33: OCA 15 pro image: example for contact angle demonstration obtain for 28hr PU electrospun web | 58 |
| 34: Contact angle results obtained for different substrates..... | 59 |
| 35: Water Resistance and Air permeability VS. Electrospinning Time | 63 |
| 36: Initial Aerosol Particle size distribution | 67 |
| 37: Aerosol Particle size distribution after filtration by ES-28h | 67 |
| 38: Interception Mechanism Scheme..... | 73 |
| 39: Diffusion Mechanism Scheme..... | 73 |
| 40: Overall results of Air Permeability, Water pressure resistance and MWTR along Electrospinning duration..... | 74 |
| 41: Overall results of Air Permeability, Water pressure resistance and MWTR along Electrospinning duration..... | 74 |

TABLES

| Table | Page |
|--|------|
| 1: Scanning Electron Microscope Setup For Morphological Analysis..... | 21 |
| 2: Solution Concentration Vs. Kinematic Viscosity..... | 41 |
| 3: Molecular Weights Of Other PU Grades..... | 43 |
| 4: Different Values Of Processing Conditions For The Preliminary Electrospinning Experiments | 46 |
| 5: Fibers Average Diameter Distribution Over Different Voltages And Tip To Collector Distances At 10 Wt% Concentration TCD = Tip To Collector Distance , *= SEM Picture Below..... | 48 |
| 6: Fibers Average Diameter Distribution Over Different Voltages And Tip To Collector Distances At 13wt% Concentration TCD = Tip To Collector Distance , *= SEM Picture Below..... | 48 |
| 7: Water Vapor Transmission Rate Of The ES Samples At Two Different Temperatures | 64 |
| 8: Filtration Efficiencies Of ES-28h | 68 |

CHAPTER 1

INTRODUCTION

Waterproof and breathable electrospun coated fabrics allow transportation of water vapor through while preventing water droplets to maintain a constantly comfortable clothing microclimate. These fabrics should normally tolerate the hydrostatic pressure as high as 80 cmH₂O before they start leaking (Kang et al., 2007) (ASTM D3393) and an acceptable water vapor transmission rate of about 49 g/m².h (Han et al., 2013) (ASTM E96).

Bearing in mind the performance and low price of using waterproof breathable membranes, scientists have focused on the development of affordable outdoor clothing using electrospinning technique which is yet a proficient fiber formation method widely used. There are several fiber spinning methods to achieve such properties. One of the oldest five methods is wet spinning in which a polymeric solution is ejected from the spinneret into a precipitating bath. The liquid in the bath causes the polymer to separate from the solution as a precipitate, hence forming fibers. Another method is the dry method which is similar in concept to the wet spinning; however, instead of precipitation, evaporation takes place. The polymer would be dissolved in a volatile solvent which will simply evaporate in air from the ejected stream, resulting in fibers. While for melt spinning, the material to be formed into fibers is actually melted, and is ejected from a multi-hole spinneret where it is subject to direct cold air. This causes the jet to solidify resulting in fiber formations. Gel spinning is also a fiber spinning technique in which high molecular weight polymers are used forming more of a gel than a solution when dissolved in solvents. This highly viscous substance results in super-strong fibers upon spinning which can be thought of as a combination of dry and wet spinning (Fibersource, 2016). Lastly, electrospinning utilizes electric force to produce nanometric fiber diameters from charged polymeric solution threads.

A typical electrospinning device consists of three key components: a high-voltage power supply, a spinneret nozzle (a metallic capillary tip), and a collector (a grounded conductor). The syringe is filled with a polymeric solution, a high voltage (typically 10–50 kV) is applied between the syringe tip and the collector, and the

solution can be fed through the spinneret at a constant and controllable rate with the use of a syringe pump.

Electrospinning phenomenon is initiated when the charge density altered by the applied high voltage overcomes the surface tension of the viscoelastic solution ejecting a jet from the tip of a Taylor cone. Upon the evaporation of the solvent, nanofibers are formed and collected (Xu et al., 2015).

Electrospinning is a promising and straightforward technique that produces continuous fibers with diameters in the range of nanometers (Demir et al., 2002). These fibers possess high surface area to volume ratios, high porosities, and other outstanding properties, making them excellent candidates for sensors, catalysts, and ultrafiltration and separation membranes (Kilic et al., 2008). Therefore, electrospun fibrous membranes have been widely used as matrixes or templates to fabricate various hierarchical nanostructures for air/water filters and other applications. Despite a large number of publications on electrospinning, only a few deal with waterproof breathable protective clothing (Bafekrpour et al., 2012).

Polyurethane (PU) can be used for coating of garments (Hohman et al., 2001), such as raincoats and industrial safety clothing against various hazards, and they are notable as being comfortable to wear and easy to care for. For breathable and waterproof clothing, the blend of high barrier performance with thermal comfort is provided by the electrospun PU nanofibers but is not attainable with available conventional protective clothing materials (Collins et al., 2012). Examining the material under high magnification, it is not difficult to anticipate better performance from

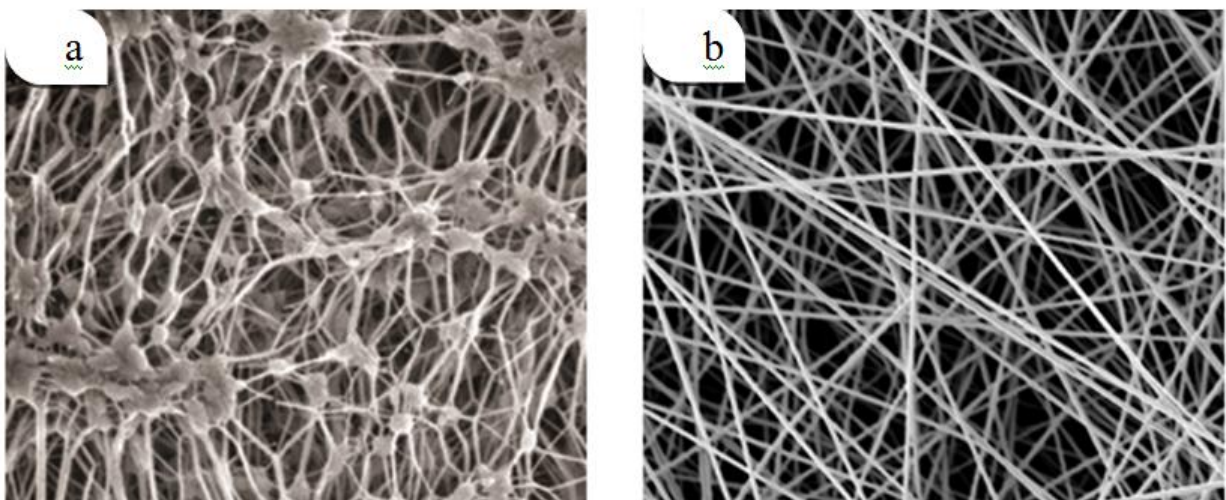


Figure 1 SEM micrographs of waterproof – breathable (a) microporous membrane (Gortex™) (Hong et al., 2015). (b) electrospun polyurethane (PU) nanofiber web (Ding et al., 2009).

electrospun membrane compared to Goretex™, eVent™ and DuPont™ Tyvek, in terms of breathability, given the larger pore size and pore coverage of electrospun membrane. SEM micrographs of expensive Goretex™ microporous membrane and electrospun PU nanofiber web can be seen in Figure 1.

Waterproof-breathable materials can be developed by fabricating layered fabric systems with varying composite structures (Deitzel et al., 2002). The layered structures based on electrospun nanofiber webs provides a higher level of resistance to water penetration (hydrophobicity) than densely woven fabrics, and a higher degree of moisture vapor and air permeability than microporous membrane laminates and coated fabrics. This is achievable with proper selection of layer structure, substrate fabric, and lamination process (Gibson et al., 2004), as illustrated in Figure 2.

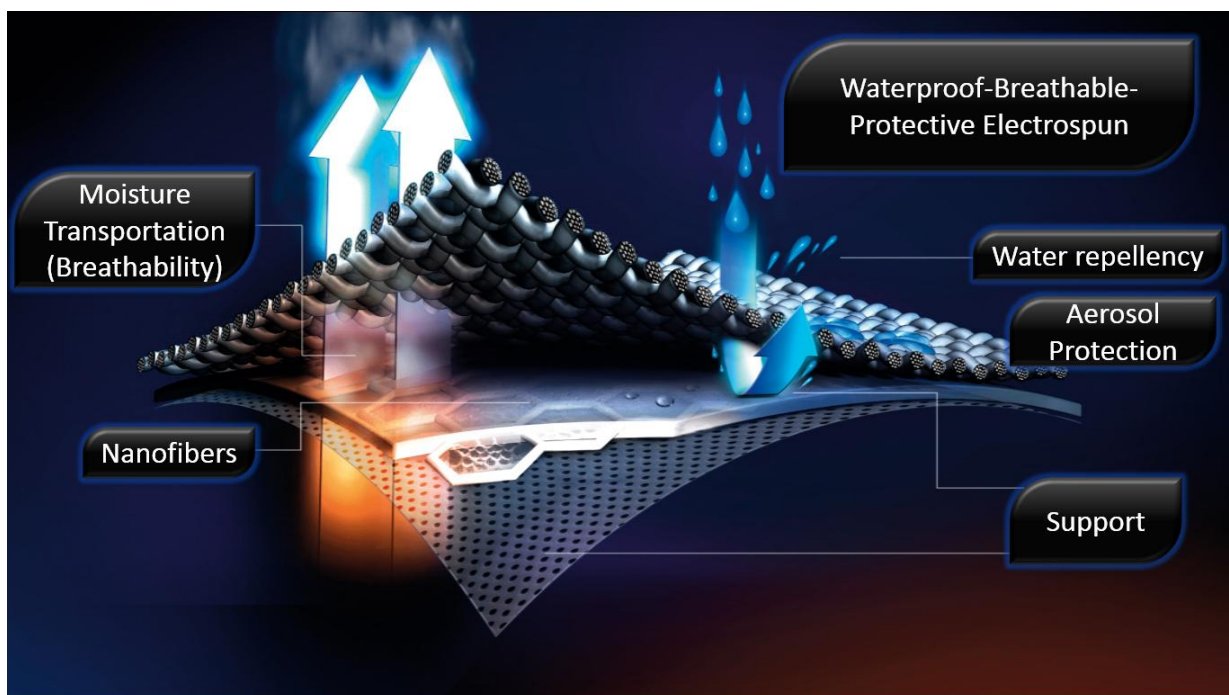


Figure 2 Illustration of a composite waterproof and breathable fabrics with electrospun membrane. (Liang Chen, 2009)

Pores of electrospun membranes are formed from inter-fiber voids. This combination satisfies the basic requirement for a waterproof and breathable fabric and has prompted researchers to investigate its characteristic for such application.

There are several factors that affect the nature and performance of the nanofibers obtained and some of which are related to the properties of the solution. Properties such as viscosity, molecular weight, surface tension, and conductivity influence the electrospun web (Karakas et al., 2013). Gibson et al. further reported that

the porosity, strength, and weight of the obtain textile depend on the polymer chosen for electrospinning (Gibson et al., 2001).

It is quite important to carefully choose the solution, more specifically the polymer used for electrospinning. In this study, industrial grade PU was used for the purpose making waterproof, breathable, protective textile. Despite a large number of publications on electrospinning, only a few deal with waterproof breathable and protective clothing. Accordingly, thermoplastic polyurethanes (TPU) have proven to demonstrate acceptable flexibility along with significant tensile strength (Karakas et al., 2013). Furthermore, Kimmer et al. reported that PUs possess excellent elasticity which eliminates the undesired weakness in nanofiber structure obtained upon electrospinning (Kimmer et al., 2009). Such properties enable PUs to have diverse applications in medicine, filtration, industry, military, and clothing (Karakas et al., 2103).

1.1 History

In his work on electrostatics and magnetism, W. Gilbert noticed the behavior of tree resins which would reconfigure into cone-shaped structures given two conditions; the resin should be stimulated with an electrical input, and then brought close to water droplets. Further tiny resin beads were detected to discharge from the very end point of the cone. This whole observation was declared as “electro-spraying” (Gilbert, Wright 1967).

The earliest trial of electrospinning led to the assertion that small filaments or threads of certain fluids (shellac, rosin, natural bee wax) can be drawn out of the edges of the support in use. (Boys, 1887). Two patents for electro-spinning were issued by J.F. Cooley in 1900 and 1902. Another patent for electro-spinning was issued by W. J. Morton in 1902.

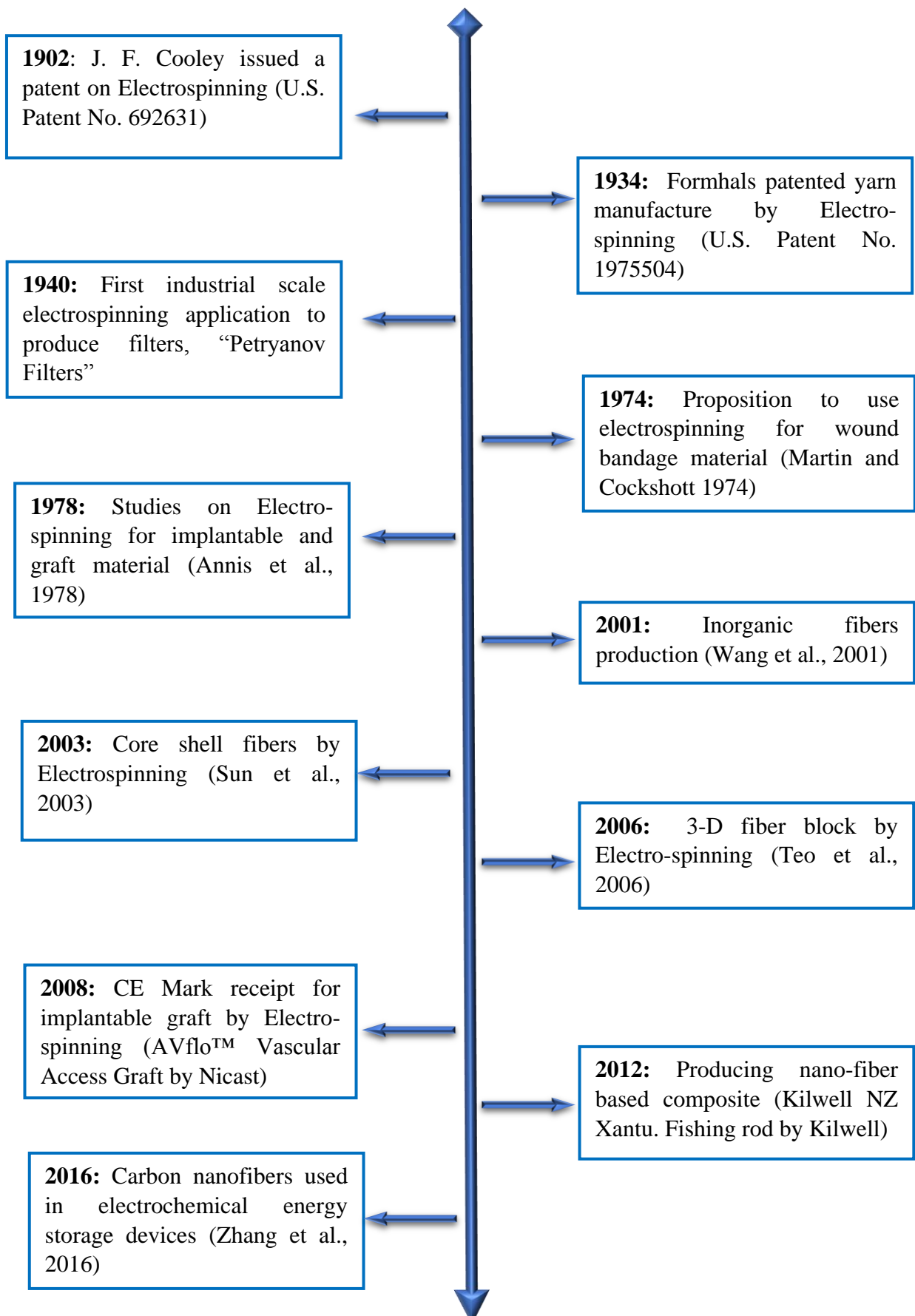
During his study of electrostatic effects on fluid performance, physicist John Zeleny worked on developing a mathematical representation of this relation. He also worked on the functionality of fluid droplets specifically at the tips of metal channels in year 1914 (Zeleny 1914). Later on, Anton Formhals made progress to take this technology to an industrial scale as explained through several patents between the years 1934 and 1944 for the formation of interweaved fibers (known as yarns). In 1936, C. L. Norton issued a patent for the electrospinning of fibers using liquefied solids instead of dissolved solutes with the aid of air blasters which enhances the formation of the fibers.

Well ahead, Sir Geoffrey Ingram Taylor's efforts played an important role in electrospinning through developing a mathematical model of the cone-like buildup (the Taylor cone) of solution droplet induced by the electrical forces. In that sense, Taylor's work between 1964 and 1969 formed the basis of the theory behind electrospinning. His later cooperation with J. R. Melcher led to the progresses in the field of high conductivity fluids developing what is known as the "leaky dielectric model" (Meltcher et al., 1969).

The research groups of Reneker and Rutledge, who made the process of electrospinning even more popular, and many other groups in the 1990s proved that numerous polymers of organic nature can actually be electro-spun into what is known as nanofibers (Doshi et al., 1995). After this year, the number of publications increased exponentially.

More theoretical progresses were made concerning electrospinning and its mechanisms starting from 1995 and on. The Taylor cone, its shape, and its consequent ejected fluid mode (Reznik et al., 2004). The unsteadiness of the formed jet induced by the applied electrical field was studied by Hohman. He further also made the effort to specifically explain the instability attributed to bending which is considered to be a significant aspect in the process (Hohman et al., 2001).

The history of electrospinning illustrated in the following timeline:



CHAPTER 2

THEORETICAL BACKGROUND

2.1 Voltage

As electrospinning process is all about the balance between electrostatic and viscoelastic forces (Rutledge & Fridrikh, 2007), voltage can be considered as one of the most important parameters that affect the results of each experiment. The voltage applied to the polymer solution causes a distribution of charges that can allow the electrostatic repulsion of the polymer from the injector, and attraction by collector. The resistance of the viscoelastic forces to such process leads to the stretching of the fibers from the needle tip until hitting the collector where the fibers are collected at the nano-scale. If the voltage is increased, more and more fluid will be ejected from the needle since the flow would have a higher velocity. Moreover, instabilities in the Taylor cone, and ultimately full withdrawal (Deitzel et al., 2001), would be observed if the velocity of the jet is increased while maintaining a constant solution volumetric flow rate (Zhong et al., 2002).

From what have been presented, the voltage applied should be able to induce the electrostatic force that can overcome the surface tension and viscoelastic forces. At low voltages, no electrospinning would take place and the solution would drop off the nozzle (Huang et al. 2003). On the other hand, several problems can be associated with very high voltage; unstable jet (Doshi et al., 1993; Zhuo, Hu et al., 2008) and beads formation (Cui et al., 2007). The instability in the form of jet pulsation occur when the voltage becomes strong enough to dismiss the jet from the cone, and the frequency of those pulsations increases with increasing electric field (Doshi & Reneker, 1993). According to Dietzel et al, the beads formation can be attributed to the instabilities in the jet; since high voltages are accompanied by greater electrostatic repulsions, and consequently increased instabilities, they tend to induce beads inside the web structure (Deitzel et al., 2001). The effect of the voltage here is opposite to the effect of the viscosity; viscoelastic forces tend to resist the instabilities and beads are formed at low viscosities (Mit-uppatham et al., 2004). Furthermore, increased voltage can disrupt the orientation of the fibers as the jet is given lower time to orient its structure (Zhao et al., 2004). Generally, the applied voltage in the electrospinning experiments of PU/DMF solutions shown in literature ranges between 12kV and 26kV (Zhuo et al., 2008).

Discontinuity can be observed in the jet flow depending on the applied voltage and the volumetric flow rate supplied by the syringe (which competes with the flow pulled out). These aspects definitely affect the region of the needle tip and thus might cause some cut-offs in the jet flow (Theron et al. 2004). Note that if this jet flow is greater or less than the supplied flow rate, instabilities and/or discontinuity in the jet occur. Knowing that the outgoing solution stream increases as the voltage increases and for a fixed solution feed, it is necessary to find the optimal voltage at which the two flows equalize in order to eliminate the instabilities. (Fallahi et al. 2008).

As for the effect of the voltage on the fiber diameter, literature show that with increasing voltage, the fibers can get larger (Pornopone et al., 2005) or smaller (Lee et al., 2004) depending on the range of voltage used. Typically, work done in the domain of optimization of experiments parameters have obtained a minimum fiber diameter at an intermediate voltage (Baumgarten, 1971; Zhuo et al., 2008), which is convenient with our findings. Figure 3 shows the evolution of the fibers morphology with increasing voltage as obtained by Zhuo et al. This is due to the fact that two opposing phenomena are competing at the same time. According to Haghi and Akbari (Haghi &

Akbari, 2007), the increased stretching due to the increased electrostatic repulsion accompanied with the high voltage causes thinner fibers. However, the increasing voltage would lead to rapid ejection of the stream giving it less time to stretch; the increased masses ejected would cause thicker fibers.

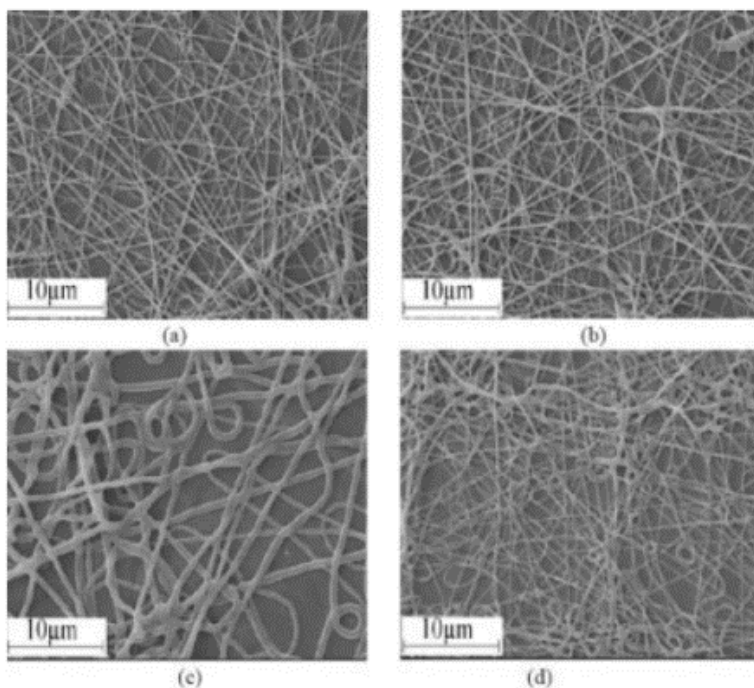


Figure 3 SEM images of the nanofibers at different applied voltages: (a) 12, (b) 15, (c) 20, and (d) 25 kV [3]. (Zhuo et al 2004)

2.2 Feed Rate

The flow rate of the solution (microliters/hr) plays rather an important role in the process especially affecting the velocity of the formed jet from the needle along with the amount of solution ejected. In general, however, an increased flow rate causes the fiber diameter to increase in addition to influencing bead formation. (Subbiah et al. 2004). Lower feed rates form discontinuous flow such the case for 450 $\mu\text{l/hr}$. Thus 500 $\mu\text{l/hr}$ have been chosen to ensure the least possible solution feeding, thus finest fiber diameter possible.

Zhuo et al. presented the solution feed rate influence on the nano-fibers produced. They observed that as the feed rate increases, the diameter of the nano-fibers increases and the opposite is true with the addition that the uniformity of the fibers would increase. More flow rate means more solution in the ejected stream; this requires more time for them to dry-out given the same distance of travel. Therefore, an increase in fiber diameter and a decrease in uniformity is obtained (Zhuo et al. 2008).

In other reports, it was observed that increasing the solution flow rate would actually cause the fiber diameter to decrease since the electrical current in the solution would increase (Theron et al. 2004).

Although increasing the solution feed rate would enhance the fiber formation in electro-spinning, it is not sufficient to maintain a web free of beads having the required smoothness (Um et al. 2004).

2.3 Tip to Collector Distance

According to Heikkila and Harlin (2008), TCD determines the flight time of the electrospinning stream and the vaporization amount of the solvent (Heikkilä & Harlin, 2008). This fact explains the range chosen for running the experiments and the results as well. Short distances might yield to fused fibers with flat cross section due to the improper vaporization of the solvent (Kidoaki, Kwon, & Matsuda, 2006; Zeng et al., 2003). At high distances, beads can be formed and the morphology of the fibers can be distorted. The results obtained were anticipated as mentioned above in the literature through obtaining dry (non-fused) fibers with diameters ranging 147-313nm, and beads obtained at high distance (26cm).

The fiber diameter showed a parabolic like behavior against TCD. It decreased until hitting a minimum at 15cm beyond which it started increasing. Similar behavior has been seen in the literature (Baumgarten, 1971; Cui et al., 2007; Heikkilä & Harlin, 2008); the minimum fiber diameter corresponded to middle TCD that is neither near nor far compared to working range. According to Heikkilä and Harlin (Heikkilä & Harlin, 2008), the decrease in the fiber diameter with distance is attributed to the fact that higher distances allows more solution vaporization and consequently thinner diameter. Humidity and solvent can affect the fiber diameter from that point of view. According to Mazoochi et al (Mazoochi et al., 2012), increasing TCD does not only enhances solution vaporization but also it gives more time for the polymer to elongate. That was approved by Karakas et al (Karakas et al., 2013) where the electrospinning of PU/DMF solution at TCD of 10cm yielded to larger fiber diameters at TCD of 12.5cm. On the other hand, the increase in the fiber diameter can be caused by a decrease in the electric field (Ding et al., 2010). When the electric field decreases, the electrostatic force of repulsion within the solution is reduced and the same apply consequently for the stretching forces. The lower the stretching the larger the fibers.

2.4 Drum Speed

The collector used in the experiments was a rotating drum on which the substrate was placed. This method of collection helps in improving the orientation of the fibers where the drum speed plays a major role; at high drum speed, air turbulence can affect the electrospinning (Tomaszewski et al.2012), as well as the appearance of necking (fibers with smaller diameter than normal) due to extensive stretching of the fibers (El-hadi & Al-Jabri, 2016), and low speed leads to poor alignment (Tomaszewski et al., 2012). In order to estimate the required drum speed that guarantee a sufficient alignment of the fibers, avoiding necking and other faulting mechanisms, we had to estimate the speed of drawing of the fibers. Assuming that the electrospun stream is continuous and the fibers has a consistent circular cross section, the velocity of drawing the fibers can be calculated from the following equation derived from the assumption the mass of the withdrawn fibers is equal the mass of solution fed through the nozzle:

$$m_{withdrawn} = m_{fed} \text{ (for polyurethane)}$$

$$\rho_{PU} \times q_{withdrawn} = m_{solution} \times \%wt$$

$$v \times \rho_{PU} \times \pi r_f^2 = q * \rho_{solution} * \%wt$$

$$v = \frac{q * \rho_{solution} * \%wt}{\rho_{PU} \times \pi r_f^2}$$

Where:

v is the velocity of drawing in m/s

q is the volumetric feed rate in m³/s

$\%wt$ is the weight of the polymer per weight of solution

$\rho_{solution}$ and ρ_{PU} are the densities of the solution and polyurethane respectively

where the density of the solution was obtained through the equation:

$$\rho_{solution} = \frac{m_{solution}}{V_{PU} + V_{DMF}}$$

$$\rho_{solution} = \frac{1}{\left(\frac{m_{PU}}{\rho_{PU}} + \frac{m_{DMF}}{\rho_{DMF}}\right) \times \frac{1}{m_{solution}}}$$

$$\rho_{solution} = \frac{100}{\frac{\%wt}{\rho_{polymer}} + \frac{100 - \%wt}{\rho_{DMF}}}$$

r_f is the expected mean radius of the collected fibers

Assuming the linear drum speed should be equal to the speed of drawing, then the speed of rotation of the drum can be calculated from the following:

$$n = \frac{v}{2\pi r_d} = \frac{q * \rho_{solution} * \%wt}{\rho_{polymer} * 2\pi^2 r_f^2 r_d}$$

Where r_d is the radius of the drum.

2.5 Electrospinning Duration

The impact of the duration of electrospinning is reflected in several physical characteristics of the electrospun web. Amini et al showed that the more time given for electrospinning lead to more frequent fibers connection, which in turn lead to webs with

better tensile strength and opposition to applied forces. (Amini et al. 2015). The experiments done for PU, Nylon, and hybrid electrospun webs also showed that the longer duration of electrospinning yielded to lower air permeability, with no major effects on the contact angle (between water drop and the webs). According to Lee and Obendorf (Lee & Obendorf, 2007), electrospinning period affects the aerial density of the fibers; higher duration is accompanied with higher basis weight. This can verify the decrease in air permeability as BANUSKEVICIŪTĒ et al has shown that increasing the number of fibers decreases the pore size yielding to lower permeability (banuškevičiūtė, 2013). That would might as well lead to an increase in the resistance to water hydrostatic pressure as the web would become thicker due to the increase in the mass deposited.

2.6 Substrate

The main concern is to obtain a fabric structure with high air permeability and water vapor transmission rate which ensure thermal comfort, and high water resistance which ensures good performance. Hence, to achieve the desired characteristics of waterproofness and breathability, the substrate or the support onto which the nano-fibers are to be deposited on is important not only for giving the web stronger mechanical properties. The “perfect” fabric would be that of high water resistance, high air permeability, and high water vapor transfer rate (WVTR). In the best case, a compromise among the three factors should be found for the optimal achievable fabric.

The final effect of the material produced is a combination of the nano-fiber web, the substrate, and the structure of the layers. In a study conducted by Yoon and Lee, different substrates were used as supports for nano-fibers as to compare the results to standard fabrics with waterproof and breathable properties. In particular, PU/DMF 13 wt% solution was electrospun on densely woven polyester, polyester fabric, and polyester fabric and tricot nylon (Yoon and Lee, 2011).

Commercial densely woven fabric on polyester gave the best water vapor transfer rate performance amongst all other substrates. PU nanofibers on densely woven polyester gave the second best performance followed by PU on polyester and PU on polyester and nylon substrates (Yoon and Lee, 2011).

Concerning water resistance, PU on Densely woven polyester and PU on polyester and nylon tricot gave similar yet best results among the studied fabrics; which were also acceptable compared to the standards. In this case, however, commercial densely woven fabric gave very poor water proof properties (Yoon and Lee, 2011).

As for the air permeability, commercial densely woven fabric also showed good results of 5.5 mm/s which were greater than those of the other fabrics followed by PU on polyester and tricot nylon with 3.1 mm/s. However, the PU on the densely woven polyester and on polyester substrate gave the poorest results (Yoon and Lee, 2011). The obtained air permeability for electrospinning of PU on nylon mesh for 28 hours was 9 mm/s which is clearly higher than the above mentioned results.

Since the substrate is an important factor to consider when analyzing the properties of the produce composite, several substrates were tested for air permeability including nylon mesh, cotton, 50:50 cotton/polyester, and polyester. Results can be summarized in appendix I.

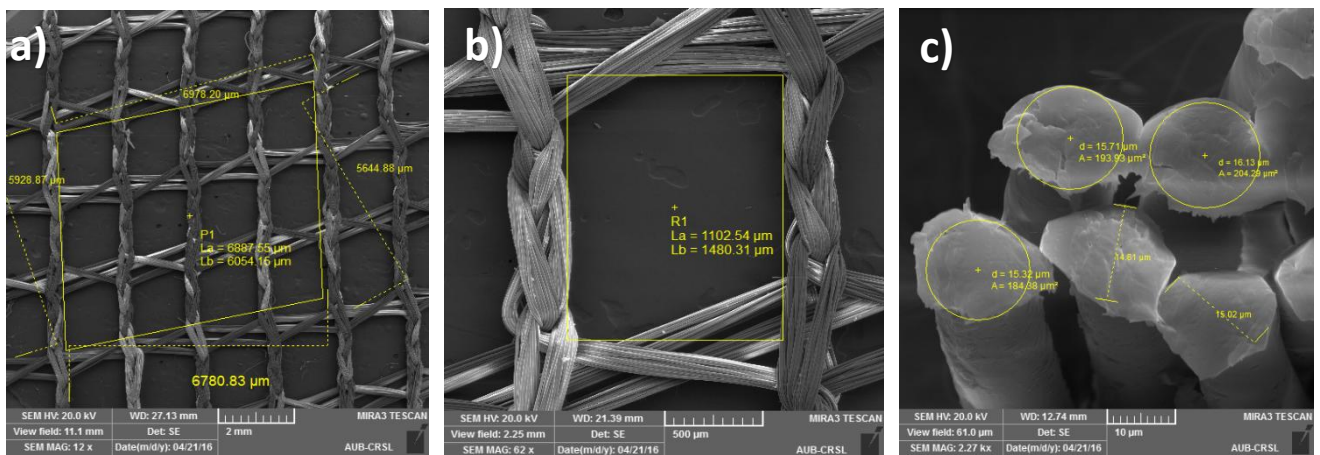


Figure 4 SEM Images for Nylon Mesh, a) Lower to c) higher magnification

Nylon mesh substrate (100%) gave the highest air permeability of 250 cm/s followed by 100% cotton with 223 cm/s. The air permeability of the remaining fabrics was considered to be poor since the values will decrease even more upon the deposit of electrospun nanofibers thus affecting the final performance of the textile. Nylon mesh was eventually chosen as the substrate since it also showed good mechanical properties which would provide the electrospun web with strength and durability. Moreover, using SEM showed that nylon mesh alone had a high porosity of 85% and

a thickness of 210 μm which is greater than that of commercial woven fabrics with 170 μm and PTFE laminate on polyester with 200 μm (Yoon and Lee, 2011). This further proves that nylon mesh has a good potential to be a reliable substrate. SEM images for the nylon mesh are shown in Figure 4 (a, b, c).

In another study by Lee and Obendorf, the nano-fiber web is better off when layered with other fabric to provide more strength and ensure the properties sought (waterproofness and good WVTR). For practicality, the performance of the produced web should be examined taking the whole layered structure into consideration. Lee and Obendorf investigated the performance of electro-spun PU/DMF solution (13 wt%) nano-fibers deposited on 100% polypropylene substrate against pesticide mixtures penetration. The substrate provided a good support in terms of weight and strength and the PU web provided good protection against penetration. Their results showed that as the web areal density increased, less and less liquid penetrated the layer, maintaining an acceptably constant level of WVTR although a decreasing trend in air permeability was observed from 240 cm^2/s at 0 g/cm^2 (substrate only) to 120 cm^2/s at 2 g/m^2 (Lee and Obendorf, 2007). Although the air permeability of polypropylene substrate is acceptable, the nylon mesh still has a higher value of 250 cm^2/s .

2.7 Limitations

Electrospinning, aside its main goal of producing polymer nanofibers, produces undesired “by-products” known as defects which are beads. This undesirable attribute is given since the beads, associated with the instability of the polymer solution, minimize the essential character of large surface area per unit mass of the nanofibers (Zuo et al., 2005). Moreover, beads formation is associated with weakened tensile strength of the web as it becomes less resistant to fracture since beads lack appropriate mechanical properties (Zhu, Yu, Chen, & Zhu, 2012). From here arise the significance of identifying the formation of these beads in order to avoid it.

According to Zuo et al, the formation of beads can be related to the instability in the solution jet. According to Fong et al (Fong, Chun, & Reneker, 1999), the capillary breakup in the electrospinning of polymeric solution can be under the effect of surface tension accompanied with beads formation as droplets might be formed with fibers in between. The droplets are formed as surface tension drives the liquid toward minimizing

the surface per unit mass. Zhu et al tried understanding the mechanism of beads formation; the suggested model is shown in Figure 5. In this mechanism, the formation of beads depends on the electric field and surface tension where electrostatic repulsion at the primary beads causes a splitting into secondary beads that get farther. According to Jaeger (Jaeger, Bergshoef, Batlle, Schönherr, & Julius Vancso, 1998), the beads shape depends on the fiber diameter as well; thinner fibers are accompanied with smaller beads that are near each other.

As beads formation is related to the instabilities, and the instability is related to the input parameters of the experiments, those parameters have their effect in beads formation. According to Fong et al, beads are formed at low viscosity (low concentration and molecular mass) and charge density, and at high surface tension. Hence, beads can be avoided by increasing the concentration of the solution to increase the viscosity, change the solvent or mix it up with other liquid with lower surface tension to reduce the surface tension, or add some salts in order to increase the net charge density of the stream.

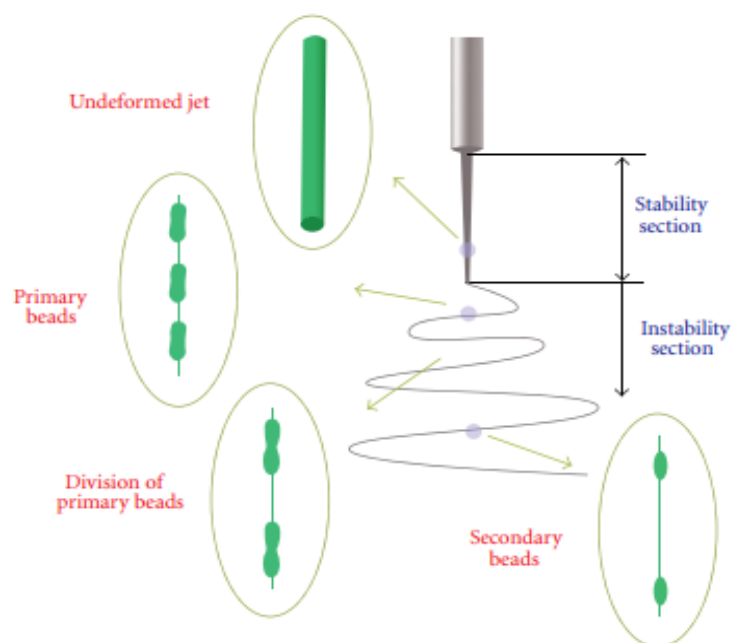


Figure 5 mechanism of beads formation (Zhu et al., 2012)

The results obtained in the experiments carried were in accordance with the literature information presented above, as beads were formed at low concentrations, low molecular weight grades, high voltage, and far TCD. Low concentration and molecular

weight resulted in low viscosity solutions. The high voltage applied to the solution resulted in the formation of neutralizing charge, decreasing the net charge density and resulting in beads formation. The results at high distance were in accordance with Zhu et al experiment where at longer distance, beads were formed, and their morphology changed with distance.

Further work should be done in studying the beads formation as they might possess various applications in catalysis, drug delivery, and photonics since they possess unique shapes and might have some important properties (Wang et al., 2015).

CHAPTER 3

MATERIALS AND EQUIPMENT

3.1 Solution Preparation

Polyurethane (PU) granules of an industrial grade, purchased from Taiwan PU Corporation (TPUCO) was intended for the production of the electrospun web. Dissolved in N, N-dimethylformamide (DMF) ($\geq 99.8\%$, A.C.S. spectrophotometric grade) purchased from Sigma-Aldrich and used as received without further purification.

Polymeric solutions of PU (polyurethane) in DMF (dimethylformamide) were prepared with different concentrations of 4% $w_{\text{PU}}/w_{\text{sol}}$, 7% $w_{\text{PU}}/w_{\text{sol}}$, 10% $w_{\text{PU}}/w_{\text{sol}}$, and 13% $w_{\text{PU}}/w_{\text{sol}}$.

The solutions were prepared for a given volume of DMF withdrawn by a micropipette, by measuring the required amount of PU on a microbalance and stirring the heterogeneous mixture through a magnetic stirrer at 700rpm until homogenization after 24 hrs at room temperature.

3.1.1 Density

To measure the density of the PU/DMF solutions, the portable density meter DMA 35 (Paar, 2010) was used (Measuring Range: 0-3 g/cm^3 , Accuracy: 0.001 g/cm^3 , Repeatability S.D.: 0.0005 g/cm^3 with 0.1 $^{\circ}\text{C}$). The measurements were taken at 25 $^{\circ}\text{C}$ and since density is a temperature sensitive parameter, it is important to carefully monitor the temperature while performing the measurements (Paar, 2010).

The density of the prepared solution may have an effect on the morphology of the electrospun web; hence it is of importance to determine the densities of the PU/DMF solutions. Obtaining the density of a solution can help determine the composition of a mixture if unknown via the density-concentration tables. Density is also important in the viscosity measurements, especially when determining the kinematic viscosity which will be used later.

3.1.2 Concentration

One of the solution parameters that may affect the conversion of polymers into nanofibers is the concentration that has direct outcomes on surface tension,

conductivity, spinning performance and viscosity, which in turn affect the electrospinning process and lead to changes in the diameters obtained (Cengiz et al., 2009).

3.1.3 Viscosity and Molecular Weight

The viscosity of the prepared PU/DMF solution is one of the important parameters on electrospinning. The solution's viscosity can affect the nanofibers produced during the electrospinning process, plus it can be used as a tool to determine the molecular weight of a solution if it was unknown, using Mark-Houwink equation:

$$[\eta] = KM^a$$

Where, η is the intrinsic viscosity, ml/g

M is the viscosity average molecular weight, g/mol

K and a are the Mark-Houwink parameters

With $a = 0.636$ and $K = 0.0087$ (Hentschel and Munstedt, 2000).

Determining the intrinsic viscosity of the solutions can be achieved graphically by plotting the viscosity against the concentration which would give the intrinsic viscosity as the y-intercept after extrapolating.

The dynamic viscosity of the solvent is known and as for that of the solution itself there are several standards for measuring the viscosity. Gravimetric Capillary, Rotational Method, Stabinger Viscometer, and Rolling Ball Method are some methods to be mentioned. However, the method that will be considered is the Rotational Method using the rotational viscometer. The general setup of the rotational viscometer consists of a container in which a measuring head is inserted. As the name suggests, rotational motion takes place.

Now, the underlying principle states that the torque required by the motor used to turn the head in the liquid is measured, and from that the viscosity is determined.

The Rotary Viscometer (FungiLab Alpha LCP, Expert Series) was used in this study to determine the viscosity of the PU/DMF solutions prepared. Before using the viscometer, a reference solution was examined in order to make sure that the machine is calibrated; Ethylene Glycol of viscosity 16.2 cP was used for that purpose. This was conducted using the spindle type L3 due to three constraints, the first is that a reasonable amount of PU/DMF was prepared (instead of preparing 150 ml, only 20 ml was used). The second constraint is that the containers in which the solution is in are not large enough for the other spindles to adequately fit. The third constraint is

that, L3 was found to cover the proper viscosity range of the solutions in hand as. When the measurements are to be taken, it is important to make sure that the solution reached the line-mark on the spindle.

In any case, the selected spindle type can be seen on the user interface of the viscometer and the density has to be changed since the solutions prepared have different concentrations. After inserting the spindle, several measurements were taken at adjusted speeds so that the torque reading indicates a number in the 50% to 90% range (Fungilab). The viscosity will be given in cSt (kinematic) and not in cP (dynamic) since the density has been modified. The viscosities of PU/DMF solutions of different concentrations, 4, 5, 6, 7, 8, 9, 10, 11, 12, 13, 14 wt%., were determined. When taking the measurements, it is quite important to ensure that there are no air bubbles under the spindle in order not to affect the shear stress.

The dynamic viscosities can then be easily obtained and will eventually lead us to the intrinsic viscosity value needed. The intrinsic viscosity was determined by extrapolating the plot of the Kraemer equation of inherent viscosity given by (PSLC) ,

$$\frac{\ln(\eta_{rel})}{C} = K''[\eta]^2 C + [\eta]$$

Where K'' is the Kraemer constant.

The process can proceed to find the molecular weight using the Mark-Houwink equation

3.2 Electrospinning of Nanofibers

PU polymeric solutions at different concentrations were prepared by dissolving PAN powder or PU granules in DMF under constant magnetic stirring of 900 rpm for 24 hr at room temperature (Gomes et al., 2007). In order to remove the entrapped air bubbles, the polymeric solutions were sonicated in Cole-Parmer 8851 sonication bath at 47 KHz for about 20 min prior to electrospinning process.

A laboratory scale electrospinning machine (FLUIDNATEK LE-10, BIOINICIA, Spain) was used for preparation of nanofibers. The inner and outer diameters of spinneret nozzle were 0.6 mm, and 0.9 mm, respectively. The collector was a rotating drum (100 mm diameter x 200 mm length) made of anodized aluminum covered by the nylon mesh substrate (Section B.6), with a variable rotational speed from 200 rpm to 2000 rpm. By specifying the flow rate, applied voltages (0-30 KV), the tip-to-collector distance, and the velocity of the collector drum a horizontal electric field was generated between the nozzle and the collector. This electric field allows the jet to leave the nozzle and to be stretched horizontally. The electrospun nanofibers were collected at controlled room temperature of 20 °C and 30% RH (Barua et al.,2015), as shown in Figure 6

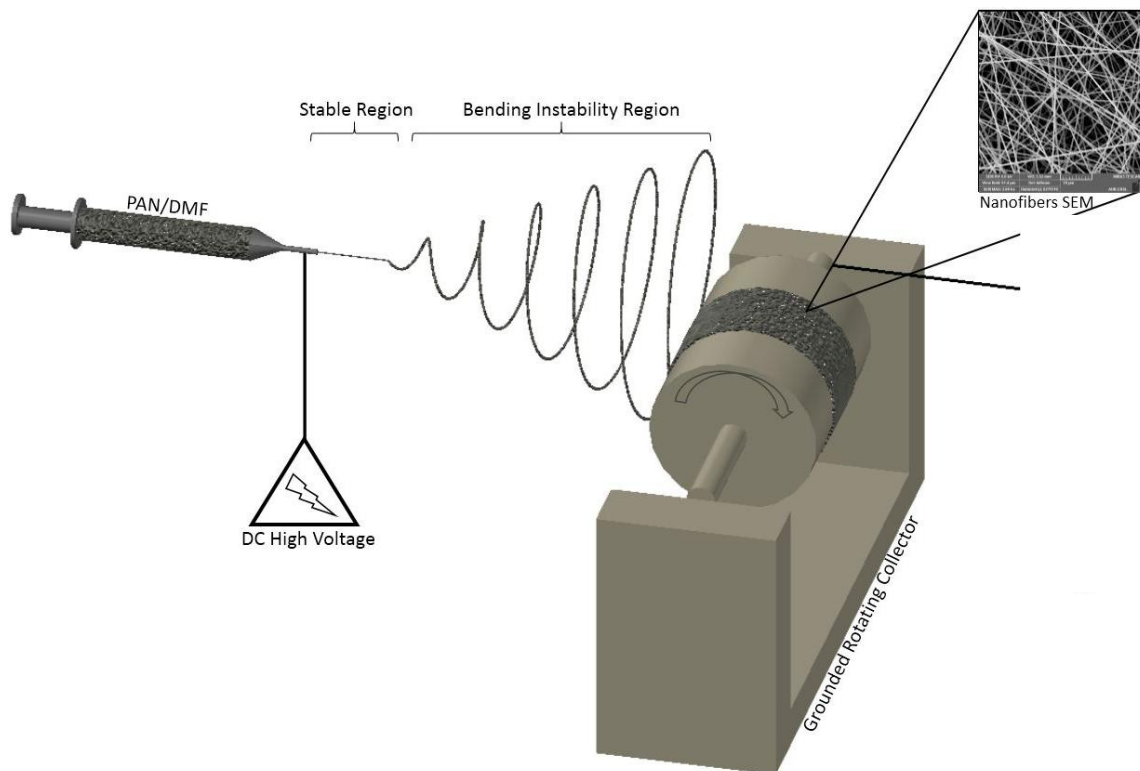


Figure 6 Electrospinning Process (Ismail et al., 2016)

Chapter 4

Experimental

4.1 Morphology

4.1.1 *Fibers diameter*

Resulting nanofibers diameter were examined using Scanning Electron Microscopy (MIRA 3 LMU tescan).

Table 1 scanning electron microscope setup for morphological analysis

| Acceleration Voltage | Working Distance | Detector | Magnification |
|----------------------|------------------|----------|-----------------|
| 15kV | 3mm | InBeam | 3000x to 50000x |

5 different round samples were obtained from each electrospun under study, then fixed onto the SEM sample holder using conductive carbon tape. They were coated with gold using Q150T Turbo-Pumped Sputter Coater (Quorum technologies) at a current of 10mA for 90 seconds. 20 different measurement of fiber diameter were obtained from each of the 5 samples under study using MIRA measurement software. Hence, 100 measurements were made for each electrospun under study.

4.1.2 *Areal Density*

For measuring the areal density of each electrospun mesh, 16 square samples (1x1 cm²) were cut from each electrospun web and weighed. The samples were taken by isolating a piece of the web cut along the width. This piece is then divided into 4 parts; left, right, middle left, and middle right, and each of those strips were cut into 4 similar squares. The areal densities taken are the average of the masses of the squares obtained from each electrospun web; micro balance with a precision of 1 microgram was used to obtain the mass of each square.

4.1.3 *Thickness*

In materials characterization and performance measurement, it is sometimes necessary to determine the thickness of the nanofiber membrane. The thickness is a function of load as the ES webs are highly porous. According to Affandi et al, the major

methods used in thickness measurements for electrospun are scanning electron microscopy and micrometers. (Affandi et al., 2010).

Some of the available methods for measuring the thickness of thin films might involve some compression upon contact with the specimen under study. In the case of electrospun web, this compression can decrease the thickness, and the measurements would be inaccurate. The problem with the existing techniques is that either they involve contact with the sample and hence can induce systematic error in the readings (like micrometer screw-gauge, cutting sample and examining using SEM, or ultrasonic technology), or they are expensive (like contactless laser measurement and Mitutoyo Litematic and Litematic Head - Series 318).



Figure 7 Brunswick thickness measuring tool

The device used for measuring thickness was Brunswick film thickness instrument (Figure 7). The sample under study is placed between the plates of the machine, and as gauge pressure is applied, the plate rotate itself to maintain its direction parallel to the surface under study to give a result with 0.0002mm precise.

This method might impose a margin of error as it involves contact. However, Scanning Electron Microscope equipped with special holders to adjust our sample in vertical position with the electron beam was used to verify the device results.

The Scanning Electron Microscopy results were in accordance with what was obtained by Brunswick thickness measuring instrument, suggesting that the pressure applied is not enough to compress the web and affect its thickness. Consequently, the Brunswick thickness measurement instrument was used being faster and easier.

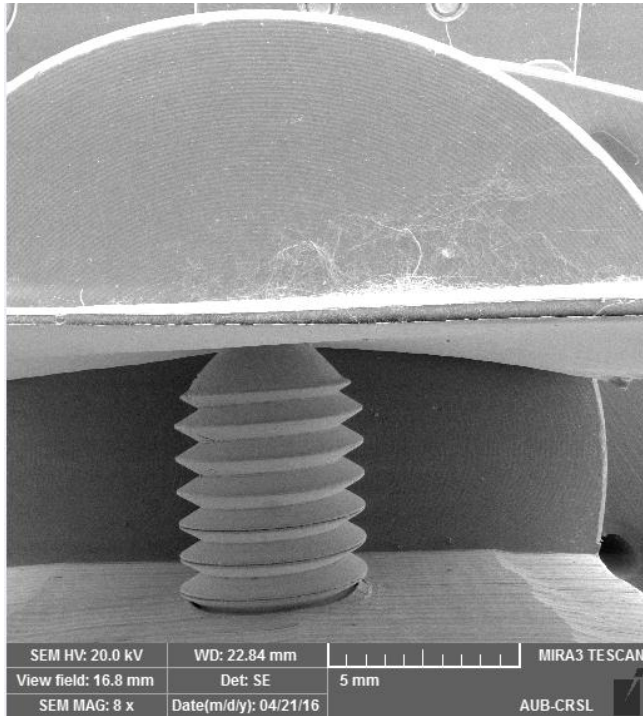


Figure 8 vertical sample holder for thickness analysis

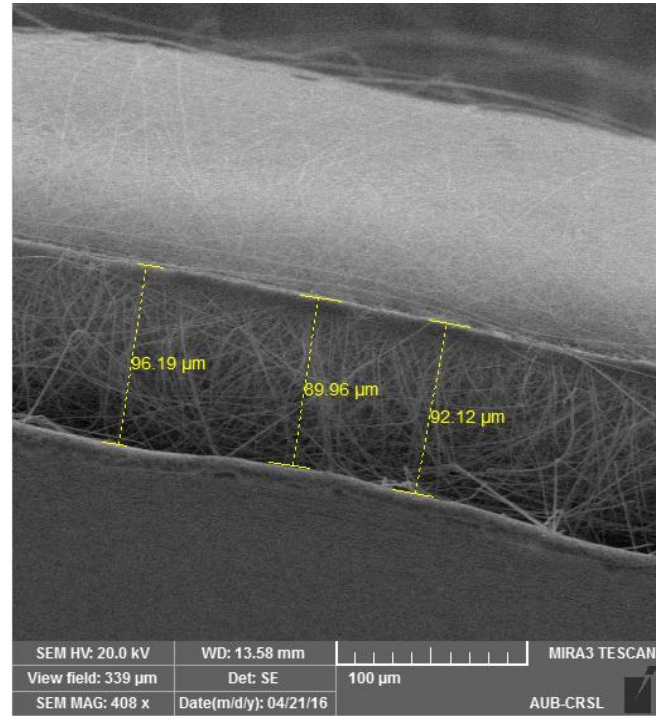


Figure 10 SEM verification of the Brunswick machine values

4.1.4 Pore Size

Porous material Inc. (PMI) capillary flow porometer has been used to study the porosity of the resulting electrospun web. A saturated sample will pass air when the applied pressure exceeds the capillary attraction of the fluid in the pores, allowing flow to pass through (De Bruyne, De Bruyne, Rosiers, & De Moor, 2005). Smaller pores have a higher capillary attraction than larger pores. Therefore, smaller pores open at higher pressures. Thus the porometer actually measures the average pore diameter using Laplace's equation:

$$d = c \frac{\gamma}{p} \text{ (Shchukin, Pertsov, Amelina, \& Zelenev, 2001)}$$

Where d= pore diameter (um)

γ = Surface tension of liquid used (dynes/cm), for Galwick, γ = 15.9 dynes/cm

P= differential pressure (psi)

C= constant = 0.415 for p in psi

Capillary flow porometer (CPF-1100AH from PMI) was used in the study of pore size profile where the membrane under study is saturated with liquid of low surface tension. Dry-up wet-up run is performed to give dry curve, half dry curve, and wet curve showing the variation of air flow with applied pressure. Upon analysis, the maximum pore size, minimum pore size, and mean pore size were determined for the webs under study.

When the sample is saturated with the low surface tension liquid, all the pores are closed. Air is then allowed to pass through the wet substrate and the pressure is measured. When the pressure becomes high enough to remove the liquid from the pores, the air flow starts increasing gradually as the pores open (Frey & Li, 2007). The relation between the pore size and the pressure required to remove the liquid is derived from the Young-Laplace's equation previously mentioned, and is given by:

$$D = \frac{4 \times \gamma \times \cos\theta}{P} \text{ (Fang, Tolley, \& Lee, 2010)}$$

Where:

D is the diameter of the pore.

P is the pressure required to open the pore.

γ is the surface tension of the wetting liquid.

θ is the contact angle

Hence, as the pressure increases, larger pores start opening before the smaller ones. The test gives the smallest, largest, and mean pore diameters. This is achieved by automatically analyzing three curves called wet curve, dry curve, and half dry curve. The wet curve shows the variation of the air flow with the change in pressure applied at the wet sample. The same is shown in the dry curve but for the pressure applied at the dry sample. The half dry curve contains the values of air flow that are half of that of the dry curve at the same pressures. For the dry curve, and consequently the half dry curve, the pressure is proportional to the air flow as all the pores are opened. That is not the case for the wet curve where the flow is zero for low pressures where no pore is opened. As the pressure increases above the minimum threshold, the air flow starts increasing as the pores are opened gradually from the largest to the smallest. This threshold corresponds to the pressure needed to open the largest pore which is referred to as bubble pressure.

When the wet curve confides with the dry curve, the smallest pore is opened, its size can be calculated from the corresponding pressure. The mean pore size can be calculated from the pressure at the intersection of the wet curve with the half dry curve; it is by definition the pressure that allows the passage of 50% of the air flow (Amini et al., 2015; Li et al., 2006).

4.2 Evaluation of waterproofness

4.2.1 HydroHead pressure test

The purpose of the hydro-head test is to measure the water-proof ability of the produced textile. The idea is to measure how much pressure of water the tested sample can withstand before leaking. As water resistance is measured by the amount of water, in mm which can be kept above the fabric before water seeps through the pores (Lou, 1987). A surface area of 4.23 cm² of the textile is subjected to a controlled water force, and a leak in the sample indicates the height of water, or hydrohead pressure, needed to penetrate through the sample. This can help determine the degree of water resistance of the textile.

The Capillary Flow Porometer CFP-1100AH from Porous Materials Inc., PMI is used to perform the hydro-head test on the produced samples. A circular sample of 2.32 cm diameter (as per the proper O-ring) is fixed in the allocated setup for hydro-head testing and the test is conducted. This test method is according to ISO 811:1981.

4.2.2 Contact Angle

The contact angle of water on the electrospun mesh was measured using optical tension meter (OCA 15EC from DataPhysics) (Figure 9). A droplet of pure water (5 microliters) was dispensed and placed directly on the surface of nanofibrous membrane. A picture was taken at each dispense through the digital camera provided and then analyzed using the SCA20 software. The data were obtained across the width of the electrospun sheet, and recorded as an average of 20 measurements.

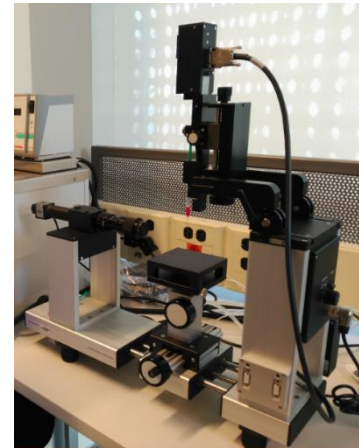


Figure 9 OCA15 Optical tensiometer

4.3 Breathability

4.3.1 Air Permeability

Air permeability of a textile material is the degree of air passage across that material. This property can be measured either by using Darcy's Law or by using what is known as the Frazier Test.

To determine the air permeability of the electrospun nanofiber samples, the Capillary Flow Porometer CFP-1100AH from Porous Materials Inc., PMI was used. The dry sample of a known area is inserted in the designated place for air permeability tests and the experiment is run. The test is in agreement with ASTM D737 and ASTM 3574.

In general, Henri Darcy described the flow of fluid through a porous medium which is known as "Darcy's Law" and is given by the following equation,

$$Q = \frac{-kA(\Delta P)}{\mu L}$$

Where, Q is the volumetric flow rate, m³/s

K is the medium permeability, m²

A is the cross sectional area perpendicular to fluid flow, m²

ΔP is the pressure drop across the path, Pa

L is the path length, m

μ is the viscosity of the fluid, Pa.s

However, this basic form of Darcy's equation is not reliable for air permeability of nano-porous membranes. Since the nanofibers diameter is so small, the movement of air particles about it can no more be neglected; this creates slip flow conditions and some modifications should be used. Nevertheless, the air permeability of fabrics can be quantified experimentally using specialized porometers, and given in Frazier units. The main concept behind it is that air is forced across the tested sample of known area under a certain differential pressure usually 1.27 cm (0.5 inches) of water. The volumetric air flow is then measured per second per area of the tested sample, and the air permeability can be given as $\text{ft}^3/\text{min}/\text{ft}^2$. This is known as the Frazier number and can be regarded as mm/sec which is actually the face velocity of air across the tested sample.

The Capillary Flow Porometer CFP-1100AH from Porous Materials Inc., (PMI) was actually used to determine the air permeability of the electrospun nanofiber samples. The dry sample of a known area is inserted in the designated place for air permeability tests and the experiment is run. The test runs conducted are in agreement with ASTM D737 and ASTM 3574.

4.3.2 Water Vapor Transmission Rate

One of the most important characteristics of electro-spun nano-fibers sought is the ability to transfer water vapor which ensures thermal comfort for the wearer known as Water Vapor Transmission Rate test (WVTR).

There are several procedures for testing the water vapor transmission rate of the electrospun webs such as the up-right cup method (known as the water method), the inverted cup method, and the desiccant method.

In the up-right cup method, a container is filled with distilled water and the fabric to be tested is sealed at the opening of the container as shown in Figure 10. The sample should be secured in place using rubber seals (gaskets). Then, air would be circulated over the setup in a controlled chamber and vapor should seep from the container, across the sample, and into the controlled chamber. According to ASTM E96, the sealing material should not allow the passage of vapor in any way and should not allow the accumulation vapor on it as well. At the same time, the sealing process should not affect the pressure inside the container as this would affect the vaporization of the water (McCullough et al., 2003) (ASTM E96). The sample should

be within 13 to 25 mm from the water and it is advised that they do not touch. In addition, the water should at least fill 3 mm depth of the container (ASTM E96). Condensation should be prevented by not allowing a temperature change of more than 3°C between the environment and the test chamber (ASTM E96).

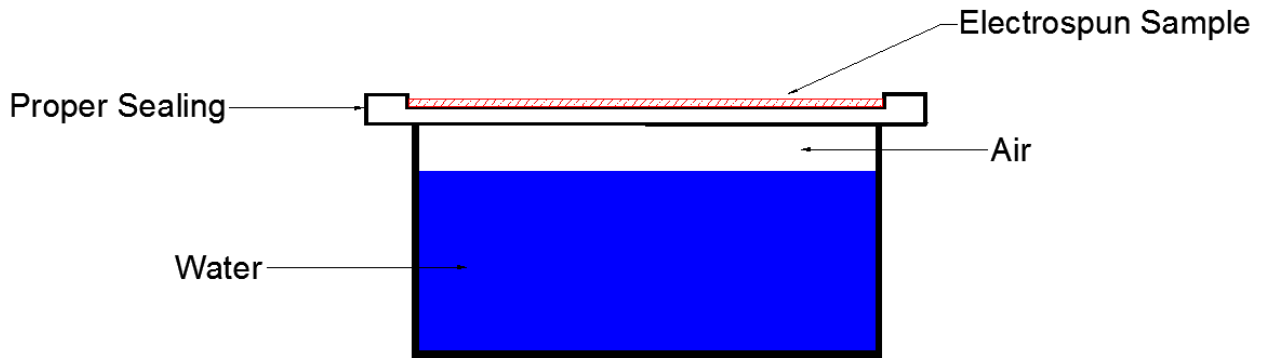


Figure 10 Up-right Cup Method Setup Scheme

When the test is running, the weight of the dish should be taken over set time intervals where it is noted that at first the rate of transfer would be high but then reaches steady state. All the measurement should be recorded with their corresponding timings (ASTM E96).

Numerically, the WVTR can be determined using the formula given by,

$$WVTR = \frac{G}{A \cdot t}$$

Where, WVTR is the rate of water vapor transfer, g/m².h

G is the weight difference, g

t is the time when weight difference occurs, hr.

A is the exposed sample surface area, m²

The inverted cup method (figure 11) includes the same setup as the above; however, the container is now inverted so that the water touches the sample being tested.

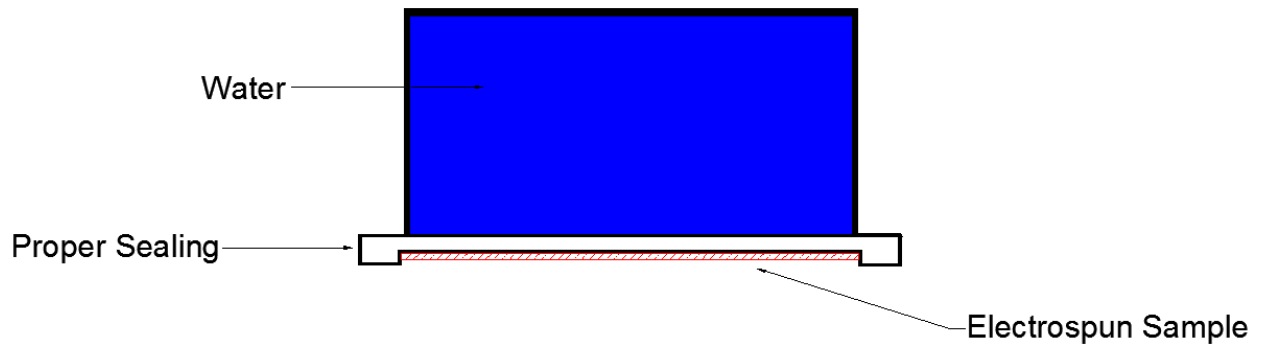


Figure 11 Inverted Cup Method Setup Scheme

As for the desiccant method, there are two types of setups. The first (figure 12) includes a container with distilled water is placed upright and another container with the desiccant placed in an inverted position on top of the water container. The second setup (figure 13) consists of a desiccant inside a container placed in a controlled humid environment. In both cases, water vapor would diffuse towards the desiccant and across the tested electrospun sample.

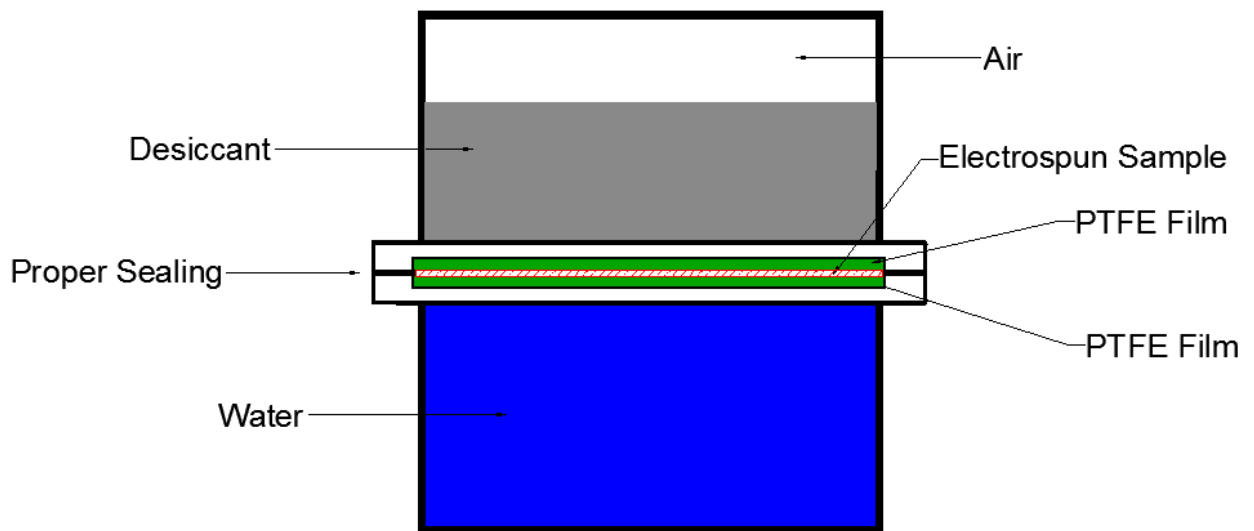


Figure 12 Desiccant Method First Type Setup Scheme

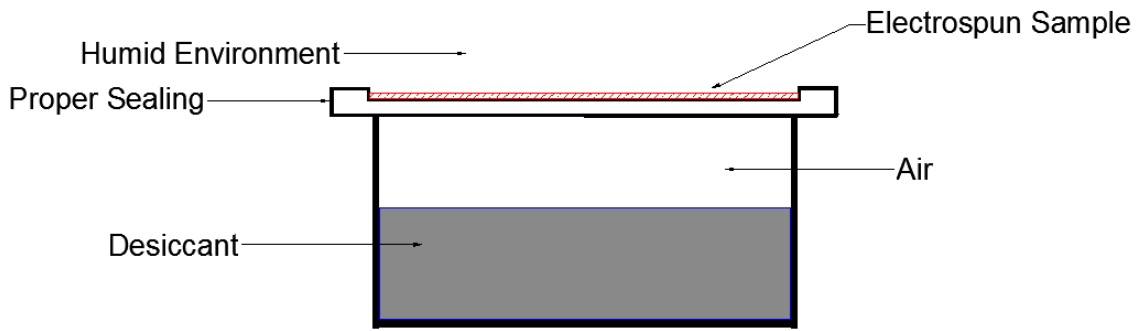


Figure 13 Desiccant Method Second Type Setup Scheme

The water method based on the ASTM E96 standards was chosen since it is of a simple setup which makes it easier to reproduce and handle, plus it was found to be the most common method used.

First, the plastic cups used were maintained clean at all times to avoid any contamination of the containers and a circular area was cut in the lids of the cups (16.33 cm^2) (figure 14.c). Then, a specific amount of water was filled in the test containers; using the digital balance, 80 grams of water was filled in each of the used containers and closed again also to avoid contamination (figures 14.a and 14.b). It was ensured that when filling water, no water droplets were deposited on the inner walls of the container as to prevent errors during the experiment.

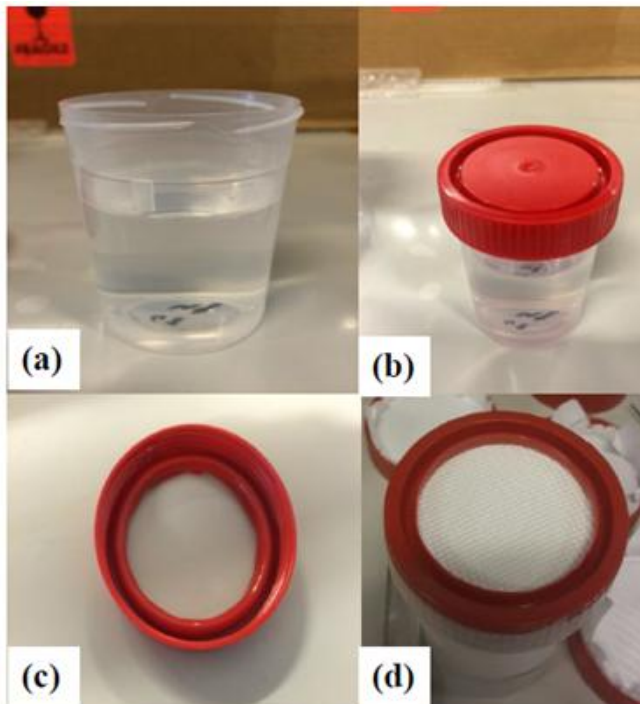


Figure 14 Assembly Steps for the Up-right Cup Method

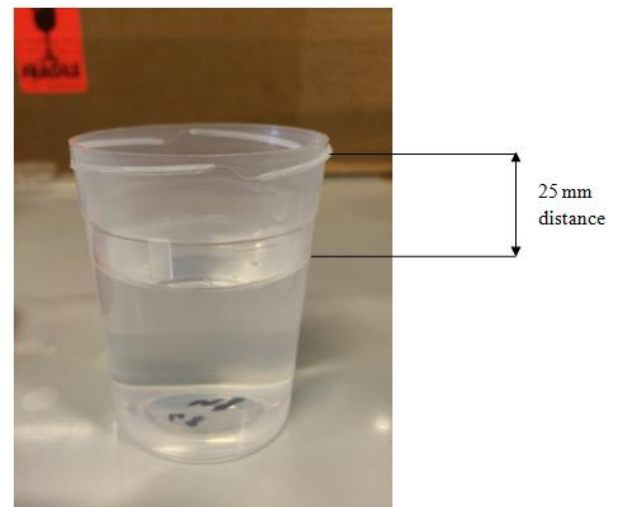


Figure 15 ASTM E96 distance requirement

Moreover, it is important to mention that the water amount was chosen to comply with the ASTM E96 which recommends leaving a distance of 25 mm between the water surface and the tested sample. The web samples were simply put on the mouth of the container and secured in place using the lid. A layer of parafilm was wrapped on the sides of the container as to avoid any leakage through the sides and to ensure that water vapor is exiting through the web sample only (figure 14.d).

The web samples were cut into 8x8 cm squares; ES-12h, ES-16h, ES-20h, ES-24h, ES-28h, ES-32h, ES-36h, ES-40h, ES-44h, and ES-48h (Electrospun-hours) were tested at the same time. The cut samples were contained in petri dishes to also prevent any contamination of the webs to be tested. In addition, a thin polymeric film of PU/DMF solution was also tested for water vapor transfer rate. The film is composed of 14 ml of the 10wt% PU/DMF solution which was intended to be similar to ES-28h with 500 ul/hrs feed rate. Nevertheless, the specified volume was poured onto a glass plate having similar dimensions as the produced webs (20cm x 31.4cm), and was allowed to dry out in the oven at 40 °C for 24 hours. After all the samples were done, they were left in the environmental chamber for a specified time period of 24 hours.

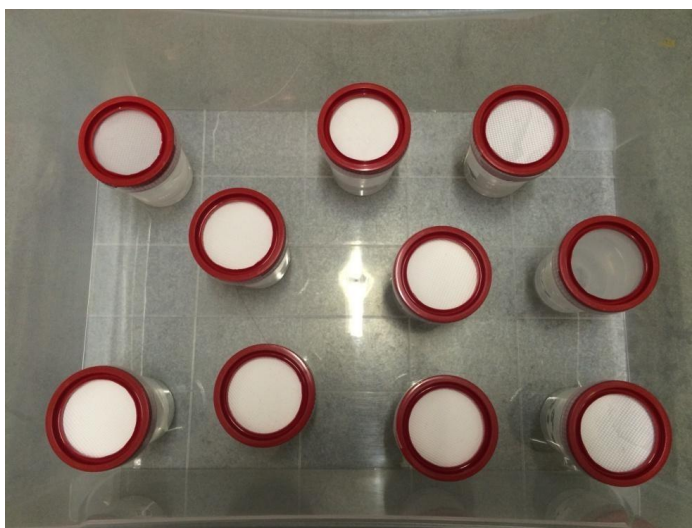


Figure 16 Placement of Samples in Environmental Chamber

The test was first conducted at 25 °C at a range of relative humidity of 65% RH. These conditions were taken as close as possible as indicated by the ASTM E96 standards. To make sure these parameters were maintained, an environmental chamber was used in which the experiment took place. When the required chamber conditions were reached, the webs were placed on the test containers inside the actual chamber as to keep the whole process under the specified conditions. The total time of the experiment was 24 hours; however, weight measurements were taken after 8, 16, and 24 hours for each sample.

For more concrete results, a second test was performed but this time with an elevated temperature of 35 °C. This value was proposed to mimic the conditions of the human body, especially skin temperature upon wearing the fabric-electrospun web composite. Human skin temperature varies within a range depending on the surrounding temperature; skin temperature increases and decreases accordingly with the surrounding temperature. At temperatures of 15 °C, the skin temperature can go down to reach 32 °C, and at 50 °C, the skin temperature rises to 37.5 °C (Elert, 2001). From these temperature ranges, it can be concluded that considering an average human skin temperature of 35 °C is relevant to the analysis. The collected data were tabulated as shown next in table (1).

4.4 Protection

4.4.1 Aerosol Filtration

Because of their good breathability and decent air permeability, electro-spun nano-fibers widen their application variety to include not only waterproof breathable fabric, but also protective clothing and adequate aerosol filters. The latter is gaining high interest recently and is being developed to give higher efficiency and comfort (Graham et al., 2003). Sundarrajan et al. further supported the use of nano-fibers for filtration purposes, as they reported that electro-spun nano-fibers perform better than traditional filters when it comes to volatile organic compounds (Sundarrajan et al., 2013).

Theory and Background

In order to clarify how crucial is the performance of these composite filters, some examples are to be given. Such fabrics can be used in the medical field, integrating them in protective masks. This should ensure, first and foremost, high performance against penetrating foreign particles and other contaminants, such as bacteria and airborne particulates. It must also provide a certain retention level of any contaminated fluids or blood. Finally, it is important that the used fabric offers acceptable levels of comfort for the wearer. Another example can be the application of such fibers in layered structures for military protective clothing. Here, the task is somehow tougher and the fabric is put under harsher conditions. Thus, the fabric system (including the nano-fibers) should give high barrier performance, strength, and

durability in order to be able to endure the outside conditions it is subject to. It must also provide adequate protection (good filtration) against harmful liquids and gases along with sustaining a certain level of waterproofness and breathability to enhance user comfort (Graham et al., 2003)

In any case, the integration of electro-spun nano-fibers in protective fabric should meet certain requirements. It is very important to choose a good support for the nano-fibers to be applied on since any fault or failure in the filter defies its purpose. The support should provide excellent durability along with adequate elasticity to maintain comfort. The overall structure should provide adequate aerosol filtration (Graham et al. reported removal at least 2 micron particles with 98% efficiency), acceptable waterproofness (when needed), good air permeability and comfort, and high durability and strength (when needed). In addition, the incorporation of chemical agents/catalysts in the web can help enhancing the filtration process in some cases

When it comes to strength and durability, which is a weak point in several applications including filtration, Zhang et al. reported that these aspects of the nano-fibers can be enhanced by piling several layers on top of each other to give added structural rigidity (Sundarrajan et al., 2013). A three-layer membrane was suggested by Podgorski et al. for the removal of nano-particles, micro-particles, and poly-dispersed aerosols. The layers include one for assuring strength and durability of the membrane, another layer for the actual filtration which is usually nano-fibers and is the middle layer, and finally another filtering layer for the removal of relatively larger particulates (Podgorski et al., 2006).

Electro-spun fiber diameter is also important when evaluating the performance of their application as filters. Altering the fiber diameter can affect the efficiency and the pressure drop of the filtering membrane; optimal fiber diameter ranges between 200 to 300 nm. Moreover, the performance is enhanced when slip flow conditions are present on the fibers. Firstly, the no slip flow conditions mean that there is zero air velocity on the fiber surface due to viscous effects, however, when slip flow conditions are present, the air velocity at the fiber surface becomes quantifiable. Slip flow conditions start to appear when the fiber diameter gets small enough such that air particles movement becomes relatively considerable. This signifies two things; the presence of slip conditions causes less drag force which eventually decreases the pressure drop, and causes more air to flow close to the fiber

surface resulting in more particle-fiber contact, thus increasing efficiency (Graham et al., 2002).

Sundarrajan et al. reported the same idea of slip flow enhancement of the filtration performance nano-fibers provide, and supported the statements of decreasing fiber diameters to increase filter efficiency (Sundarrajan et al., 2013). By using nano-fibers, decreasing the most penetrating particle size (MPPS) and increasing the efficiency with minimal increase in pressure drop, is achievable (Podgorski et al., 2006). They also reported that the high surface-area-to-volume-ratio of nano-fibers ensures elevated efficiencies when it comes to filtering since such properties increases the chances of aerosol particles getting trapped, hence increases retention levels.

Based on the mentioned above, the nano-fiber performance in filters can be assessed by using a factor known as the “quality factor” given by (Yun et al., 2010) as,

$$q_f = \frac{\ln\left(\frac{1}{p}\right)}{\Delta P}$$

Where, q_f is the quality factor (higher values means better performance)

ΔP is the pressure drop

p is the amount of penetration

In another study, the focus was on the performance of electro-spun nano-fibers as aerosol protection in apparel textile. Although such membranes can serve as good water proofs, maintaining acceptable breathability, and aerosols retention, there are weak spots in some locations such as the knees and the elbows (Gibson & Gibson, 2004). The bending movements impose relatively higher stretches and strains on these spots than other areas, thus making it a notable investigation field. It was indeed found that as the strain percentage increases, the air permeability showed an increasing trend which indicates an increase in spacing within the nano-fibrous web (Gibson & Gibson, 2004).

As a final thought, the perfect nano-fiber based aerosol filter is still unachievable, but there must be a compromise between pressure drop and aerosol filtration efficiency. Smaller fiber diameters (in 200 nm range) and tighter pores result in higher efficiency, but on the other hand results in a higher pressure drop (Qin & Wang, 2006). The best filter is that of ideal filtration properties and minimal

pressure drop, but unfortunately this is unattainable so far. However, an optimum can be found among the present properties and it surely differs from one application to another (Qin & Wang, 2006).

Experimental Method

To test the aerosol filtration efficiency of ES-28h, a setup was used in which aerosol particles were addressed across the web via a directed air flow. Two square tunnels were assembled concentrically; the larger one was of 15 cm sides and 1 m length with an attached fan at the entrance and served as the main aerosol-particle/air flow path, while the smaller tunnel was of 5 cm sides and 40 cm length and served as the holder of the nanoweb sample (figures 17.a and 17.b). The aerosols are introduced at close proximity to the fan which provides the air flow necessary to carry the aerosols towards the nanoweb. To quantify the upstream and downstream particle concentrations, a quick response, high resolution particle analyzer was used. A mass flow regulator (0-5 L/min) and a small motor and pump (2-5 L/min) were used to control the face velocity of the air flow.

To generate the actual aerosols, a Condensation Monodisperse Aerosol Generator (M 3475) was used. The principle is rather simple, as NaCl is used as a support onto which the aerosol material will be deposited (Figure 18).

The used aerosol material was di-2-ethyl hexyl sebacate (DEHS) in which particles of size range between 0.1 μ m and 8 μ m can be produced. Concentration of more than 10⁶ particles/cm³ can be produced with flow rates of 3.5-4 L/min. The generator is fed with filtered nitrogen gas to prevent any contamination. This nitrogen flow serves as the carrier to the atomized NaCl solution (20 mg/L) dispensed to form droplets 1-3 μ m in size. The stream enters a dehydration process in diffusion dryer as to form crystal-like particles with sizes of 10-100 nm and to produce the actual aerosols, the stream is allowed to bubble through the DEHS. The concentration of the produced aerosols can be controlled either by adjusting the NaCl concentration using a screen bypass, or by varying the temperature and the vapor pressure. The mixture is finally passed through a heater at 300 °C and then cooled off in order to condense the aerosol vapor on the NaCl particles. The produced aerosols can be characterized by determining the particle diameter and what is known as the geometric standard deviation (ideally 1).

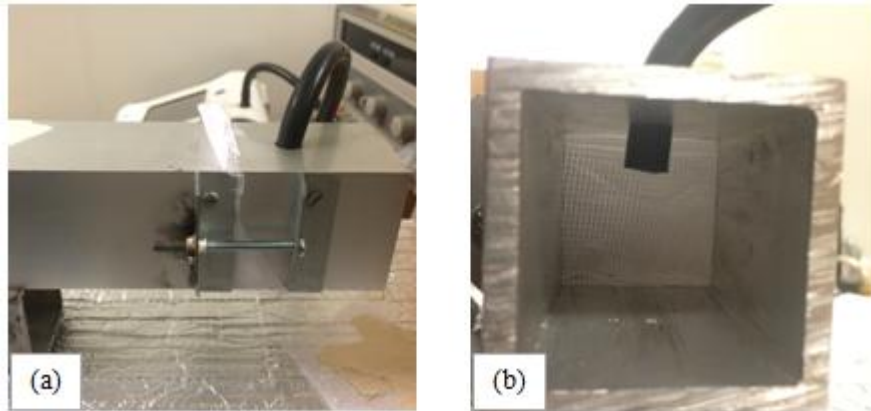


Figure 18 Smaller Tunnel; Nano web Sample Holder (made in AUB shops)

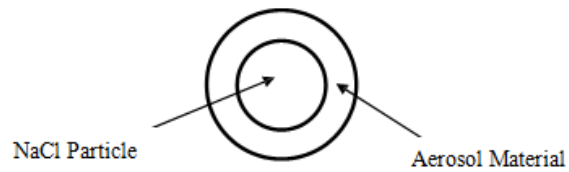


Figure 17 Aerosol Particle Schematic (not to scale)

The presented formula was used to determine the efficiency of the nanofiber filter,

$$\eta = \frac{C_u - C_d}{C_u}$$

Where, η is the efficiency

C_u is the upstream particle concentration (particles/cm³)

C_d is the downstream particle concentration (particles/cm³)

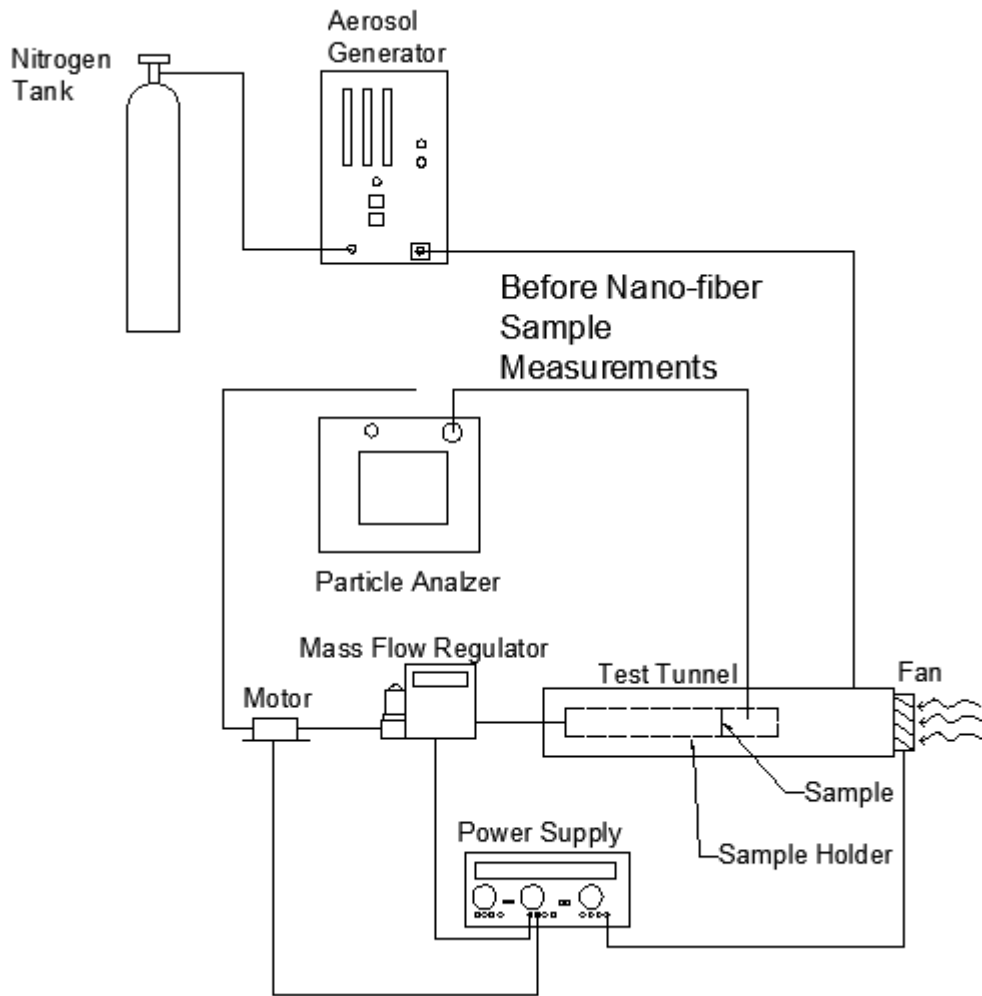


Figure 19 Aerosol Filtration Experimental Setup Scheme

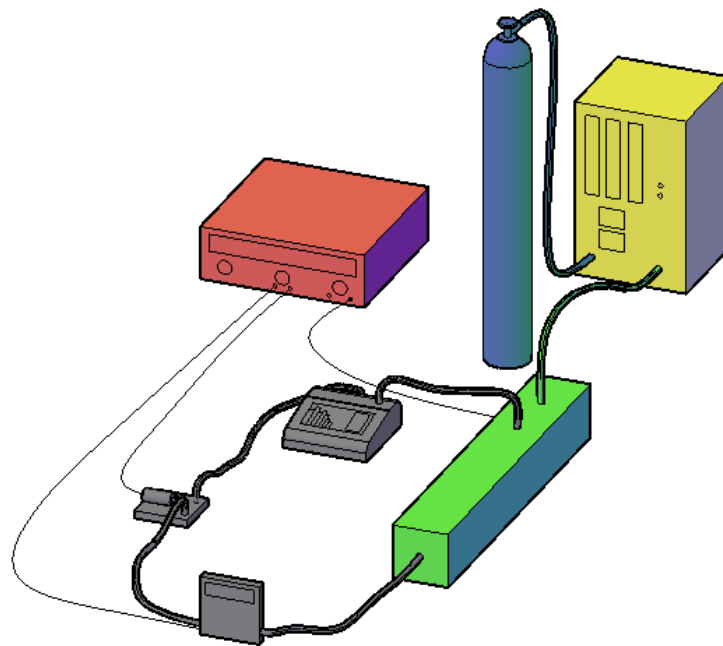


Figure 20 3D Representation of the Experimental Setup (AutoCAD)

CHAPTER 5

RESULTS AND DISCUSSIONS

5.1 Raw material specifications

5.1.1 Density

The density was determined for 4, 5, 6, 7, 8, 9, 10, 11, 12, 13, and 14 wt% PU/DMF experimentally using the DMA 35

The results for the theoretical method and experimental are plotted below.

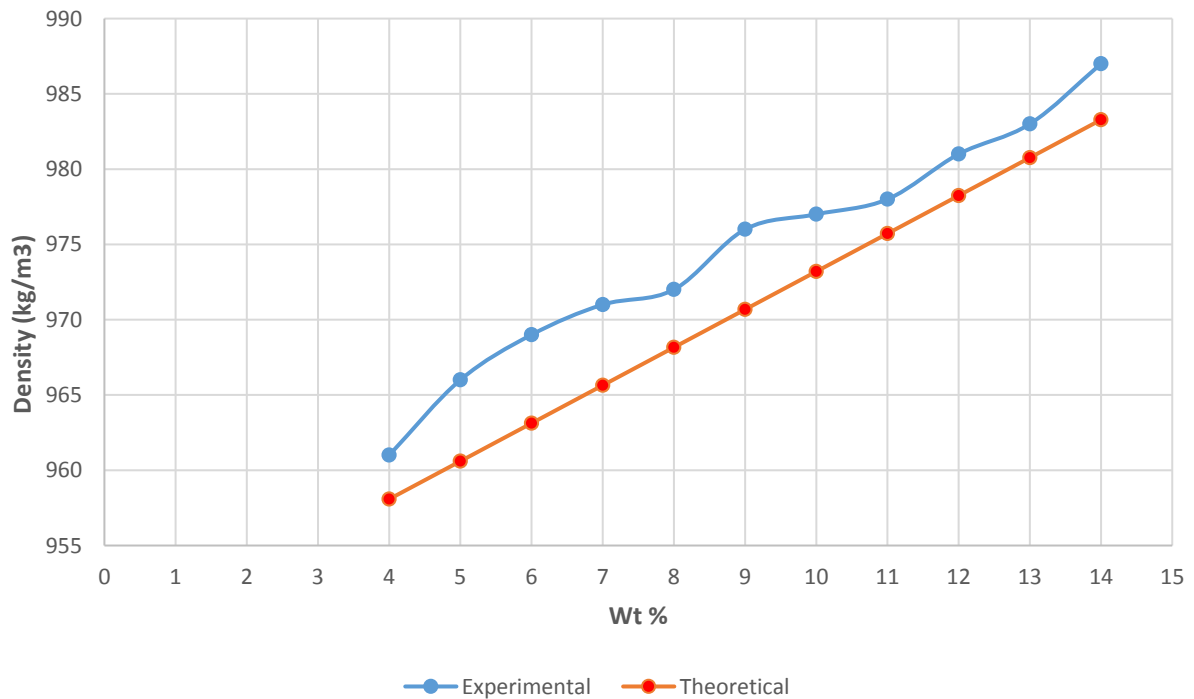


Figure 21 Density vs. Wt% PU/DMF (Experimental and Theoretical)

Figure 21 shows that as the concentration of the solution increases, the density increases as well. Although density and concentration are different concepts, in which density is an inherent property of the solution as opposed to concentration, the relation here is observed to be linear. For instance, at 10 wt %, the theoretical method gave a density of 973 kg/m³.

Concentration

Increasing concentrations would lead to an eventual increase in viscosity – due to an increase in the mix-up polymer chain numbers - and decrease in the surface tension, and consequently, larger fibers. In addition, literature showed that nanofibers get fragmented into droplets at low concentrations, and found a limit for increased concentrations above which the formation of nanofibers becomes harder, what implied a certain optimum range found to be the best for smooth nanofibers formation (Deitzelet al., 2001).

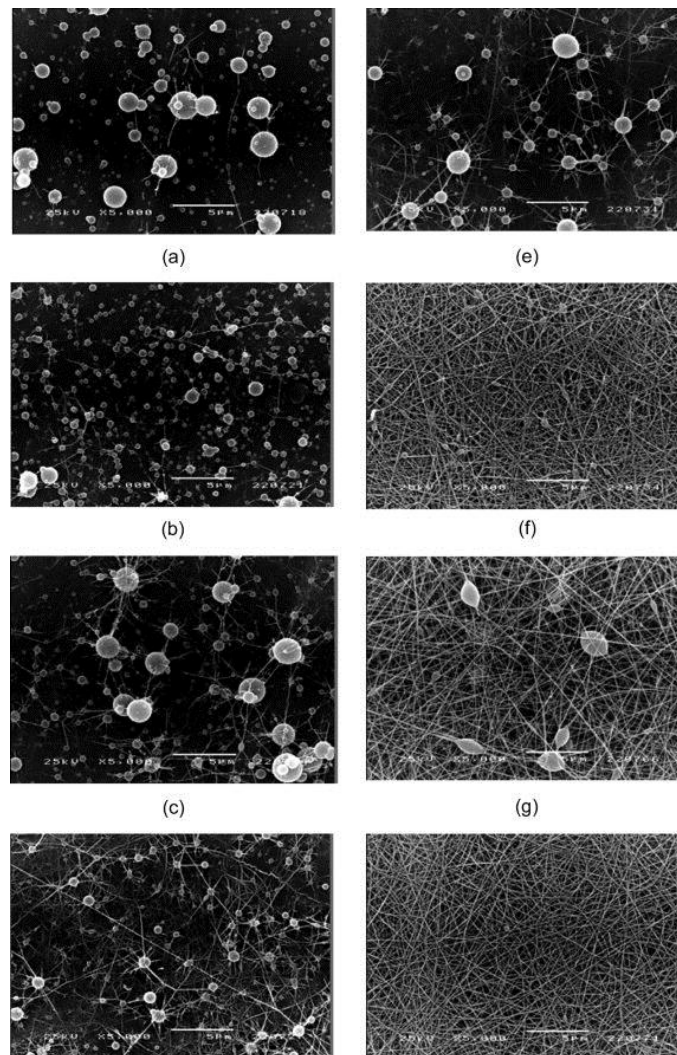


Figure 22 Evolution of fiber morphology with increasing concentration from a to h (Supaphol et al., 2005)

At very low concentrations, electrospinning takes place instead of electrospinning. Increasing the concentration beyond that would lead to electrospinning with beads formation (Supaphol et al., 2005). That phenomenon can be attributed to the

fact that the viscoelastic forces within molecules are not strong enough to resist the electrostatic repulsion between the charges. On the contrary, increasing the concentration beyond a certain level would induce strong viscoelastic resistance to the electrostatic repulsion necessary to carry electrospinning; in other words, excessive concentration would lead to dripping off instead of electrospinning (Zhuo et al., 2008).

The aim from optimizing the experiments from this perspective was to obtain uniform distribution of smooth fibers with minimum diameter. Previous work done in literature concerning the electrospinning of PU used concentrations ranging from 3 wt% (Zhuo et al., 2008) to 16 wt% (Cha et al., 2006).

Karakaş et al has shown that solution concentration has the major effect among other parameters in PU electrospinning. The experiments were carried at a voltage of 15kV, a feed rate of 0.5ml/hr, at 15cm TCD with solutions of PU/DMF of concentrations 8wt%, 10wt%, and 12wt%. Although the lowest concentration yielded to the lowest fiber diameter, the morphology showed un-wanted beads. The beads starts disappearing at a concentration of 10wt%; that was the best solution obtaining the finest diameters with no beads. A much lower concentrations, electro spraying instead of electrospinning take place (Karakas et al., 2013). Demir et al showed that for PU/DMF solution at concentrations below 3.8wt%, the stream is broken into drops due the low viscosity of the solution (Demir et al., 2002). The lower the concentration of the solution (PU/DMF was used in the study), the less uniform the fibers assembly become (Zdraveva, 2011); 10wt% solution gave the best result and it was chosen for the rest of the experiments.

The concentrations tested were 3wt%, 4wt%, 7wt%, 10wt%, 13wt%, and 14wt% where there was droplets when using 3% wt, beads at 7% wt and 4%, the beads vanished at 10% wt and 13% wt, and at 14% no electrospinning took place.

Viscosity and Molecular Weight

Over the numerous investigations in nanofiber electrospinning, it is well known that the fiber diameter depends on the polymeric solution concentration and viscosity. Hence, viscosity- measurements during electrospinning experiments is an important aspect for optimizing the finest fiber diameter.

In a study concerning the matter on Polyacrylonitrile (PAN) in Dimethylformamide (DMF). The viscosity of the polymeric solution tends to increase as the concentration of the solution increases. The viscosity was monitored for solutions with concentrations in the range of 4 to 20 wt % with increments of 2 wt%. The results show that the viscosity increased from 97.2 cP to 5238.6 cP as the concentration increased from 4 to 20 wt %, respectively (Nasouri et al., 2012).

Zhang et al., determined the viscosity of polyvinyl alcohol (PVA)/distilled water solution. The results show that the viscosity range was between 75 cP to 232 cP for 6 g PVA in 94 ml pure water and 8 g PVA in 92 ml pure water, respectively. However, increasing the concentration too much (above 8.3 wt%), hence the viscosity, would make it difficult to eject fibers from the needle tip (Zhang et al., 2005).

However, in the conducted experiment, six measurements were taken for each concentration by varying the rounds per minute (RPM) while staying within the torque range of 50 to 90%. Table 3 shows the results.

Table 2 Solution Concentration vs. Kinematic Viscosity

| Concentration % | 4 | 5 | 6 | 7 | 8 | 9 | 10 | 11 | 12 | 13 | 14 |
|---|----|----|----|-----|-----|-----|-----|-----|------|------|------|
| Measured Kinematic viscosity Average (cSt) | 27 | 49 | 63 | 126 | 235 | 357 | 699 | 916 | 2166 | 2818 | 4413 |
| Dynamic Viscosity (cP) | 26 | 47 | 61 | 122 | 227 | 346 | 680 | 893 | 2119 | 2763 | 4341 |

As can be seen from Table 3 the measured kinematic viscosity, hence the dynamic viscosity, increases as the concentration increases. This is a similar trend as the ones observed by Nasouri et al. 2012 and Zhang et al. 2004. At zero concentration, there is no need to take measurements since the viscosity is that of the solvent which is DMF with 0.92 cP. Viscosity of the electrospun solution has proven to be an important parameter since it can effect formation of the ejected stream, the needle-tip drop, and the formed fiber diameters. Proper electrospinning cannot be achieved when the

viscosity of the polymeric solutions are too low or too high. Viscosities less than 100 cP would affect the fiber structure and entertain the formation of droplets rather than fibers. On the other hand, viscosities higher than 2000 cP would result in difficulties in stabilizing the jet formed (Deitzel et al., 2001). Deitzel et al. investigated the above mentioned situation by using Polyethylene Oxide in water solutions. The operational range was determined to be within the concentration range of 4 to 10 wt%. In addition, the measured viscosity range was between 100 and 2000 cP which is the acceptable range as stated before (Deitzel et al., 2001).

After obtaining the relative viscosity, which is simply the ratio of the viscosity of the solution to that of the solvent, the inherent viscosity was determined and the values are shown in appendix I. The inherent viscosity is then plotted against the PU/DMF solutions as shown in Figure 23. Extrapolating the inherent viscosity graph gives a y-intercept of 82: the intrinsic viscosity.

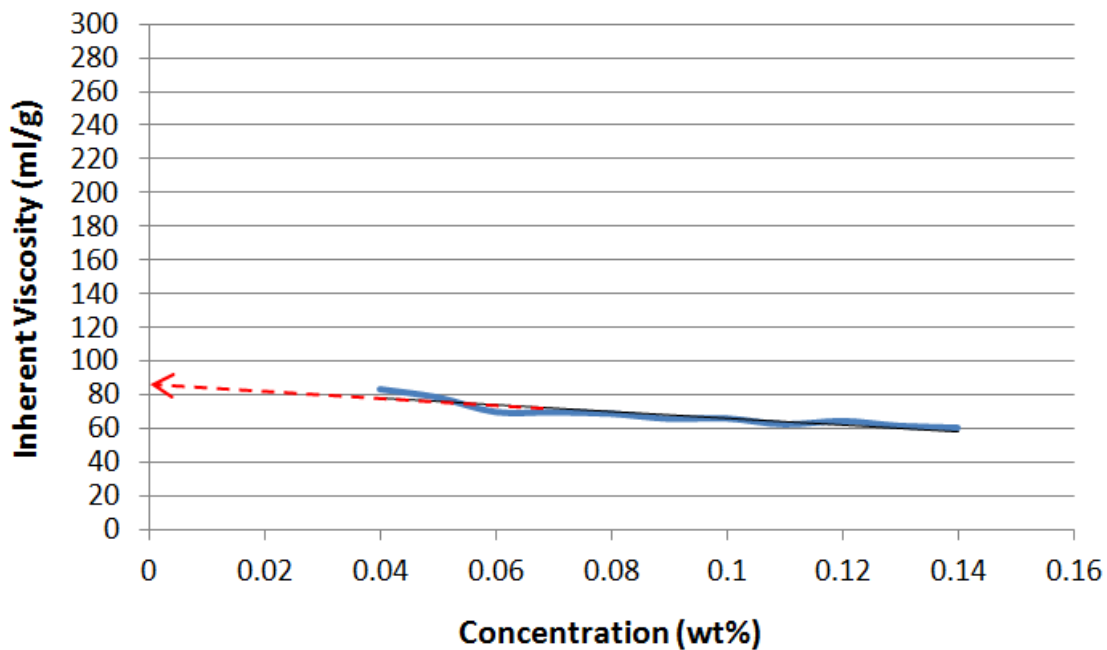


Figure 23 Inherent Viscosity VS. Concentration

Cengiz and Jirsak reported that pure 15 wt% PU/DMF solution had a viscosity of 760 cP (Cengiz and Jirsak, 2009). This can be considered to be close to the viscosity of the 10 wt% PU/DMF obtained which had a value of 680.2 cP. Stenhouse et al. also reported the intrinsic viscosity of liquid-crystalline PU in DMF to be between 0.32 and

0.57 dL/g depending on the molecular weight. As the molecular weight increases so does the intrinsic viscosity (Stenhouse et al., 1988). Tuzar et al. reported the intrinsic viscosity (using Ubbelohde viscometer) of PU in different DMF based solvents. In DMF/Acetone solvent (DMF fraction by volume varying between 0.4 and 1), the intrinsic viscosity varied between 0.455 and 0.580 dL/g. On the other hand, in DMF/Toluene solvent (DMF fraction by volume varying between 0.9 and 0.25), the intrinsic viscosity varied between 0.5 and 0.632 dL/g (Tuzar et al., 1971). Vasconcelos et al. reported the viscosity of 10wt% PU solutions using different solvents. In pure DMF the intrinsic viscosity was 54ml/g, in 70/30-Xylene/DMF the intrinsic viscosity was 53ml/g, and in 70/30-DMSO/DMF the intrinsic viscosity was 52.7ml/g (Vasconcelos et al., 2001).

Finally, the Mark-Houwink equation can now be used to determine the molecular weight. Plugging in the inherent viscosity along with the mark-Houwink constant mentioned earlier, gives a molecular weight of approximately 199,000 g/mol. It is noteworthy to mention that seven other PU grades were prepared in DMF and tested but all failed to have merit to be chosen for electrospinning. Table 4 shows the molecular weights of the other PU grades.

Table 3 Molecular Weights of other PU Grades

| Polyurethane Grade | Molecular Weight (g/mol) |
|---------------------------|---------------------------------|
| TPUA-265A | 47517 |
| TPUI-E61D | 75943 |
| TPUI-E80 | 15868 |
| TPUI-E95 | 90514 |
| TPUI-G95 | 1334 |
| TPUI-H95 | 793 |
| TPUI-T95 | 11087 |

The main reason, however, based on the above analysis, is that they all had low viscosities even for high concentrated solutions which is not desirable. The highest among the tested PU grades was TPUI-E95 with a viscosity of 642 cP at 13wt% and 1002 cP at 14 wt% and a molecular weight of \approx 90,000 g/mol. This can probably

perform well but is limited by the concentration needed as compared to the chosen grade, TPUA-760, with a more flexible range at a practical concentration of 10 wt%.

5.2 Electrospun Morphology

Fibers diameter

The study concerning the fibers morphology and the effect of various electrospinning parameter on the nanostructure of the web was aiming at optimizing the conditions for best uniformity (no beads) and minimum fiber diameter. The uniformity is important in improving the mechanical property of the final web (Zhu et al., 2012), while reduced fiber diameter enhances the waterproof ability of the final product as a result of smaller pores (Eichhorn & Sampson, 2010).

8 different types of industrial grad PU granules were used for electrospinning at a fixed concentration of 10wt.% , at a flow rate of 0.5 ml/hr., DC voltage of 25 KV and tip to collector distance of 15 cm.

Figure 24 shows SEM images obtained from each electrospinning experiment.

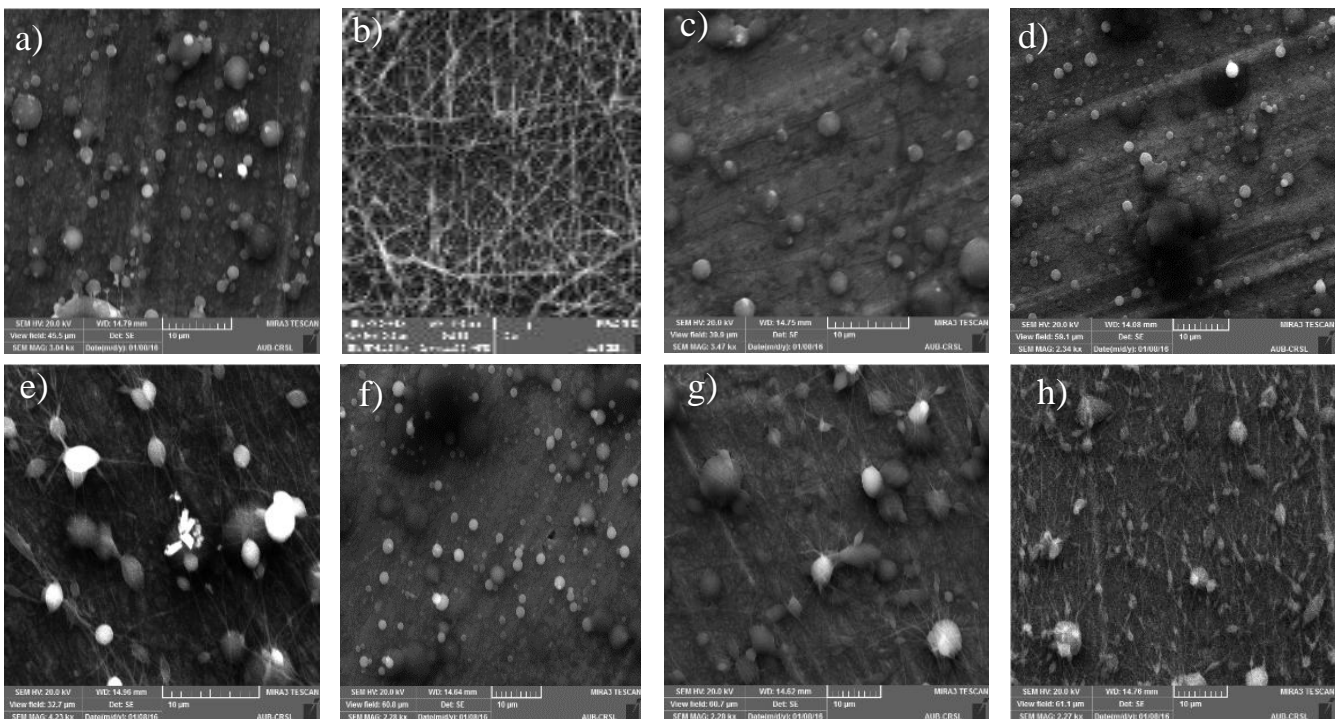


Figure 24 SEM images of electrospun obtained at same conditions from different PU grades: a) TPUI-95, b) TPUA 760, c) TPUA-265 A, d) TPUI-E61D, e) TPUI-E80, f) TPUI-T95, g) RWTPUIG95, h) TPUI-H95

As shown in Figure 24, fibers were formed only upon using TPUA-760 grade PU polymer (10wt.% in DMF). This shows again the importance of molecular weight of polymer and the viscosity of the polymeric solution.. Based on these screening experiments, we chose to investigate only this grade and perform the rest of the experiments

The process of electrospinning is highly dependent on the balance between the electrostatic and viscoelastic forces (Rutledge & Fridrikh, 2007); only when the electrostatic repulsion exceeds surface tension and viscoelastic stability the jet is ejected. Viscoelastic forces play a role in formation of elongated jet. When the viscosity of solution is not high enough beads formation is occurred (Fong et al., 1999). Electrospinning occurs at low viscosities when electrostatic repulsion overcome the viscoelastic forces which is responsible for jet stability and continuity. In fact, the viscosity of the solution is dependent on overlapping of the polymeric chains; the higher the overlapping, the greater the viscosity (Shenoy et al., 2005). therefore, the higher the concentration or molecular weight, the greater the entanglement (Koski et al.,2004). So it is expected that with increasing the concentration or molecular weight, the behavior would develop from beads formation to smooth fibers. High viscosities would lead to dripping off the nozzle as viscoelastic forces dominate over electrostatic repulsion.

The relation between concentration and viscosity is shown in Table 3. As was expected, the viscosity deferred between the solutions, increasing with concentration. The consequences are shown in the electrospinning results obtain in Figure 25.

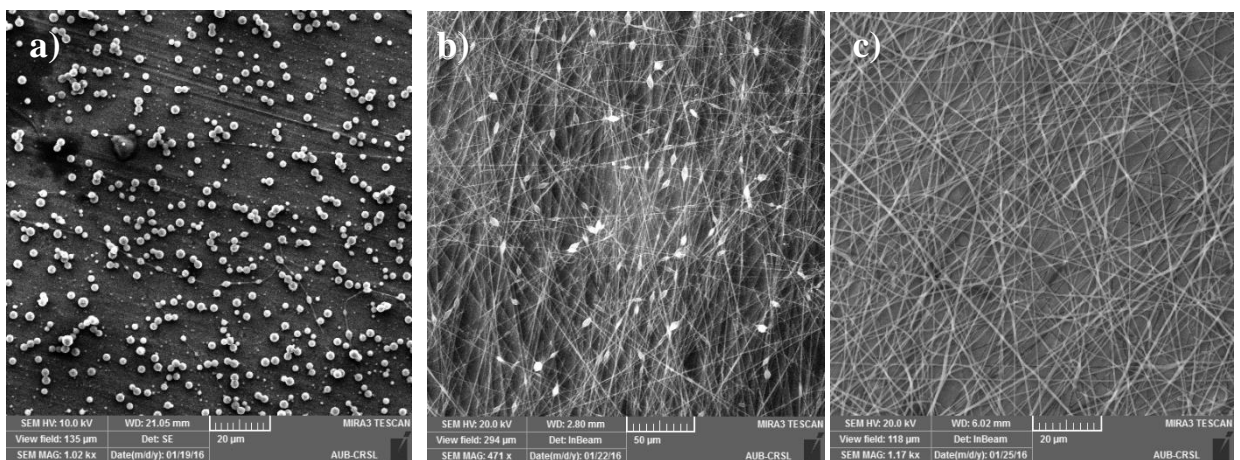


Figure 25 SEM images of electrospun obtained at same conditions for different concentrations, a) 4% wt, b) 7 % wt, c) 10 % wt

It is shown that no electrospinning occurred at 4wt% concentration. Formation of beads was evident at 7wt%, and the web uniformity was attained at concentrations of 10wt%.

The next step was to optimize the nano-structure of the web; beadless with minimal fiber diameter. The two major parameters affecting from that point of view are voltage, tip to collector distance, and concentration. 210 electrospinning experiments were performed in order to determine the minimum fiber diameter that can be obtained, with the corresponding voltage and tip to collector distance. The experiments were designed as combinations of the parameters value present in the following table:

Table 4 Different values of processing conditions for the preliminary electrospinning experiments

| Drum Speed (r.p.m) | Flow Rate (ml/h) | Concentration | Tip-to-Collector Distance (cm) | Voltage (kV) |
|--------------------|------------------|---------------|--------------------------------|--------------|
| 680 | 0.5 | 4wt% | 12 | 13 |
| | | 7wt% | 14 | 15 |
| | | 10wt% | 15 | 17 |
| | | 13wt% | 16 | 19 |
| | | 18 | 21 | |
| | | 20 | 23 | |
| | | 22 | 25 | |
| | | 24 | 27 | |
| | | 26 | 29 | |
| | | 31 | | |
| | | 33 | | |
| | | 35 | | |
| | | 37 | | |

The flow rate was maintained at 0.5ml/hr and the drum speed at 680rpm. The voltage was varied between 13kV and 37kV. The tip to collector distance was varied between 12cm, and 26cm. 4 different polymeric concentrations were used (4wt%, 7wt%, 10wt%

and 13 wt%). The fiber diameter in addition to the beads formation in each of the obtained electrospun was studied in order to optimize the process. Concerning the former, the morphology of the web was characterized by the degree of beads formation. The characterization goes from least amount of beads present to higher amounts as: no beads, minor beads, major beads, and full of beads. Figure 26 shows example of each of the degrees of beads formation obtained when changing parameters during experiments. The degree of bead formation observed after each experiment is presented in tables 6 and 7. The tables show that although beadless fibers can be obtained at both 10% and 13%, the range of the conditions at which those fibers are obtained is wider at 10% which allows for further control of the fiber diameter and consequently the web characteristics.

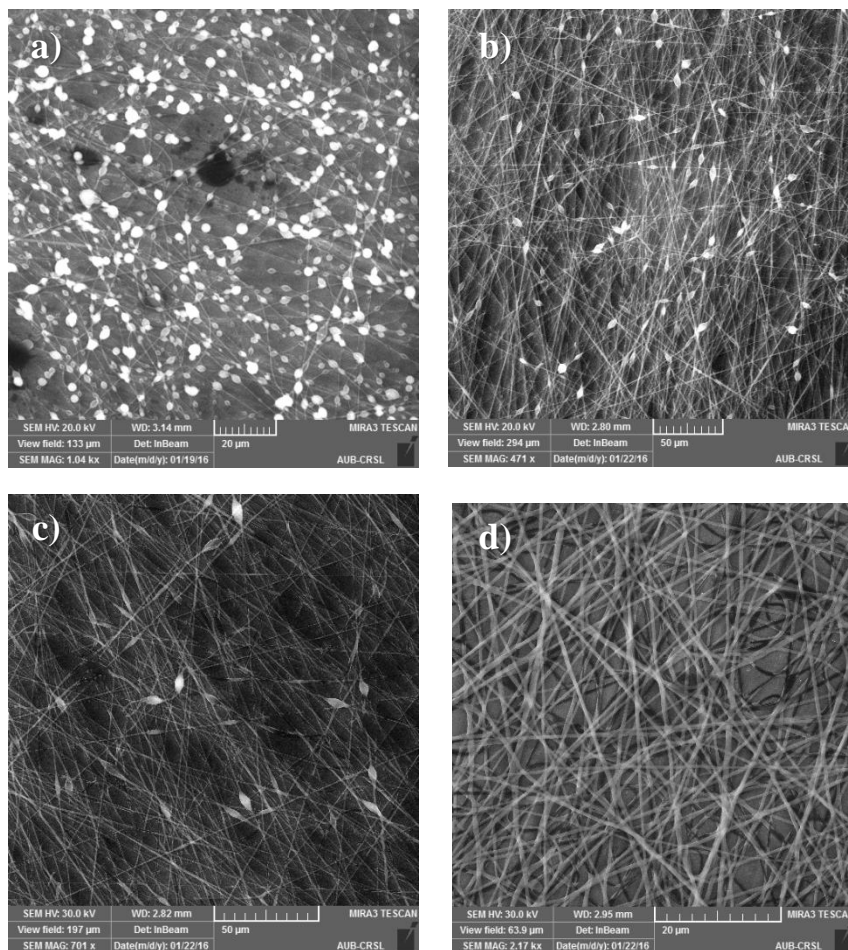


Figure 26 different examples of fibers morphology and degrees of beads formation a) full beads, b) Major beads, c) Minor beads d) No beads

Table 5 fibers average diameter distribution over different voltages and tip to collector distances at 10 wt% concentration TCD = Tip to Collector Distance , *= SEM picture below

| TCD/V | 11 | 13 | 15 | 17 | 19 | 21 | 23 | 25 | 27 | 29 | 31 | 33 | 35 | 37 |
|-------|----------|-------------|-----|-----|-------------|-----|-----|-------------|-------------|----------------|-------------|----|----|------------|
| 12 | NO ES | 312 | 309 | 301 | 297 | 290 | 285 | 273 | 260 | Minor Beads | Major Beads | | | Full Beads |
| 14 | | 281 | 276 | 269 | 261 | 246 | 238 | 231 | 219 | | | | | |
| 15 | | 257 | 253 | 241 | 228 | 215 | 209 | 193* | 171 | | | | | |
| 16 | | 265 | 257 | 243 | 240 | 236 | 231 | 229 | 220* | | | | | |
| 18 | | 271 | 264 | 259 | 257 | 254 | 251 | 248 | 232 | | | | | |
| 20 | | 289 | 286 | 279 | 274 | 271 | 265 | 261 | 247 | | | | | |
| 22 | | 303 | 295 | 289 | 281* | 278 | 273 | 269 | 263 | | | | | |
| 24 | | 309 | 304 | 299 | 295 | 287 | 282 | 276 | 269 | | | | | |
| 26 | | Minor Beads | | | | | | | | | | | | |

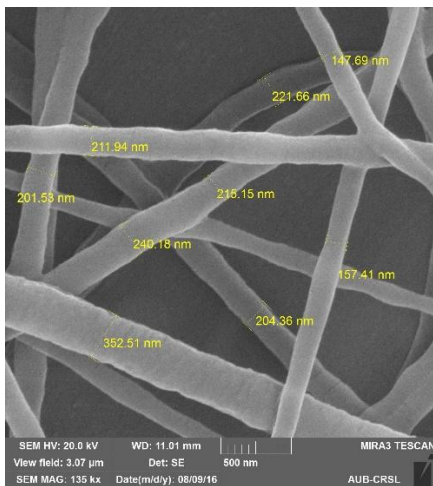
Table 6 fibers average diameter distribution over different voltages and tip to collector distances at 13wt% concentration TCD = Tip to Collector Distance , *= SEM picture below

| TCD/V | 11 | 13 | 15 | 17 | 19 | 21 | 23 | 25 | 27 | 29 | 31 | 33 | 35 | 37 |
|-------|----------|---------------|-------------|-----|-----|-------------|-------------|----|----|-------------|----------------|----|----|----|
| 12 | NO ES | No Bending | | | | | | | | Minor Beads | Major beads | | | |
| 14 | | | 421 | 415 | 406 | 399 | 382 | | | | | | | |
| 15 | | | 376 | 365 | 344 | 333* | 323 | | | | | | | |
| 16 | | | 337 | 320 | 301 | 293 | 270* | | | | | | | |
| 18 | | | 340 | 335 | 330 | 323 | 319 | | | | | | | |
| 20 | | | 362 | 360 | 355 | 352 | 348 | | | | | | | |
| 22 | | | 391* | 384 | 379 | 370 | 366 | | | | | | | |
| 24 | | | 405 | 393 | 389 | 382 | 376 | | | | | | | |
| 26 | | | 419 | 413 | 401 | 393 | 385 | | | | | | | |

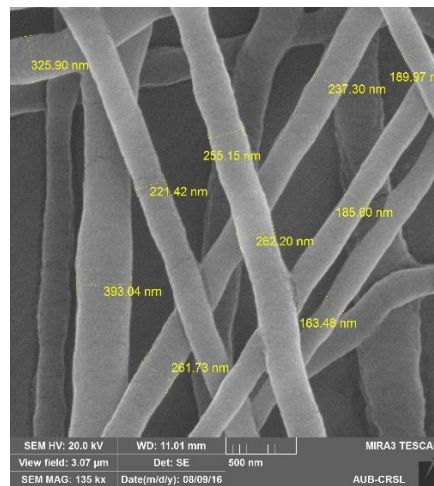
For the 10% wt solution, no beads formation at tip to collector distance below 26cm and voltage below 27kV, exclusively. As the voltage increased from 25kV to 29 kV. At 26cm, minor beads were observed for voltage up to 25kV, and major beads for

voltage beyond that up to 35kV. Major beads were present at voltages beyond 29kV up to 35kV. At 37kV, full of beads were observed at every tip to collector distance.

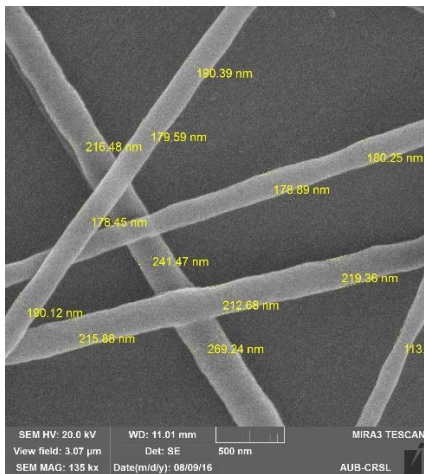
Figure 27 shows SEM images obtained with the electrospinning of 10% wt and 13% wt PU/DMF at different conditions. It appears that finer fibers are obtained at 10% concentration, which is in accordance with literature results described later. Hence, choosing 10% wt PU/ DMF solution for running the electrospinning experiments plays a role in optimizing the results.



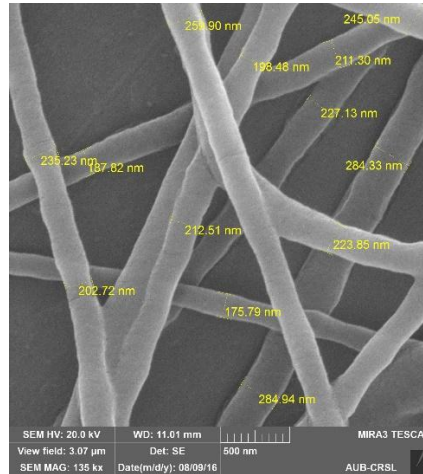
10%wt, 19kV, 22cm



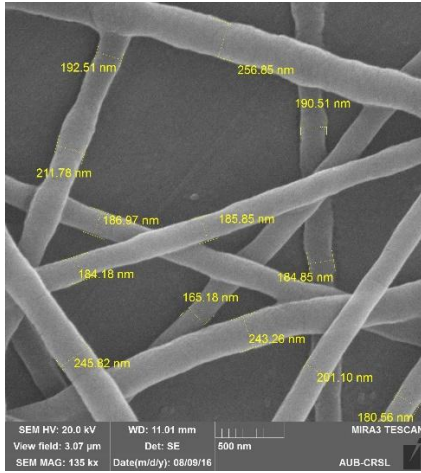
13%wt, 19kV, 22cm



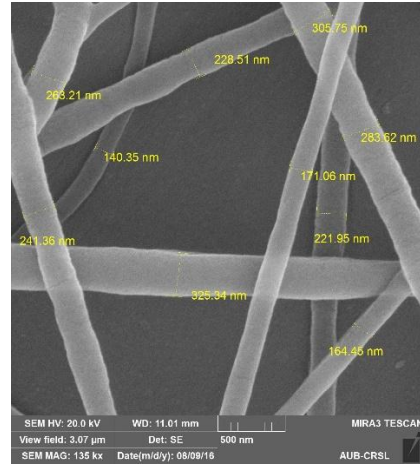
10%wt, 25kV, 15cm



13%wt, 25kV, 15cm



10%wt, 27kV, 16cm



13%wt, 27kV, 16cm

Figure 27 SEM micrographs from some of the samples prepared at various conditions.

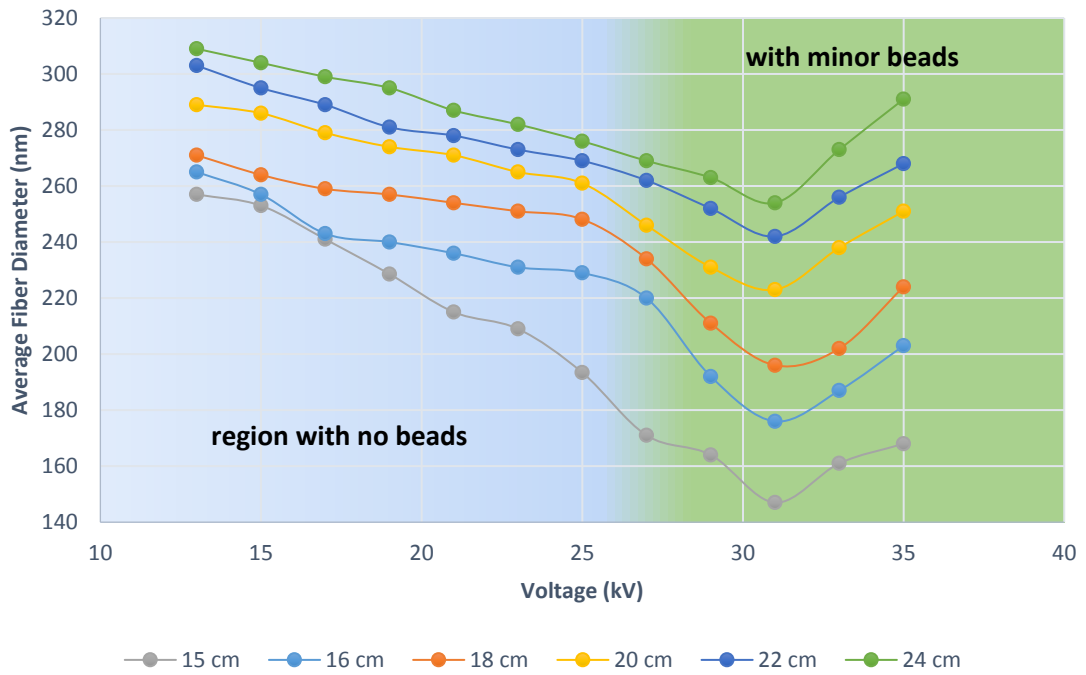


Figure 28 Variation of fiber diameter with the applied voltage at different tip to collector distances

As shown in the graph of Figure 28, for a constant distance, the fiber diameter decreases with increasing the voltage (since stretching forces increase the intensity of drawing fibers) until achieving a minimum beyond which it starts increasing (as the

flight time decrease with extensive voltage, the stretching time for fibers to get thinner is reduced). It has been shown that for any distance, the minimal diameter is obtained at a voltage of 31kV where the formation of minor beads takes place. The fiber diameter showed similar behavior at a constant voltage increasing the tip to collector distance. The diameter decreased until achieving a minimum at 15cm tip to collector distance at various voltages; Increasing the distance leads to increasing stretching time of the correspondent electric field. Above certain TCD (15cm), fibers diameter start to increase due to weakening in the electric field and consequently the stretching forces. From the data shown, it appears that the finest fiber diameter with no beads in the structure can be achieved at a voltage of 25kV and a tip to collector distance of 15cm.

Areal Density

Areal density of electrospun membrane is defined as the mass of the fibers collected over a unit area; it is considered as a reflection of continuity of the process homogeneity of the web, plus its effect on the web porosity (Krifa & Yuan, 2016) which is a critical property of breathable and protective fabrics. Studying the basis weight helps mainly in establishing an idea about the distribution of the nanofibers on the used support.

In this context, the formula used to obtain the theoretical value of the areal density can be derived by calculating the mass deposited on the collector from the flow rate of the polymer and dividing it by the area. The equation is follows:

$$w = \frac{\rho * C * Q * t}{A_c}$$

Where, w is the areal density, mg/cm^2

ρ is the density of the used solution, g/ml , and it can be calculated from the densities of solute and solvent by the following equation:

$$\rho_{solution} = \frac{100}{\frac{\%wt}{\rho_{polymer}} + \frac{100 - \%wt}{\rho_{solvent}}}$$

C is the mass fraction of the solute present in the solution

Q is the flow rate at which the solution is ejected from the needle tip, and it is presented in $\mu\text{l/hr}$

t is the run time of the electro-spinning, hr

A_c is the collector surface area, cm^2 The value of the area can be calculated from the diameter of the drum (d) and its width (b) by the following equation:

$$A_c = \pi \times d \times b$$

d and b are presented in cm.

When carrying the experiments, several observations could be done that can give some hints to potential errors in such procedures. Although the electrospinning was performed with sweeping on, the fibers were mostly concentrated at the middle section. That can be referred to the fact that sweeping was turned after the electrospinning is started and steady flow achieved, besides, some frequent cuttings in the flow of the electrospun solution happened at the edges. The ununiformed distribution lead to the appearance of some outliers for each web while carrying the experiments where the masses of some samples deferred significantly from others. Statistically, and for a certain amount of time, the nozzle will be in the middle position more than both corners of the electrospinning area. Therefore, the produced mesh will be thicker in the middle.

As for the relation between electrospinning time and areal density, Figure 29 shows the trend obtained from theoretical calculations and experimental data:

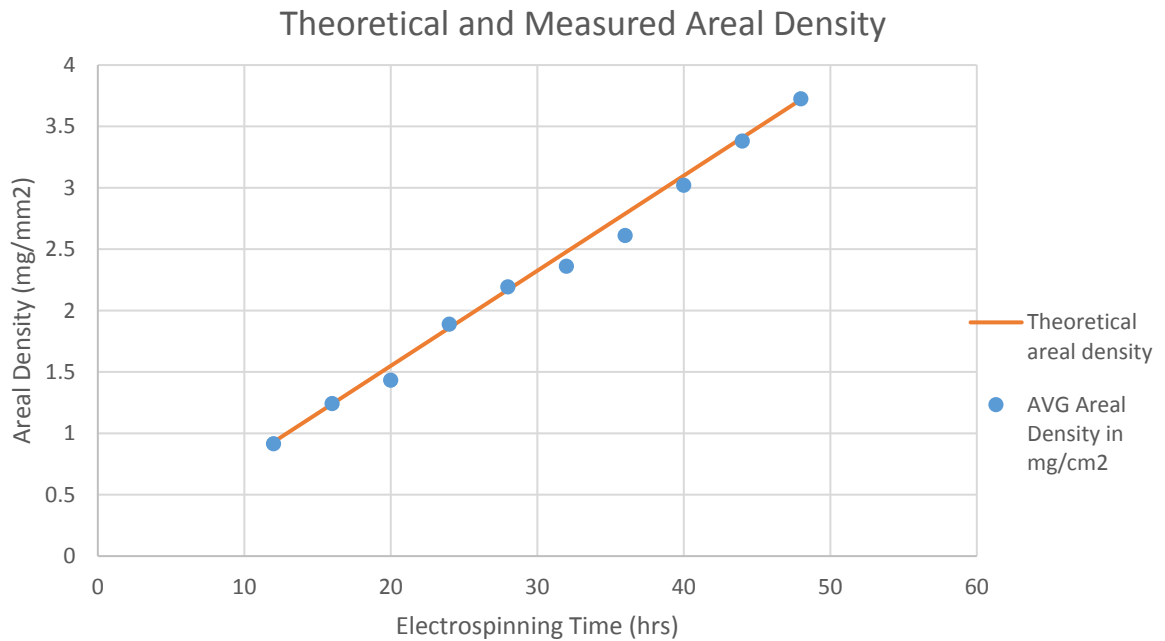


Figure 29 relation between areal density and electrospinning time theoretically and experimentally

Since the only changing parameter is the electrospinning time, the theoretical data of areal density increased with time. The experimental data showed also an increment in the areal density with time, with negligible error characterized by minor deviation from linearity; the error present is insignificant although the fibers were not distributed uniformly because of the procedure follow and take sample from all over the width of the electrospun web. There is a good agreement between the measured and calculated values; more electrospinning time means more fibers deposition and consequently more mass over the constant surface area of the rotating drum.

In fact, failure to find an agreement between theoretical and experimental values indicates that there are errors: in cutting *and/or* weighing *and/or* fiber distribution. That was not the case as the procedure followed precise steps in taking the sample and cutting them; cutting is a very crucial step as the square pieces must be cut as precise and consistent as possible. To verify the precision, SEM measurements were done to calculate the area of randomly chosen square sample and the results showed that the area of the squares can be considered as 1 cm² since the error is negligible.

Thickness

In order to obtain reliable results of the web thickness, different parts were examined, similar to areal density measurement technique.

Figure 30 shows that the thickness increased with electrospinning duration. Thus, increasing the amount of polymer coating the mesh would lead to an increase in the volume of deposition; as the area of the drum is constant, the increase in the volume would take place in the thickness. The polymeric film had low thickness as it has no pores to increase the occupying space; the high standard deviation signifies a nonuniform distribution of the polymer all over the film.

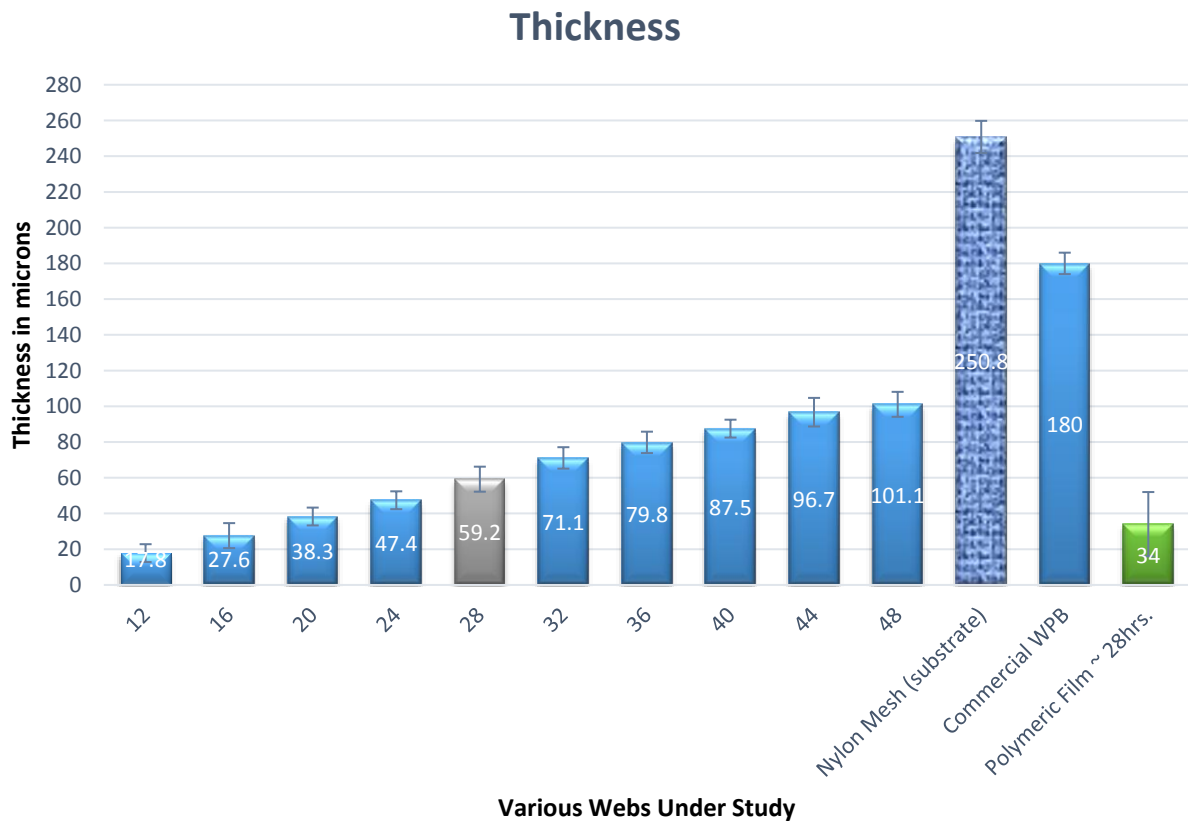


Figure 30 thickness results obtained by Brunswick film thickness measurement device in microns

WPB: Waterproof Breathable textile, DuPont™ Tyvek, model PT31L0

Pore Size

As the idea of water proof breathable fabric depends on the fabric acting like a filter allowing water vapor and air to pass through and blocking the passage of water, pore size become an essential characteristic that permit achieving protective yet thermally comfortable fabric.

A summary of the mean size data for all the electrospun layers and for commercial water proof breathable fabric is shown in Figure 31. The average pore size distribution of the electrospun meshes are between 2 and 5 micrometers. The value decreases by increasing the time of electrospinning. This trend is in agreement with what have been found in literature (Han, Chung, & Park, 2013a). According to Han et al, the thickness of the electrospun web is related to the fibers packing which can be manipulated by electrospinning; the increase in web thickness signifies an increase in the degree of packing, which yields to a decrease in the pore size.

Banuškevičiūtė et al showed that increasing the thickness of electrospun web would lead to a decrease in the pore size; as a result, the water permeability was reduced (Banuškevičiūtė et al., 2013). The increase in waterproofness accompanied by the reduction of pore size can be on the expense of the fabric breathability. Increasing the fiber density in mesh lowers the pore size which can result in blocking the air flow (Lee & Obendorf, 2007). Hence, it is important to measure the pore size and study the pore size distribution in order to show the effect of electrospinning time (which in turn affects the areal density and layer thickness) on the characteristics of the fiber. (Frey & Li, 2007)

Moreover, the structure of the pores play a role in the functionality of the produced web, and herein another parameter comes into consideration: pore tortuosity. According to Shirazi et al pore tortuosity is a measurement of pore shape randomness and lack of uniformity. It is supposed that as the thickness of the web increases (in our case due to the increase in electrospinning time), the tortuosity of the pores increases and lowers the air permeability (Shirazi et al., 2013).

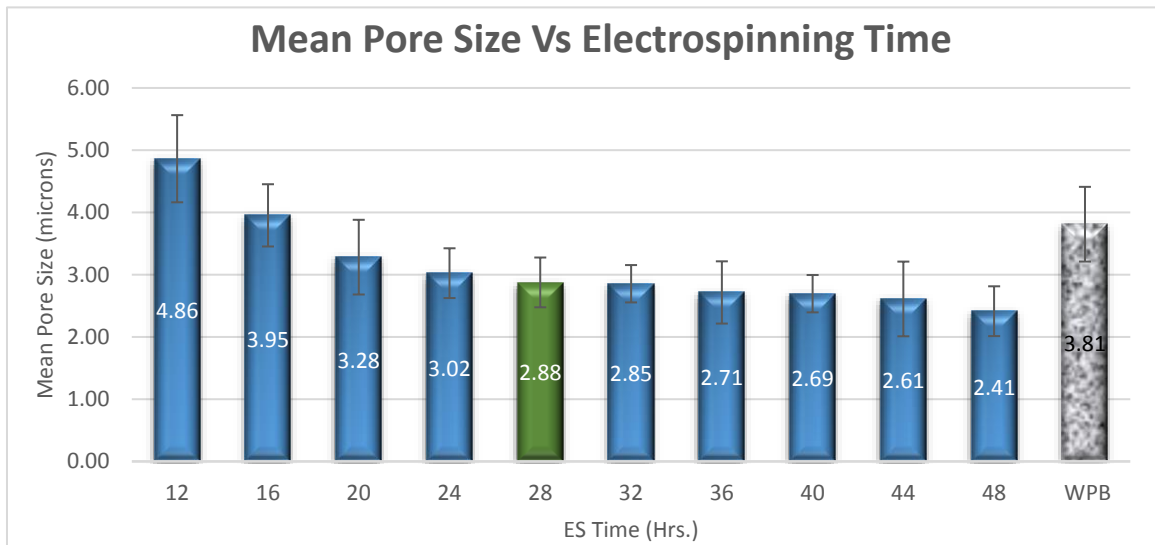


Figure 31 Pore size analysis results of different electrospun membranes obtained at different running times in comparison with Waterproof Breathable (WPB) textile, DuPont™ Tyvek, model PT31L0.

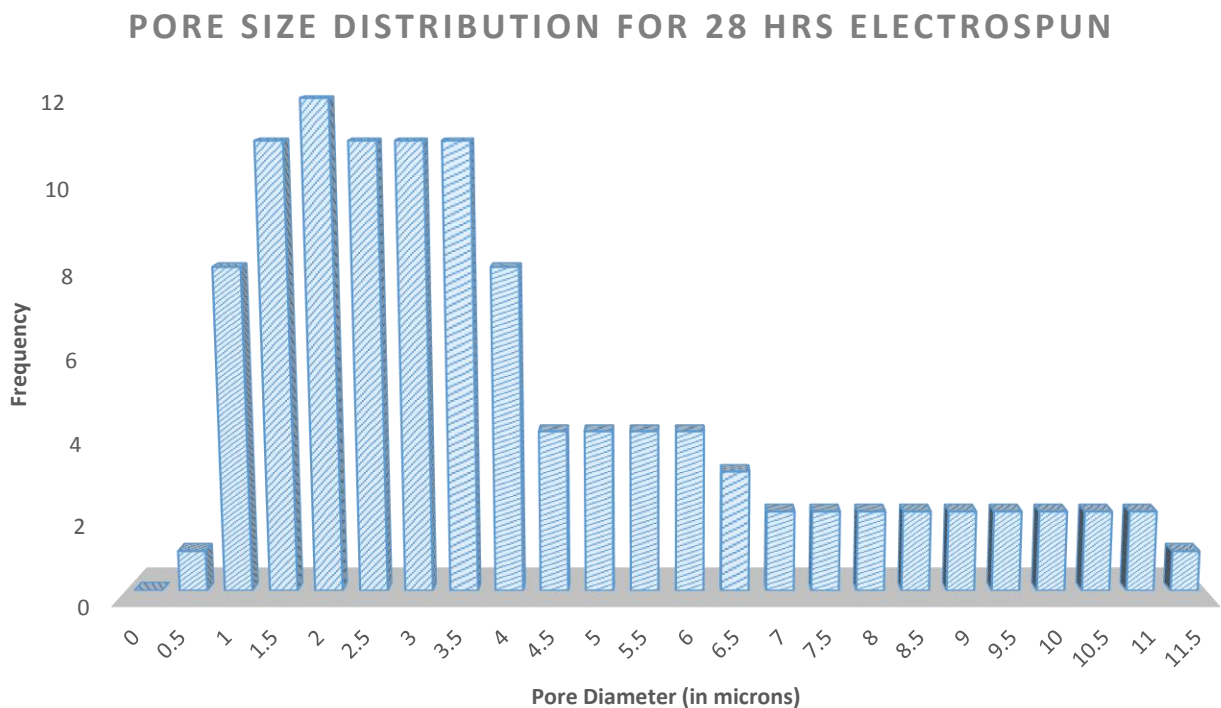


Figure 32 Pore size distribution of 28hrs electrospun web

Figure 32 shows that although the distribution is wide, with pore sizes ranging from 0.5 to 11.5 microns, there appears a mode region in which the pore diameter lies

between 1.5 and 3.5 microns, and this region includes the mean diameter which was 2.88 microns for the tested specimen.

The nanofibers obtained from electrospinning result in highly porous web with small pores that can be used in different applications; filtration, tissue engineering, thermal comfort and protective clothing (Yoon & Lee, 2011) (Gibson et al., 2001). For further illustration about the importance of the electrospinning technique in obtaining waterproof breathable fabric, a PU film was produced to compare with 28hrs electrospun. 14ml of 10wt% PU/DMF solution was spread over the 31.4cm × 20cm glass sheet (same dimensions of nylon mesh substrate used in electrospinning experiments), and then dried at 40°C in an oven for 24 hrs. The resulted PU film was not porous based on pore size measurement. Although the film is water proof, it is not breathable.

By changing the effective parameters on electrospinning, one can have control over the size of pores which directly determines the transport of water, water vapor and air through the membrane. A polymeric film with the same polymer, thickness and areal density does not have any pores and therefore it cannot be used as a breathable fabric.

5.3 Waterproofness

Contact Angle

Optical Contact Angle (OCA) 15 EC measuring and contour analysis system is used to measure the wettability of the resulting electrospun web, where the angle formed between the liquid–solid interface and the liquid–vapor interface is the contact angle to be captured and analyzed employing high resolution camera and software of dataphysics instrument.

Since resistivity to water is an important characteristic, the final web should have a certain interaction with water. According to De Shoenmaker this interaction is governed by the following considerations: the repulsive/attractive forces at the interface of the contact between water and the surface, and the porosity (De Shoenmaker et al., 2011). The first consideration introduces to the idea of the surface tension; the attraction force at the surface that tends to keep the particles of the liquid together; the interfacial

tension (force of interaction at the interface) tend either to repel water from the electrospun substrate (in this case the electrospun is hydrophobic), or to attract it to it (hydrophilic). Contact angle is a good representation of the interfacial interaction formed at the contact of the liquid with the solid surface and ambient gas (Kwok et al., 1997), as Figure 33 shows. Contact angle measurement is used to describe and study the interfacial interaction between the liquid (water in this research) and solid surfaces (the electrospun web) (Moghadam & Hasanzadeh, 2013); it is an indication of the adhesion between the surface and the water molecules. High contact angle shows the repellence of water by the surface, and low contact angles show wettability; surfaces with contact angle with water greater than 90° are considered hydrophobic, while below 90° are considered hydrophilic (Amini et al., 2015). Superhydrophobic surfaces have contact angles higher than 150° (Park et al., 2010).

The contact angle measurement experiments were done according to the aforementioned procedure for the 10 electrospun webs obtained. For comparison, the measurements were made for commercial water proof breathable fabric: Waterproof Breathable textile, DuPont™ Tyvek, model PT31L0, and for the appropriate polymeric film as shown in Figure 34.

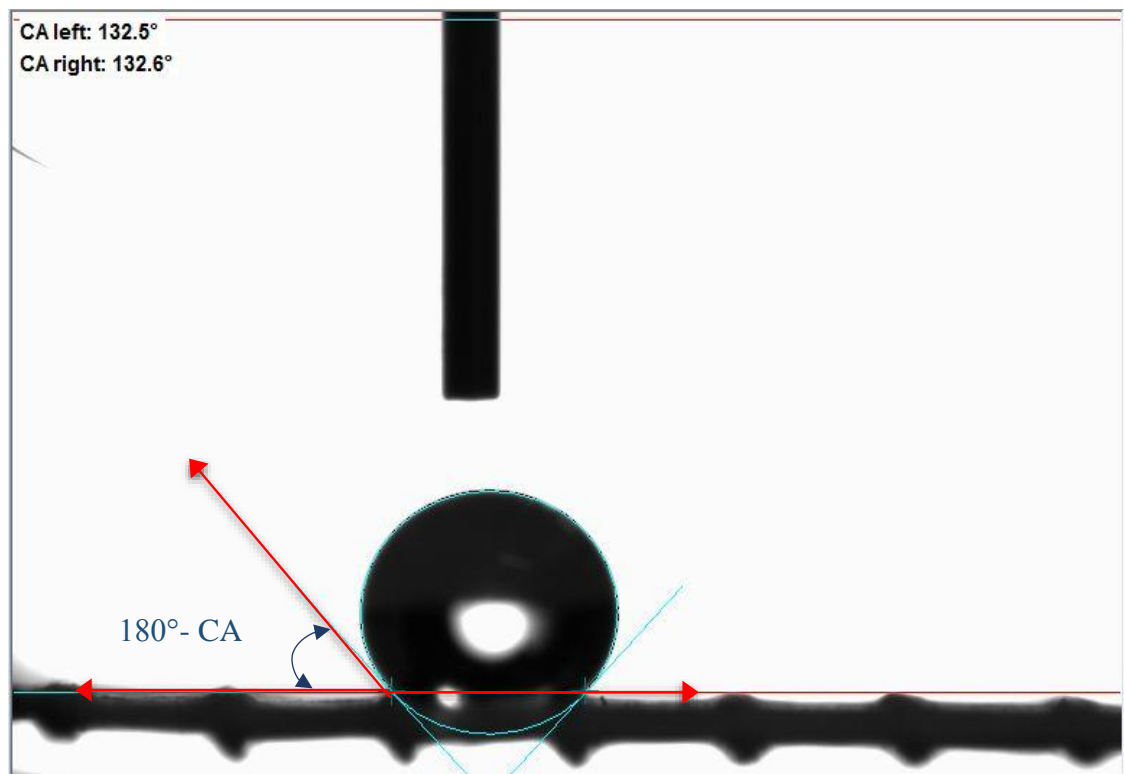


Figure 33 OCA 15 pro image: example for contact angle demonstration obtain for 28hr PU electrospun web

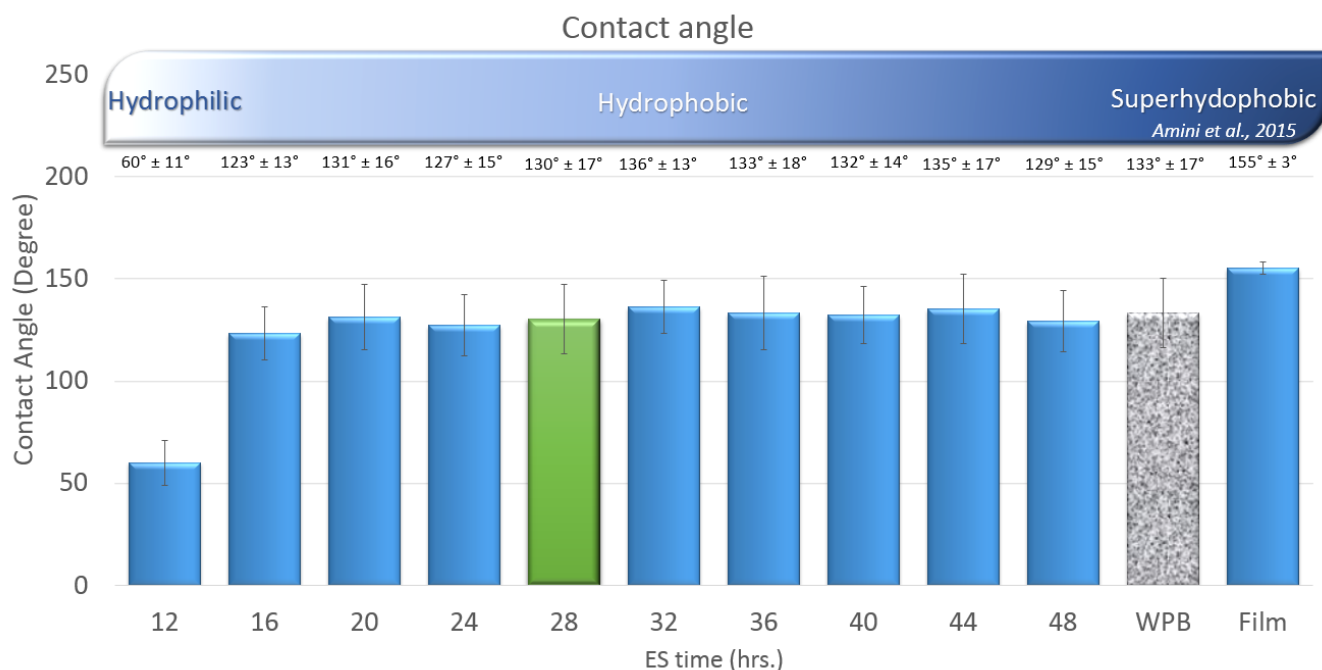


Figure 34 Contact angle results obtained for different substrates

The results show that all of the electrospun webs (except the one after 12h of electrospinning) can be considered hydrophobic, as the values are between 120° and 140°. For this sample, the pore size and porosity effects overwhelmed the effect of interfacial repulsion allowing quick absorption of water into the layer. The contact angle of water on the webs at different electrospinning duration (between 16 and 48h) was almost the same. A good idea for increasing contact angle further is to coat the fibers with further more hydrophobic polymer in order to lower the surface free energy and increase water repulsion. The PU film was more hydrophobic than the electrospun, and that is due to the lack of pores (which is evident in the pore size testing). Figure 34 shows the extensive repulsion of water by the polymeric film. Comparison of standard deviations between all electrospun webs and PU film shows that the hysteresis in contact angle is referred to the pore size and pore distribution. Although the polymeric film is superhydrophobic, it is not breathable. Thus the importance of electrospinning to make use of a superhydrophobic polymer (like PU), and introduce pores to achieve breathability on the expense of hydrophobicity. A balance between these two values is important.

Results show that electrospun webs resemble in their interaction with water the behavior of the commercial water proof breathable layer (that is known for its waterproofness), and can be a good substitution in case breathability requirements are attained.

HydroHead pressure test

The graph in Figure 35 shows that as the electrospinning time increases, the water pressure resistance (Hydrohead) of the electrospun nanofiber web increases. That is, as more fibers are electrospun, more water pressure can be held up by the web without leakage. The 12-hour sample had the lowest value, indicating low water resistance. The highest value was recorded by the 48 hrs sample, which can nearly withstand 300 cmH₂O. The commercial waterproof and breathable textile, DuPont™ Tyvek, model PT31L0 had a relatively low hydro-head value among the other samples with slightly higher than 100 cmH₂O.

According to the British Ministry of Defense, textiles withstanding 80 cm of water are considered to be water proof; hence, 20 hours of electrospinning, as shown in figure 35, are enough to get close to that threshold. However, waterproof textiles can be categorized as: below 80 cmH₂O is regarded as a low level of water-proof, between 100 and 250 cmH₂O is medium water-proof, and anything above 500 cmH₂O is highly water-proof (Kang et al., 2007).

Hydrohead pressure as high as 75 cm H₂O had been previously reported for electrospun PU/DMF-THF (Gorji et al., 2011). Which is considered to be in the low range of water resistance below the standard level , similar to the 20-hour electrospun sample. Comparable results in which the hydrohead of electrospun PU/DMF was 74 cmH₂O (Yoon and Lee, 2010).

In another study, a hydrohead of 37 cmH₂O of PU/DMAC has been reported with a low areal density (Kang et al., 2007).

Ahn et al. reported a high hydro-head value of 305 cmH₂O for electrospun PU with areal density of 4.3 mg/cm² (Ahn et al., 2010). This value is between the range of medium to high water resistant fabrics and comparable to the 48-hour electrospun sample presented above.

Controlling the electrospinning duration, hence the areal density of the produced fiber sample, has an influence on the capability of the produced web to

withstand water pressure. This, along with adjusting the pore size of the electrospun web, makes it possible to achieve higher water resistance of the produced textile.

However, as mentioned earlier, there should be a trade-off between the air permeability and the water resistance of the electrospun nanofiber sample. As the electrospinning duration increases, the water resistance increases while the air permeability decreases (figure 35).

Deciding on a very high water resistance level would negatively affect the air permeability aspect of the textile making it uncomfortable although highly water proof. Therefore, an agreement must be narrowed down to the intermediate region of the above graphical representation. Taking the commercially present DuPont™ Tyvek waterproof and breathable textile, model PT31L0 as a benchmark, it lies between ES-28h and ES-32h when it comes to air permeability; and between the ES-20h and the ES-24h sample when it comes to water resistance. Considering ES-32h sample, which is above commercial present fabric, it can be observed that it has a high level of water pressure resistance but a poor air permeability performance. ES-24h seems to be better since it has a relatively high level of air permeability, but when it comes to water resistance it scores comparably to DuPont™ Tyvek fabric. ES-28h, however, proved to be the best compromise since it has a very good water resistance (155 cmH₂O) level well above the needed limit, along with an acceptable level of air permeability (9 mm/s) higher than that of the benchmark.

5.4 Breathability

Air Permeability

It can be seen from the graph in Figure 35 that as the electrospinning time increases, the air permeability of the produced sample decreases. The ES-12h showed the highest air permeability value of 29 mm/s, while the ES-48h showed the lowest value of 4 mm/s. The commercially available DuPont™ Tyvek water proof and breathable fabric was used as a benchmark. The ES-28h proved to be more air permeable.

As the time of electrospinning increases, more and more nanofibers are accumulating hence increasing the tortuosity of the membrane; this creates more resistance against the passage of air across.

Results were in agreement with other reports; Kang et al. showed that a 12 wt.% PU/DMAC solution electrospun on a polyester/nylon substrate, gave an air permeability of 6 mm/s (Kang et al., 2007). Electrospinning of PU/DMF on polypropylene support resulted in a relatively high air permeability of 1160 mm/s, with an area as low as 0.2 mg/cm² (Lee and Obendorf., 2007). This is significantly higher than the results obtained even when compared to the 12-hour sample (least electrospinning time) which gave an air permeability value of 29mm/s having higher areal density of 0.91 mg/cm². Indeed, all the other sample electrospun for longer durations will have smaller air permeability values with higher areal densities. For a 1 mg/cm² areal density, the resulting web have an air permeability of 3.2 mm/s (Yoon and Lee., 2010).

Accordingly, electrospinning of PU on nylon support resulted in a web with 4.3 mg/cm² areal density results of an air permeability in the range of 9.1 mm/s.

Several factors affect the air permeability of the PU electrospun web including the type and structure of substrate used and the time of electrospinning which translates into areal density. If the substrate is more densely woven with lower void fraction, the air permeability of the overall resulting textile should decrease. But most importantly, as the electrospinning time increases, the areal density of the resulting nanofiber web increases. As per above results, the air permeability proved to be inversely proportional to the electrospinning time and hence to the areal density. Decreasing the areal density from 0.2 to 0.1 mg/cm² increases the air permeability from 1160 mm/s to 1587 mm/s (Lee and Obendorf., 2007). For example, increasing the web density from 1.89 mg/cm² to 2.19 mg/cm² decreases the air permeability from 13 mm/s to 9 mm/s, respectively.

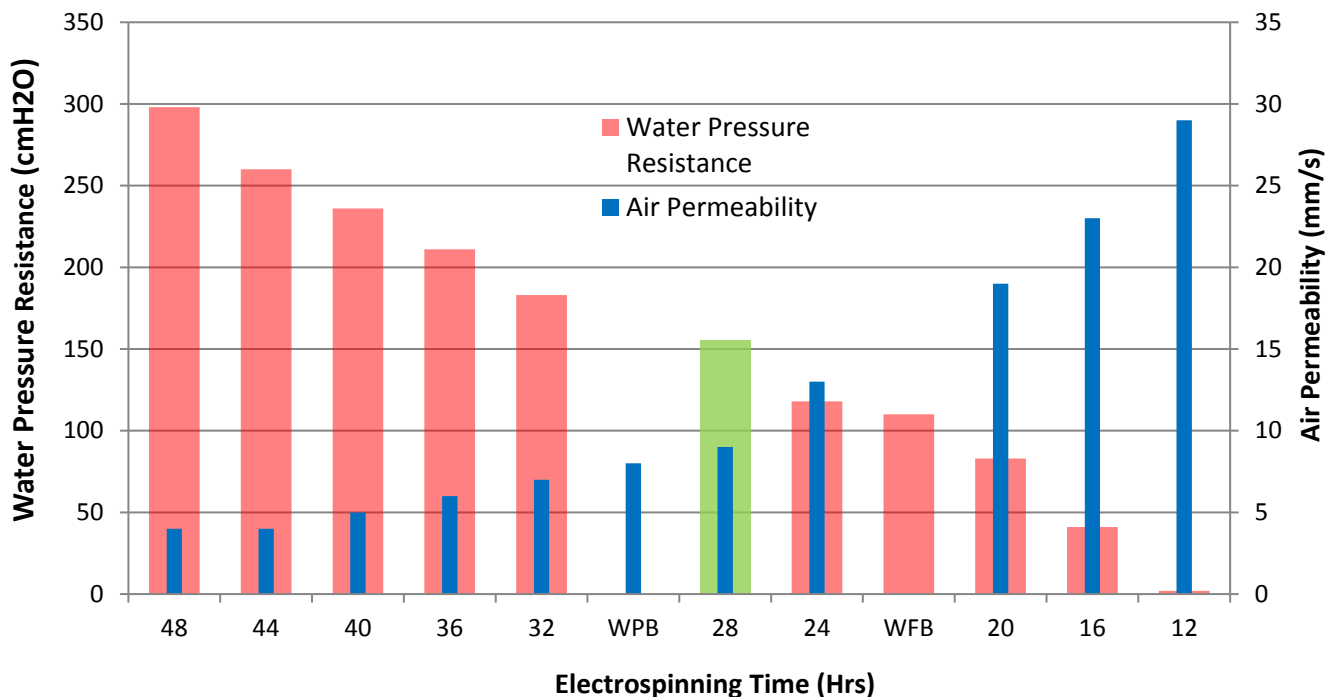


Figure 35 Water Resistance and Air permeability VS. Electrospinning Time

WPB: Waterproof Breathable textile, DuPont™ Tyvek, model PT31L0

Water Vapor Transmission Rate

As can be seen from results in table 6 (Detailed in Appendix I), disregarding the polymeric film momentarily, the highest water vapor transfer rate was achieved by ES-12h and the lowest by the ES-48h for both temperature conditions. It can also be observed that, the highest weight difference was recorded by the 12-hour sample as compared to the lowest weight difference recorded by the 48-hour web sample.

Table 7 Water Vapor Transmission Rate of the ES samples at two different temperatures

| Samples | Water Vapor Transmission Rate (g/m².hr) | |
|--------------------------|---|-----------------|
| | At 25 °C | At 35 °C |
| PU ES-12h | 61.99 | 68.52 |
| PU ES-16 hrs. | 56.5 | 62.07 |
| PU ES-20 hrs. | 52.65 | 58.14 |
| PU ES-24 hrs. | 45.5 | 50.27 |
| PU ES-28 hrs. | 42.56 | 46.77 |
| PU ES-32 hrs. | 39.56 | 43.64 |
| PU ES-36 hrs. | 35.14 | 38.65 |
| PU ES-40 hrs. | 30.98 | 34.13 |
| PU ES-44 hrs. | 26.36 | 28.82 |
| PU ES-48 hrs. | 21.36 | 23.43 |
| PU Polymeric Film | 0.03 | 0.028 |

As it can be seen from Table 8, by increasing the thickness of the ES samples by prolonging the duration of ES, the tortuosity of the web increases, therefore less water vapor can pass through the web.

The progress of the weight difference of the samples was monitored by recording them at three different times; 8, 16, and 24 hours. As the time increases, the weight difference increases indicating more transfer of water vapor across the web samples. Note that the weight difference for the polymeric film sample remains constant and negligible. The graphs in Appendix I show how the weight differs as a function of time.

Table 8 (detailed in Appendix I) shows the same trend of increasing weight difference as the experiment time increases. However, there is a shift upwards higher temperature indicating that temperature has an effect on the rate of water vapor transfer; as the temperature increased from 25 °C to 35 °C, the weight difference of all the electrospun samples increased. Take for instance the 24-hour sample, the weight

difference at 25 °C was 0.59, 1.178, and 1.78 g after 8, 16, and 24 hours, respectively, while the weight difference at 35 °C was 0.65, 1.3, and 1.97 g after 8, 16, and 24 hours, respectively. The WVTR also increases from 45.5 g/m².hr to 50.27 g/m².hr as the temperature increase from 25 °C to 35 °C for the 24-hour sample. Which is consistent with a study by Huang and Chen on the effect of air temperature on the WVTR of air permeable fabrics. Where four different fabrics were tested for WVTR at increasing temperatures, and all gave the same result; the WVTR increased as the temperature increased. The mean free path and the mean velocity of the gaseous particles (water vapor) can have an effect on the gas diffusion coefficient (Huang & Chen, 2010). Moreover, the mean velocity is a function of temperature, hence increasing the temperature would actually increase the mean velocity the higher diffusion rate observed (Huang & Chen, 2010).

PU ES-28h proved to have good air permeability along with acceptable water resistance. Thus, the main concern in this analysis of WVTR was ES-28h which recorded 42.56 g/m².hr at 25 °C, and this then increased to reach 46.77 g/m².hr at 35 °C.

In another study, also concerning the breathability of PU layered fabric; Yoon & Lee used a 13 wt.% PU/DMF solution electro-spun on pure polyester support. Two different samples were tested for WVTR, the first having a web density of 5.6 g/m² and the other having a web density of 10.2 g/m². The test method used was that of ISO 2528:1995 with anhydrous calcium chloride as the desiccant at 38 °C and 90% RH. The reported WVTRs were 120.7 and 179.1 g/m²/h for the samples with 10.2 and 5.6 g/m² areal density, respectively (Yoon & Lee, 2010). Thus, as the areal density of the produced web increase, the WVTR decreases where more nanofibers are packed up in the same area. The increased areal density is also attributed to the increased electrospinning duration.

Furthermore, Lee & Obendorf examined the WVTR of PU in another study. Here, they used a 13 wt.% PU/DMF solution for electrospinning. Note that the nanofibers were electro-spun on pure polypropylene substrate and the WVTR method used was based on the ASTM E96. Also PU web samples of different densities were used, the first having a density of 1 g/m² and the other 2 g/m². The results show that the former had a WVTR of 19.9 g/m².hr while the latter had a WVTR of 19.35 g/m².hr (Lee

& Obendorf, 2007). These values are low compared to the above obtained results for ES-28h which was 46.77 g/m².hr.

McCullough et al. reported the WVTR of several water proof breathable fabrics using the ASTM E96 standards. Among were the PU integrated fabrics, and the WVTR results of these was 35.95 g/m².hr (McCullough et al., 2003) which quite the closest to but still less than the 28-hour sample with 42.56 g/m².hr. Note that the electrospinning duration was unknown but McCullough used similar conditions and test method; 23 °C, 50 % RH, and the Upright-cup method (McCullough et al., 2003).

Han et al. reported other WVTR results for electrospun 12 wt. % PU/DMF using ASTM E96 desiccant method. The values were 49.13 g/m².hr for WVTR at 20 °C (Han et al., 2013), although the electrspinning duration is also unknown, which is just above than the obtained WVTR result for ES-28h with 42.56 g/m².hr.

Based on the above analysis, it is noticeable that the process of electrospinning gives the produced textile unique properties. The electrospun PU/DMF webs are permeable to air and water vapor but are at the same time efficiently water resistant. A comparison between the PU film and ES-28h further supports this notion. The polymeric film is simply 14 ml of PU/DMF solution in which ES-28h is its corresponding electrospun web. The polymeric film recorded negligible WVTR and negligible weight difference throughout the whole time course, whereas, ES-28h resulted in a WVTR of 42.56 and 46.77 g/m².hr at 25 and 35 °C, respectively. This huge difference is highly expected and shows that the film is one solid piece of dried solution with no pores. The electro-spun webs, however, are porous structures and would allow the channeling of water vapor.

5.5 Protection

Aerosol Filtration

The diameter of aerosol particles generated for the test was in the range of 0.3 to 2 μm , as it has been show in Figures 36.

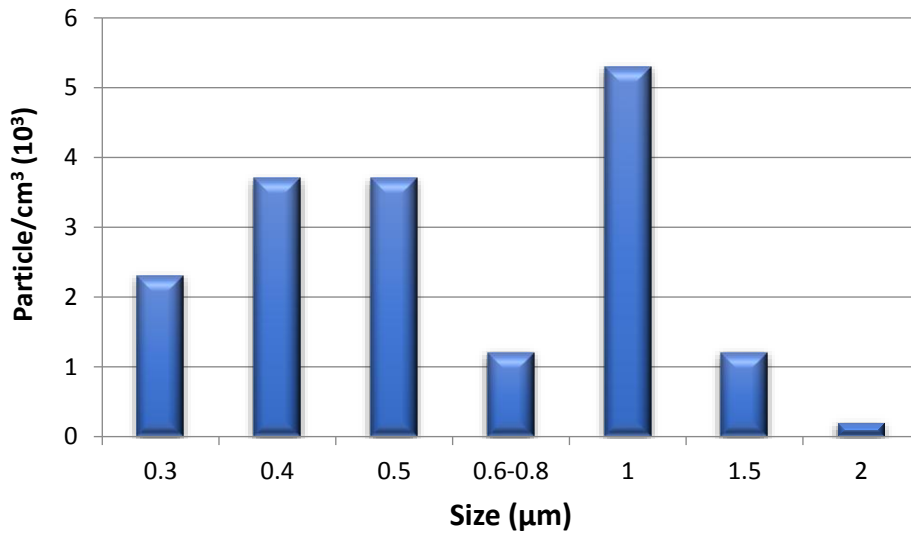


Figure 36- Initial Aerosol Particle size distribution

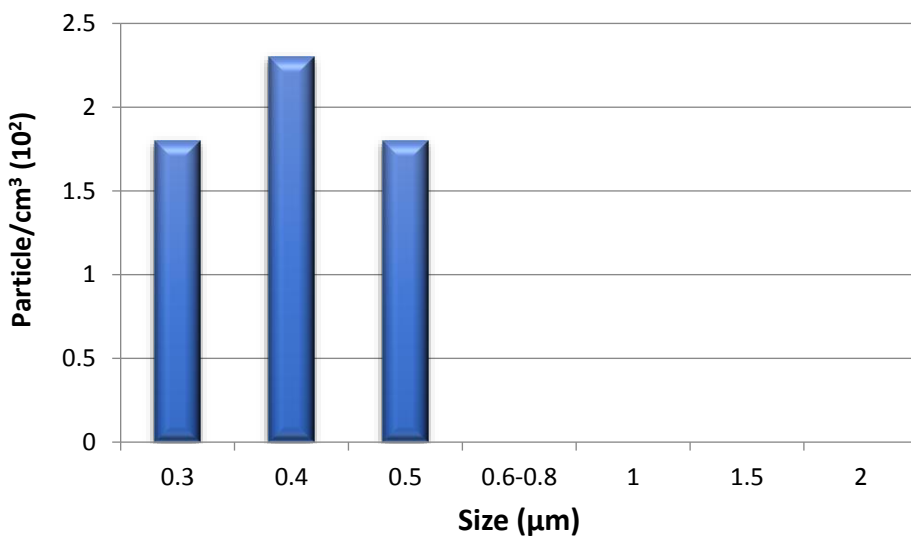


Figure 37- Aerosol Particle size distribution after filtration by ES-28h

Figures 36 and 37 show the particle size distribution and their concentrations before and after filtration by ES-28h , respectively. It is important to point out such a particle size distribution which can be attributed to the inconsistency of the aerosol

generator itself, along with the fact that the particles are naturally present in the atmosphere which affects the particle analyzer readings hence alters the distribution. However, this should not impose any problem on the analysis since most of the particles are actually retained as will be explained later. It is clear from Figure 37 that the particles larger than 0.5 μm are filtered off completely, while the concentration of smaller particles (between 0.3 and 0.5 μm) dropped by 94%. This indicates that ES-28h can easily retain particles larger than 0.5 μm with 100% efficiency. For such smaller particle sizes, other unavailable specific conditions must be present; sensitive detectors should be used to monitor the particles size distribution and concentration, and the test should be conducted in a specifically controlled environment. Because some of the penetrating particles (0.5 μm and below) may already well be present in the atmosphere after the web filter altering the results.

Nevertheless, the overall filtration performance of the web is good with total particle retention efficiency of 99.5 % fulfilling its desired purpose adequately.

Table 8- Filtration Efficiencies of ES-28h

| Particle Concentration (particles/cm³) | | | |
|--|--------------------------|-------------------------|-------------------|
| Size | Before filtration | After Filtration | Efficiency |
| 0.3 μm | 2.3×10^3 | 1.8×10^2 | 92.2% |
| 0.4 μm | 3.7×10^3 | 2.3×10^2 | 93.8% |
| 0.5 μm | 3.7×10^3 | 1.8×10^2 | 95.1% |
| 0.6-0.8 μm | 1.2×10^3 | 0 | 100% |
| 1 μm | 5.3×10^3 | 0 | 100% |
| 1.5 μm | 1.2×10^3 | 0 | 100% |
| 2 μm | 0.2×10^3 | 0 | 100% |
| Total < 2 μm | 1913 | 53.79 | 97.2% |

It is noteworthy to mention that these results are obtained for ES-28h that presents adequate performance regarding waterproofness, breathability, and aerosol filtration; hence any extension in the electrospinning duration would at least give the same retention results if not better. However, arbitrarily increasing the electrospinning duration is undesirable since other factors of air permeability, water vapor transmission

rate, and water resistance are other important factors that should be taken into consideration.

It was further reported by Hung et al that increasing the areal density of the nanofiber web to a value of 0.33 g/m^2 , actually increases the web efficiency in filtration (Sundarrajan et al., 2013). ES-12h gave an areal density of 0.91 mg/cm^2 which is significantly higher than 0.33 g/m^2 . This proves ES-28h, which has even higher areal density, has a high efficiency in filtration of aerosols.

For electrospinning the webs, including ES-28h, a nylon mesh support with areal density of 3.53 mg/cm^2 was used. This gives the layered structure required for an increase in the quality factor, and hence the filtration efficiency.

Wang et al. investigated the filtration properties of polyacrylonitrile (PAN) in which some samples were PAN/DMF solutions and others PAN/SiO₂ in DMF. The used aerosols particles were NaCl with size ranges of 300 to 500 nm and the two sample types were tested (Wang et al., 2014). First, it was observed that as the fiber diameter increases; hence the sizes of the present pores, more and more NaCl particles pass through which leads to a decrease in filtration efficiency (roughly, from 74 to 11 %) (Wang et al., 2014). As for the PAN/SiO₂ that had a filtration efficiency of around 69% (Wang et al., 2014). Wang et al. also reported electrospun nanofiber webs from PVC/PU and its performance in filtering aerosols of sizes 300-500 nm, recorded a good efficiency of 99.5% and an acceptable pressure drop of 144 Pa (Sundarrajan et al., 2013). This is close to the results obtained for ES-28h with a 94% efficiency to filter 300-500 nm particles. Increasing the electrospinning time may as well increase the filtration efficiency close to that reported, but as previously mentioned other factors should be considered when doing so.

Barhate et al. also reported that Nylon6 nanofibers proved to have a filtration efficiency good enough to exceed that of HEPA filters. It is important to mention that High Efficiency Particulate Arrestance (HEPA) is an air filter made up of fiberglass with diameters ranging between 0.5 and 2 μm and retains 99.97% of the 0.3 μm particulates. The fiber diameter distribution of the Nylon6 nano-fibers, however, was in the range of 80 to 200 nm with areal density of 10.75 g/m^2 and the filtration tests were conducted with a face velocity 3-10 cm/s of 300 nm aerosols (Barhate et al., 2007).

Gibson et al. compared the penetration percentage of aerosol particles across different filtration membranes. The first category was the commercially used fabrics in which army protective fabric, cotton, and nylon microfibers allowed 5-10% penetration of aerosols; normal nylon fibers and other liners exceeded 50%. The other category was the electrospun membranes in which Nylon6 based on carbon foam allowed less and less penetration of aerosols as the spinning time increased to reach only 0.05% penetration after sufficient time. On the other hand, PBI and PU electrospun membranes did not allow any penetration (0%) of aerosols which was found to be comparable to the commercial filters in use (PTFE and PVDF) (Gibson et al., 2001). However, the electrospinning duration was not specified hence it might be for a long period of time (more than 32 hours) which as mentioned earlier can affect air permeability and WVTR negatively. Nevertheless, taking this into consideration, the filtration efficiency results obtained for ES-28h of 94% are perfectly acceptable in comparison with Gibson et al. report.

Filtration performance of PU/DMF was also studied by Choi et al. in which a 10wt% solution was used to produce the nanofibers (1.3 mg/cm² areal density).

Compared to general filters where the minimum efficiency of filtration is for sizes of 100-300 nm, the PU filters performed better having a minimum efficiency of filtration for particle sizes of 80 to 100 nm. The factors involved here are similar to the ones in the conducted experiment for ES-28h (10wt % PU/DMF solution, 2 mg/cm² areal density, and 5cm/s velocity of the aerosols). However, the particle sizes were in the range of 20-300 nm (well below the range of 300-1000 nm used in the conducted experiment) and no filtration efficiency was mentioned for this range.

Gibson and Gibson studied electro-spun PU/THF/DMF (10:80:10) for filtration; the substrate used was mainly aluminum surface.. The results showed that a filtration efficiency of 99.5% was achieved, which is in perfect agreement with the results obtained although a different support was used, and this percentage increases as the duration of electrospinning increases. This good performance, as compared to other filters or methods, was attributed to high surface area of the web (Gibson & Gibson, 2002).

Effective Parameters on Aerosol Filtration

As the duration of electrospinning increases, the air permeability of the web decreases. This can be explained by the high dependability of air permeability on the web thickness and void fraction. The web develops more resistance to air flow across the fibers since the time spent under electro-spinning not only increases the web thickness but also decreases its porosity. Faccini et al., (2012) reported similar results concerning the matter.

Electrospun nano-fibers proved to have good aerosol filtration properties as the results show that more electrospinning duration leads to a thicker web and less porosity, thus increasing filtration efficiency. Based on the Brownian diffusion, the aerosols were observed to abide by the traditional model which states that when particle size is decreased the filtration must be increased; particles of 300 nm size were the least retained particles by the tested filter.

Yun et al. confirmed that the traits of nano-fibers such as small pore size, decent pore channeling, and good surface area to mass ratio, makes them a significant candidate in aerosol filtration. NaCl nano-particles with size range of 20 to 300 nm were generated and tested on the nano-fiber filters with flow rates of 0.3 to 2 L/min (Yun et al., 2010). The results showed that as the fiber web thickness increases, the particle penetration decreases. Increased thickness can be achieved by increasing the time of the electro-spinning process, however, increased thickness means increased pressure drop across the membrane (Yun et al., 2010). A linear relationship was established between the web thickness and the resulting pressure drop (Podgorski et al., 2006).

Zhang et al. electrospun Nylon6/Formic Acid solutions with concentrations of 15 wt% at a voltage of 15,000 V and 20 cm TCD. To test the filtration efficiency of the produced web, collision atomizer was used to generate NaCl as aerosols. The produced aerosols had a size range of 50 to 400 nm and solely uncharged aerosols were allowed to enter the filtration test setup. With the aid of a particle size scanner, the results showed that the produced nanofibrous meshes were more effective to remove the smaller sized aerosols (50 nm) rather than the bigger ones. Moreover, they explained that the factor truly affecting the filtration efficiency is the fiber size

distribution rather than its average in a sense that when more fibers of at least 100 nm diameters were present, the filtration efficiency increased (Zhang et al., 2009).

Sambaer et al. reported several conditions affecting the filtration efficiency of PU nano-fibers. The solution used was PU/DMF with 13.5 wt% electro-spun on polyester substrate. The filtration experiment was performed using di-ethyl hexyl sebacate (DEHS) aerosol particles with velocities of 5.7 cm/s. In general, the most penetrating particle size was in the order of 100 nm and as the particle size increased so did the filtration efficiency (Sambaer et al., 2010). First, they varied the air velocity was to study its effect on filtration; it turned out that as the air velocity increases the filtration efficiency decreases as more and more particle go through (from 90% at 2 cm/s to 40% at 8.5 cm/s for the most penetrating particle size). Moreover, the air temperature was another condition studied whereas the temperature increase, the filtration efficiency increases (from 30% at 100K to 90% at 1000K for the most penetrating particle size). Note that at 300K (room temperature) the results show that the most penetrating particle size is in the 100 nm range and the efficiency increases as the size increases. Finally, the air pressure was varied and the results revealed that as the pressure increases, the filtration efficiency decreases (from about 75% at 0.05MPa to 40% at 0.3MPa for the most penetrating particle size) (Sambaer et al., 2010).

It is noteworthy to mention that as the diameter of particles increases, the penetration increases to a certain level called the “most penetrating particle size” or the “MPPS” after which increasing the particle diameter results in decreased penetration again (Yun et al., 2010). This is attributed to the fact that there are different effects according to the particle size. When particles are bigger, filtration occurs under the effect of “interception” (figure 38), on the other hand, when particles are smaller, filtration occurs under the effect of “diffusion” (figure 39). However, in the MPPS region, both effects occur but none is actually significant (Lee and Liu, 2012). Yun et al. reported in an earlier study that according to the theory of filtration, decreasing the fiber diameters can result in increased filtration efficiency; this is exactly what electro-spun nano-fibers can provide which further advocates the use of nano-fiber webs for filtration (Yun et al., 2007).

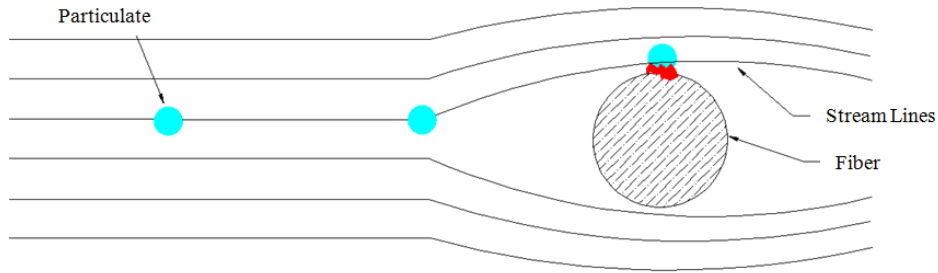


Figure 38 Interception Mechanism Scheme

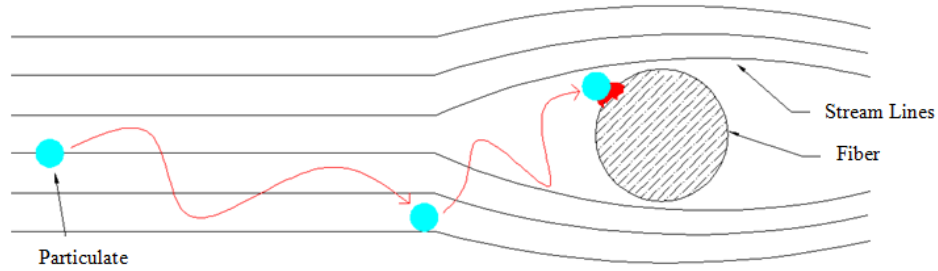


Figure 39 Diffusion Mechanism Scheme

When increasing the fiber diameter to reach the critical fiber diameter, the void fraction of the web increases for the sake of conserving the same porosity which increases air permeability, hence affects the filtration efficiency negatively. At any point past the critical fiber diameter, porosity is counterbalanced by increased thickness which will eventually decrease air permeability but increase filtration efficiency.

CHAPTER 6

CONCLUSION

It appears from the overall results (Figure. 40) of air permeability and water resistance that ES-28h web is more permeable than our benchmark taken as the commercial water proof breathable fabric, DuPont™ Tyvek, model PT31L0, yet more water repellent. In fact, compared to the results obtained by the other electrospun, the data obtained at 28hrs web form a median of the overall data, which proof that the range chosen for the study is convenient with the aims of the experiments.

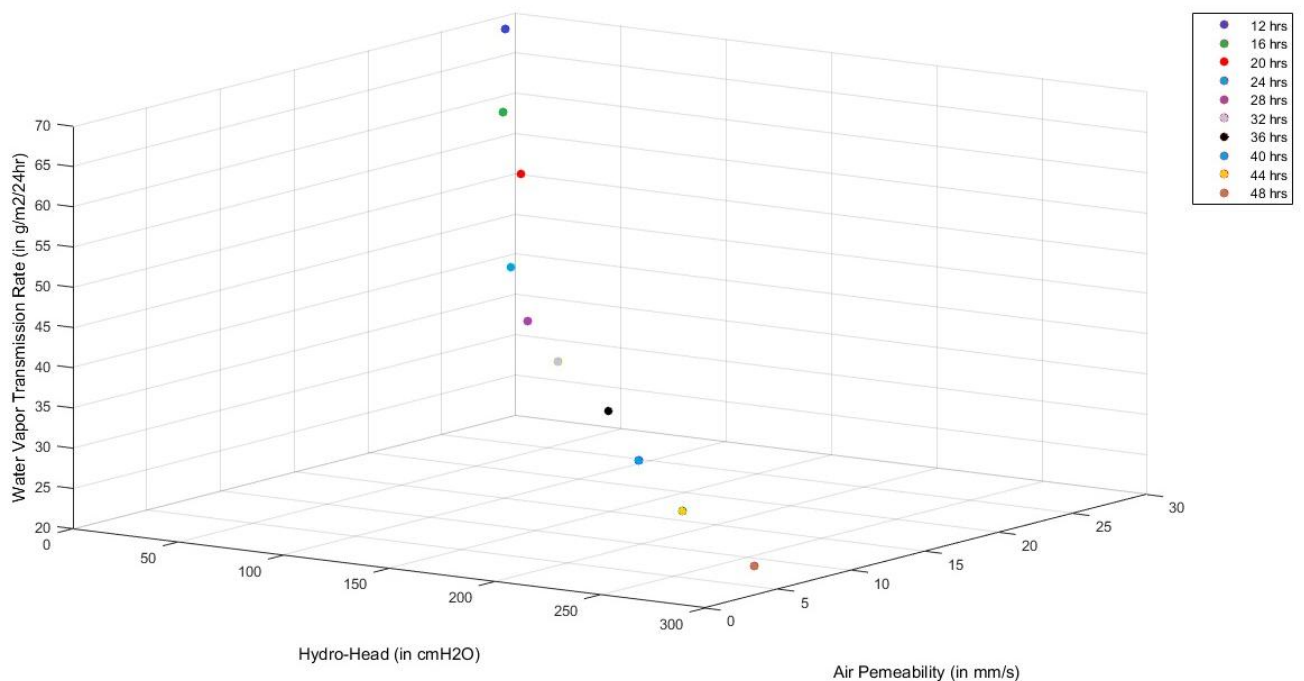


Figure 40 overall results of Air Permeability, Water pressure resistance and MWTR along Electrospinning duration

A great work has been done for fabricating water proof breathable fabrics, and many publications involved the usage of PU dissolved in DMF as well. While the scientific grades of PU is expensive and can hit a price of 100\$ for few grams, the industrial grades used in this research were costing few dollars for 500g of PU that can produce up to 24 m² of electrospun coated fabric with a production rate of 22.4 cm²/hr

using our lab-scale FLUIDNATEK LE-10 electrospinner. Moreover, the significance of the work is that it can be considered a first step toward producing such nanofiber on industrial scale with green technology where a recovery system is adapted on AT711 β electrospinner (Section G) with a production rate of 3000 cm²/hr.

Waterproof protective clothing that is used in oil, soil and water protection can be transformed to waterproof breathable protective clothing by using the electrospun nano-fibers that allows the water and dirt to roll off the surface, but leaving water vapor to pass from the skin to the outer surface of the fabrics. Thus, a new approach to heat stress relief in chemical protective clothing was forwarded by the nanotechnology that allows protection with normal cooling of the human body. The novelty of this research is that it optimizes the operating conditions of the electrospinning process experimentally to control the nano-sized mesh physical dimensions and properties to meet the required degree of protection and comfort for a worker in specific environmental conditions. Which set an example of technical advance to serve the need of sustainable development.

Future Prospective

6.1 AT711 β Industrial electrospinner

Shifting from medical, pure grade to industrial polymers as raw materials was the first step to transfer the electrospinning process from lab scale to an industrial one.

AT711 β is an industrial electrospinner equipped with 100 spinneret nozzles, 2 screw pumps, a positive DC high voltage power supply and a negative one, ± 30 KV each. A conductive rotating drum collector (35 cm diameter x 100 cm length) with a variable rotational speed from 100 rpm to 1500 rpm.

Electrospun nanofibers were collected in a chemical hood equipped with a solvent recovery system (Liquid-Gas scrubber and a distillation column).

APPENDIX

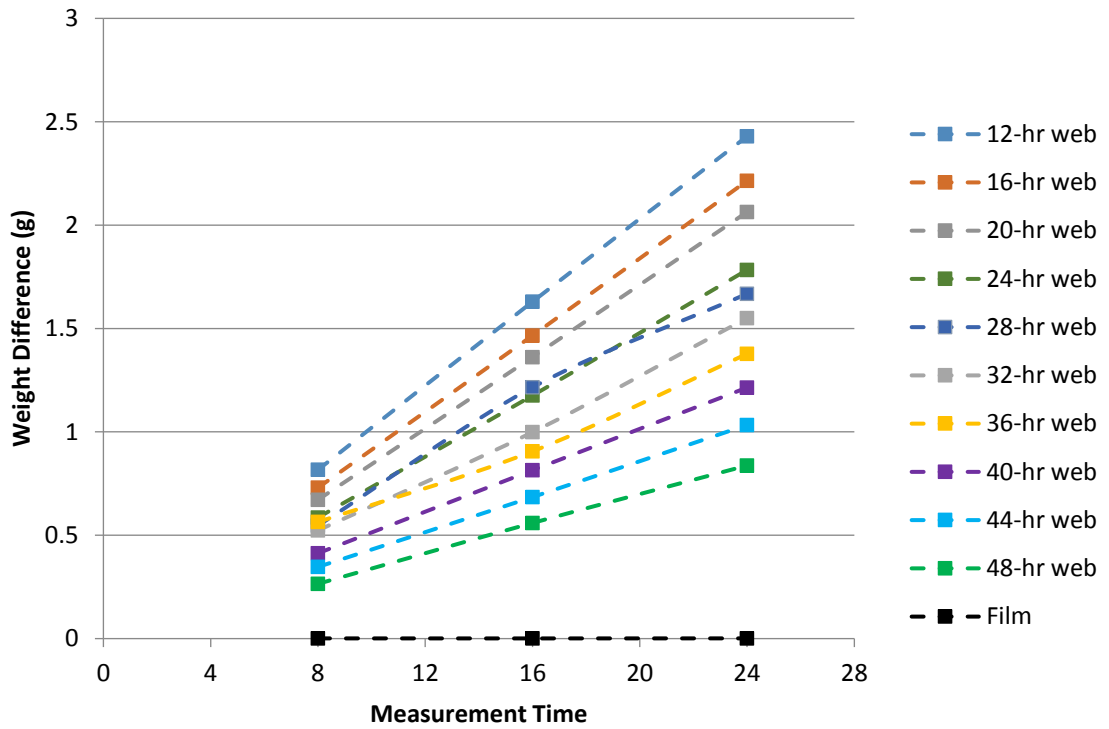
1. Experimental Data

- *Air Permeability of Different Substrates (ASTMD 737)*

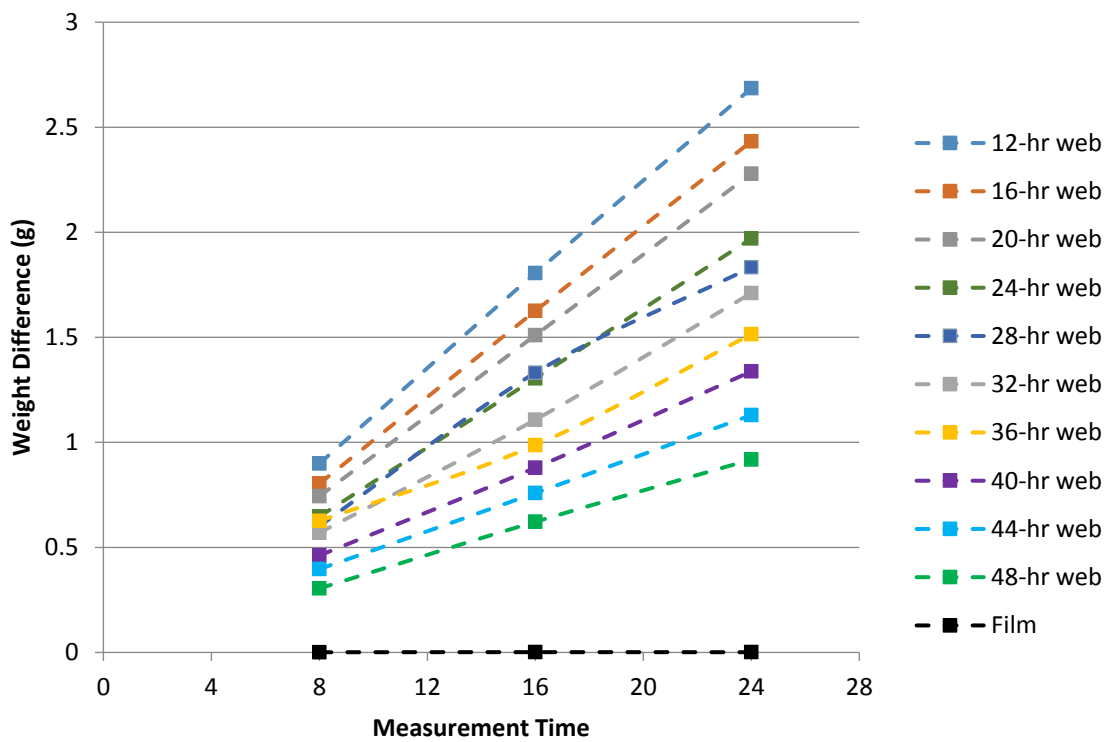
| Substrate | Air Permeability (cm/s) |
|----------------------------|--------------------------------|
| 100 % Nylon Mesh | 250 |
| 100 % Cotton | 223 |
| 50% / 50% Cotton/Polyester | 76 |
| 100% Polyester | 62 |

- *Water Vapor Transmission Rate Detailed Results*

| Sample | WD after 8 hrs. (g) | | WD after 16 hrs. (g) | | WD after 24 hrs. (g) | | WVTR (g/m ² .hr) | |
|------------|---------------------|----------|-------------------------|----------|-------------------------|----------|-----------------------------|----------|
| | At 25 °C | At 35 °C | At 25 °C | At 35 °C | At 25 °C | At 35 °C | At 25 °C | At 35 °C |
| PU 12 hrs. | 0.82 | 0.9 | 1.63 | 1.81 | 2.43 | 2.69 | 61.99 | 68.52 |
| PU 16 hrs. | 0.73 | 0.8 | 1.47 | 1.63 | 2.21 | 2.43 | 56.5 | 62.07 |
| PU 20 hrs. | 0.67 | 0.74 | 1.36 | 1.51 | 2.06 | 2.28 | 52.65 | 58.14 |
| PU 24 hrs. | 0.59 | 0.65 | 1.178 | 1.3 | 1.78 | 1.97 | 45.5 | 50.27 |
| PU 28 hrs. | 0.55 | 0.6 | 1.22 | 1.33 | 1.67 | 1.83 | 42.56 | 46.77 |
| PU 32 hrs. | 0.52 | 0.57 | 1 | 1.11 | 1.55 | 1.71 | 39.56 | 43.64 |
| PU 36 hrs. | 0.56 | 0.63 | 0.91 | 0.99 | 1.38 | 1.51 | 35.14 | 38.65 |
| PU 40 hrs. | 0.41 | 0.46 | 0.81 | 0.88 | 1.21 | 1.34 | 30.98 | 34.13 |
| PU 44 hrs. | 0.35 | 0.4 | 0.68 | 0.76 | 1.03 | 1.13 | 26.36 | 28.82 |
| PU 48 hrs. | 0.26 | 0.3 | 0.56 | 0.62 | 0.84 | 0.92 | 21.36 | 23.43 |
| PU Film | 0.001 | 0.001 | 0.001 | 0.001 | 0.001 | 0.001 | 0.03 | 0.028 |



Weight Difference as a Function of Time at 25 °C



Weight Difference as a Function of Time at 35 °C

- *Dynamic, Kinematic, and Inherent viscosities for the different Solution Concentrations*

| Concentration (wt%) | Dynamic Visc. (cP) | Relative Visc. | Inherent Visc. (ml/g) |
|---------------------|--------------------|----------------|-----------------------|
| 4 | 26 | 28.2609 | 83.54 |
| 5 | 47 | 51.087 | 78.67 |
| 6 | 60.93 | 66.2232 | 69.88 |
| 7 | 121.6 | 132.181 | 69.77 |
| 8 | 227.2 | 247.004 | 68.87 |
| 9 | 346.3 | 376.424 | 65.9 |
| 10 | 680.2 | 739.368 | 66.06 |
| 11 | 893.5 | 971.193 | 62.53 |
| 12 | 2119 | 2302.9 | 64.52 |
| 13 | 2763 | 3003.48 | 61.6 |
| 14 | 4341 | 4718.45 | 60.42 |

- **Viscosity Measurements of Different Polymer Solutions Obtained from Literature**

| Source | Polymer | Solvent | Concentration | Viscosity | Intrinsic Viscosity | Measuring Tool |
|-----------------------|---------|-----------------|---------------|----------------|---------------------|-------------------|
| Nasouri et al. 2012 | PAN | DMF | 4-20 wt% | 97.2-5238.6 cP | - | - |
| Zhang et al., 2004 | PVA | Distilled water | 6.38-8.69 | 75-232 cP | - | Rotary viscometer |
| Deitzel et al., 2000 | PEO | Distilled water | 4-10 wt% | 100-2000 cP | - | - |
| Cengiz & Jirsak, 2009 | PU | DMF | 15 wt% | 760 cP | - | - |

| | | | | | | |
|---------------------------------|-------------|-------------|--------|---|---|----------------------|
| Stenhouse et al., 1989 | LCPU | DMF | - | - | 0.32-0.57 dL/g (depending on MW) | Ubbelohde viscometer |
| Tuzar et al., 1971 | PU | DMF/Acetone | - | - | 0.455-0.580 dL/g (depending on DMF fraction) | Ubbelohde viscometer |
| Tuzar et al., 1971 | PU | DMF/Toluene | - | - | 0.5-0.632 dL/g (depending on DMF fraction) | Ubbelohde viscometer |
| Vasconcelos et al., 2001 | PU | DMF | 10 wt% | - | 54 ml/g | Fenske viscometer |
| Vasconcelos et al., 2001 | PU | DMF/Xylene | 10 wt% | - | 53 ml/g | Fenske viscometer |
| Vasconcelos et al., 2001 | PU | DMF/DMSO | 10 wt% | - | 52.7 ml/g | Fenske viscometer |

2. Calculations

- *Drum Speed*

$$v = \frac{q * \rho_{solution} * \%wt}{\rho_{PU} \times \pi r_f^2}$$

Where:

- *v* is the velocity of drawing in m/s
- *q* is the volumetric feed rate in m³/s
- %wt is the weight of the polymer per weight of solution
- where the density of the solution was obtained through the equation:

- $\rho_{Solution} = \rho_{Polymer}x_{Polymer} + \rho_{Solvent}x_{Solvent}$

- ρ is the density, Kg/m³
- *x* is the fraction of Polymer/Solvent
- *r_f* is the expected mean radius of the collected fibers

Assuming the linear drum speed should be equal to the speed of drawing, then the speed of rotation of the drum can be calculated from the following:

$$n = \frac{v}{2\pi r_d} = \frac{q * \rho_{solution} * \%wt}{\rho_{polymer} * 2\pi^2 r_f^2 r_d}$$
$$= \frac{0.5 \times 3600 \times 10^{-9} \times 973.2 \times 0.1}{1.2 \times 2 \times \pi^2 \times (193 \times 10^{-9})^2 \times 0.1} = 680 \text{ r.p.m}$$

Where *r_d* is the radius of the drum.

- **Viscosity and Molecular Weight Calculation**

There are several types of viscosities given as:

$$\text{Relative Viscosity} = \eta_{rel} = \frac{\eta}{\eta_0}$$

$$\text{Specific Viscosity} = \eta_{sp} = \eta_{rel} - 1$$

$$\text{Reduced Viscosity} = \eta_{red} = \frac{\eta_{sp}}{C}$$

$$\text{Inherent Viscosity} = \eta_{inh} = \frac{\ln(\eta_{rel})}{C}$$

Mark-Houwink equation given by,

$$[\eta] = KM^a$$

Where, η is the intrinsic viscosity, ml/g

M is the viscosity average molecular weight, g/mol

K and a are the Mark-Houwink parameters

The shear stress and the shear rate can be calculated as (Viscopedia, Measuring Principles),

$$\tau = \frac{T}{2 * \pi * R_b^2 * L}$$

Where, τ is the shear stress, Pa

T is the torque of the motor, N.m

R_b is the head radius, m

L is the head length, m

$$\gamma = \frac{2 * \omega * R_c^2}{(R_c^2 - R_b^2)}$$

Where, γ is the shear rate, s^{-1}

ω is the angular velocity, rad/s

R_b is the head radius, m

R_c is the container radius, m

The dynamic viscosity can be then determined by,

$$\tau = \eta\gamma$$

Where, τ is the shear stress, Pa

γ is the shear rate, s^{-1}

η is the dynamic viscosity, Pa.s

Furthermore, the kinematic viscosity can be determined using,

$$v = \frac{\eta}{\rho}$$

Where, v is the kinematic viscosity, m^2/s

η is the dynamic viscosity, Pa.s

ρ is the density, kg/m^3

The intrinsic viscosity is determined by extrapolating the plot of the Kraemer equation of inherent viscosity given by (PSLC) ,

$$\frac{\ln(\eta_{rel})}{C} = K''[\eta]^2 C + [\eta]$$

Where K'' is the Kraemer constant

REFERENCES

- Choi, H., Kim, S. B., Kim, S. H., & Lee, M. (2013). Preparation of electrospun polyurethane filter media and their collection mechanisms for ultrafine particles. *Journal of the Air & Waste Management Association*, 64(3)
- Demir, M. M., Yilgor, I., Yilgor, E., & Erman, B. (2002). Electrospinning of polyurethane fibers. *Polymer*, 43(11), 3303-3309.
- Fibersource, American Fiber Manufacturer Association. (2016). *Manufacturing: Synthetic and cellulosic fiber formation technology.*, 2016
- Gibson, P., Schreuder-Gibson, H., & Rivin, D. (2001). Transport properties of porous membranes based on electrospun nanofibers. *Colloids and Surfaces A: Physicochemical and Engineering Aspects*, 187–188, 469-481.
- Han, H. R., Chung, S. E., & Park, C. H. (2013). Shape memory and breathable waterproof properties of polyurethane nanowebs. *Textile Research Journal*, 83(1), 76-82.
- Kang, Y. K., Park, C. H., Kim, J., & Kang, T. J. (2007). Application of electrospun polyurethane web to breathable water-proof fabrics. *Fibers and Polymers*, 8(5), 564-570.
- Karakas, H., Sarac, A. S., Polat, T., Budak, E. G., Bayram, S., Dag, N., et al. (2013). Polyurethane nanofibers obtained by electrospinning process. *International Scholarly and Scientific Research & Innovation*, 7(3), 607-610.
- Kimmer, D., Zatloukal, M., Petras, D., Vincent, I., & Slobodian, P. (2009). Investigation of polyurethane electrospinning process efficiency. *AIP Conference Proceedings*, 1152(1), 305-311.
- Baumgarten, P. K. (1971). Electrostatic spinning of acrylic microfibers. *Journal of Colloid and Interface Science*, 36(1), 71-79.

- Cui, W., Li, X., Zhou, S., & Weng, J. (2007). Investigation on process parameters of electrospinning system through orthogonal experimental design. *Journal of Applied Polymer Science*, 103(5), 3105-3112.
- Deitzel, J. M., Kleinmeyer, J., Harris, D., & Tan, N. B. (2001). The effect of processing variables on the morphology of electrospun nanofibers and textiles. *Polymer*, 42(1), 261-272.
- Doshi, J., & Reneker, D. H. (1993). Electrospinning process and applications of electrospun fibers. *Industry Applications Society Annual Meeting, 1993., Conference Record of the 1993 IEEE*, pp. 1698-1703.
- Haghi, A., & Akbari, M. (2007). Trends in electrospinning of natural nanofibers. *Physica Status Solidi (a)*, 204(6), 1830-1834.
- Lee, J. S., Choi, K. H., Ghim, H. D., Kim, S. S., Chun, D. H., Kim, H. Y., et al. (2004). Role of molecular weight of atactic poly (vinyl alcohol)(PVA) in the structure and properties of PVA nanofabric prepared by electrospinning. *Journal of Applied Polymer Science*, 93(4), 1638-1646.
- Mit-uppatham, C., Nithitanakul, M., & Supaphol, P. (2004). Ultrafine electrospun polyamide-6 fibers: Effect of solution conditions on morphology and average fiber diameter. *Macromolecular Chemistry and Physics*, 205(17), 2327-2338.
- Pornsopone, V., Supaphol, P., Rangkupan, R., & Tantayanon, S. (2005). Electrospinning of methacrylate-based copolymers: Effects of solution concentration and applied electrical potential on morphological appearance of as-spun fibers. *Polymer Engineering & Science*, 45(8), 1073-1080.
- Zhao, S., Wu, X., Wang, L., & Huang, Y. (2004). Electrospinning of ethyl-cyanoethyl cellulose/tetrahydrofuran solutions. *Journal of Applied Polymer Science*, 91(1), 242-246.
- Zhuo, H., Hu, J., Chen, S., & Yeung, L. (2008). Preparation of polyurethane nanofibers by electrospinning. *Journal of Applied Polymer Science*, 109(1), 406-411.
doi:10.1002/app.28067

- Zhong X H, Kim K S, Fang D F, Ran S F, Hsiao B S, Chu B (2002) *Structure and process relationship of electrospun bioabsorbable nanofiber membranes*. *Polymer* 43 pp.4403
- Fong, H., Chun, I., & Reneker, D. H. (1999). Beaded nanofibers formed during electrospinning. *Polymer*, 40(16), 4585-4592.
- Jaeger, R., Bergshoeff, M. M., Battle, C. M. I., Schönherr, H., & Julius Vancso, G. (1998). Electrospinning of ultra-thin polymer fibers. *Macromolecular Symposia*, , 127. (1) pp. 141-150.
- Wang, L., Topham, P. D., Mykhaylyk, O. O., Yu, H., Ryan, A. J., Fairclough, J. P. A., et al. (2015). Self-Assembly-Driven electrospinning: The transition from fibers to intact beaded morphologies. *Macromolecular Rapid Communications*, 36(15), 1437-1443.
- Zhu, S., Yu, H., Chen, Y., & Zhu, M. (2012). Study on the morphologies and formational mechanism of poly(hydroxybutyrate-co-hydroxyvalerate) ultrafine fibers by dry-jet-wet-electrospinning. *Journal of Nanomaterials*, 2012, 1-8. doi:10.1155/2012/525419
- Zuo, W., Zhu, M., Yang, W., Yu, H., Chen, Y., & Zhang, Y. (2005). Experimental study on relationship between jet instability and formation of beaded fibers during electrospinning. *Polymer Engineering & Science*, 45(5), 704-709. doi:10.1002/pen.20304
- Baumgarten, P. K. (1971). Electrostatic spinning of acrylic microfibers. *Journal of Colloid and Interface Science*, 36(1), 71-79. doi:10.1016/0021-9797(71)90241-4
- Cui, W., Li, X., Zhou, S., & Weng, J. (2007). Investigation on process parameters of electrospinning system through orthogonal experimental design. *Journal of Applied Polymer Science*, 103(5), 3105-3112. doi:10.1002/app.25464
- Ding, W., Wei, S., Zhu, J., Chen, X., Rutman, D., & Guo, Z. (2010). Manipulated electrospun PVA nanofibers with inexpensive salts. *Macromolecular Materials and Engineering*, 295(10), 958-965. doi:10.1002/mame.201000188
- Heikkilä, P., & Harlin, A. (2008). Parameter study of electrospinning of polyamide-6. *European Polymer Journal*, 44(10), 3067-3079.

- Karakas, H., Saraç, A., Polat, T., Budak, E., Bayram, S., Dag, N., et al. (2013). Polyurethane nanofibers obtained by electrospinning process. *Proceedings of World Academy of Science, Engineering and Technology*, (75) pp. 607.
- Kidoaki, S., Kwon, I. K., & Matsuda, T. (2006). Structural features and mechanical properties of in situ-bonded meshes of segmented polyurethane electrospun from mixed solvents. *Journal of Biomedical Materials Research Part B: Applied Biomaterials*, 76B(1), 219-229. doi:10.1002/jbm.b.30336
- Mazoochi, T., Hamadani, M., Ahmadi, M., & Jabbari, V. (2012). Investigation on the morphological characteristics of nanofibrous membrane as electrospun in the different processing parameters. *International Journal of Industrial Chemistry*, 3(1), 1-8.
- Zeng, J., Chen, X., Xu, X., Liang, Q., Bian, X., Yang, L., et al. (2003). Ultrafine fibers electrospun from biodegradable polymers. *Journal of Applied Polymer Science*, 89(4), 1085-1092. doi:10.1002/app.12260
- El-hadi, A. M., & Al-Jabri, F. Y. (2016). Influence of electrospinning parameters on fiber diameter and mechanical properties of poly(3-hydroxybutyrate) (PHB) and polyanilines (PANI) blends. *Polymers*, 8(3), 97. doi:10.3390/polym8030097
- Tomaszewski, W., Kudra, M., Ciechańska, D., Szadkowski, M., & Gutowska, A. (2012). Electrospinning of aligned fibrous materials on an inner rapidly rotating cone surface. *Fibres & Textiles in Eastern Europe*,
- AMINI, G., SAMIEE, S., GHAREHAGHAJI, A. A., & HAJANI, F. (2015). Fabrication of polyurethane and nylon 66 hybrid electrospun nanofiber layer for waterproof clothing applications. *Advances in Polymer Technology*, , n/a. doi:10.1002/adv.21568
- BANUŠKEVIČIŪTĖ, A., Aušra BANUŠKEVIČIŪTĖ, Erika ADOMAVIČIŪTĖ, & Rimvydas MILAŠIUS. (2013). Investigation of water permeability of thermoplastic polyurethane (TPU) electrospun porous mat. *Medžiagotyra*, 19(2), 178-183.
- Lee, S., & Obendorf, S. K. (2007). Use of electrospun nanofiber web for protective textile materials as barriers to liquid penetration. *Textile Research Journal*, 77(9), 696-702. doi:10.1177/0040517507080284

- Lee, S., & Obendorf, S. K. (2007). Use of electrospun nanofiber web for protective textile materials as barriers to liquid penetration. *77*(9), 696-702.
- Yoom, B., & Lee, S. (2011). Designing waterproof breathable materials based on electrospun nanofibers and assessing the performance characteristics. *12*(1), 57-64.
- GPS, I. L. (2014). *Density meters - measuring principle.*, 2016
- Paar, A. (2010). *DMA 35 portable density meter* (Instruction Manual). Austria: Anton Paar GmbH.
- Cengiz, F., & Jirsak, O. (2009). *The effect of salt on the roller electrospinning of polyurethane nanofibers*. Heidelberg: The Korean Fiber Society.
doi:10.1007/s12221-009-0177-7
- Cha, D. I., Kim, K. W., Chu, G. H., Kim, H. Y., Lee, K. H., & Bhattarai, N. (2006). Mechanical behaviors and characterization of electrospun Polysulfone/Polyurethane blend nonwovens. *Macromolecular Research*, *14*(3), 331-337. doi:10.1007/BF03219090
- Deitzel, J. M., Kleinmeyer, J., Harris, D., & Beck Tan, N. C. (2001). The effect of processing variables on the morphology of electrospun nanofibers and textiles. *Polymer*, *42*(1), 261-272.
- Demir, M. M., Yilgor, I., Yilgor, E., & Erman, B. (2002). Electrospinning of polyurethane fibers. *Polymer*, *43*(11), 3303-3309.
- Karakas, H., Saraç, A., Polat, T., Budak, E., Bayram, S., Dag, N., et al. (2013). Polyurethane nanofibers obtained by electrospinning process. *Proceedings of World Academy of Science, Engineering and Technology*, (75) pp. 607.
- Supaphol, P., Mit-uppatham, C., & Nithitanakul, M. (2005). Ultrafine electrospun polyamide-6 fibers: Effects of solvent system and emitting electrode polarity on morphology and average fiber diameter. *Macromolecular Materials and Engineering*, *290*(9), 933-942. doi:10.1002/mame.200500024
- Zdraveva, E. (2011). Electrospinning of polyurethane nonwoven fibrous mats. *TEDI Međunarodni Interdisciplinarni Časopis*, *1*(1), 55-60.

- Zhuo, H., Hu, J., Chen, S., & Yeung, L. (2008). Preparation of polyurethane nanofibers by electrospinning. *Journal of Applied Polymer Science*, *109*(1), 406-411.
doi:10.1002/app.28067
- AMINI, G., SAMIEE, S., GHAREHAGHAJI, A. A., & HAJIANI, F. (2015b). Fabrication of polyurethane and nylon 66 hybrid electrospun nanofiber layer for waterproof clothing applications. *Advances in Polymer Technology*, , n/a.
doi:10.1002/adv.21568
- Baji, A., Mai, Y., Wong, S., Abtahi, M., & Chen, P. (2010). Electrospinning of polymer nanofibers: Effects on oriented morphology, structures and tensile properties. *Composites Science and Technology*, *70*(5), 703-718.
- BANUŠKEVIČIŪTĖ, A., Aušra BANUŠKEVIČIŪTĖ, Erika ADOMAVIČIŪTĖ, & Rimvydas MILAŠIUS. (2013). Investigation of water permeability of thermoplastic polyurethane (TPU) electrospun porous mat. *Medžiagotyra*, *19*(2), 178-183.
- Bhattarai, N., Cha, D. I., Bhattarai, S. R., Khil, M. S., & Kim, H. Y. (2003). Biodegradable electrospun mat: Novel block copolymer of poly (p-dioxanone-co-L-lactide)-block-poly(ethylene glycol). *Journal of Polymer Science Part B: Polymer Physics*, *41*(16), 1955-1964.
- Chen, D. W., Liao, J., Liu, S., & Chan, E. (2012). Novel biodegradable sandwich-structured nanofibrous drug-eluting membranes for repair of infected wounds: An in vitro and in vivo study. *International Journal of Nanomedicine*, *7*, 763-771.
doi:10.2147/IJN.S29119
- De Bruyne, M. A. A., De Bruyne, R. J. E., Rosiers, L., & De Moor, R. J. G. (2005). Longitudinal study on microleakage of three root-end filling materials by the fluid transport method and by capillary flow porometry. *International Endodontic Journal*, *38*(2), 129-136. doi:10.1111/j.1365-2591.2004.00919.x
- De Schoenmaker, B., Van der Schueren, L., De Vrieze, S., Westbroek, P., & De Clerck, K. (2011). Wicking properties of various polyamide nanofibrous structures with an optimized method. *Journal of Applied Polymer Science*, *120*(1), 305-310.
doi:10.1002/app.33117

- Eichhorn, S. J., & Sampson, W. W. (2010). Relationships between specific surface area and pore size in electrospun polymer fibre networks. *Journal of the Royal Society, Interface / the Royal Society*, 7(45), 641-649. doi:10.1098/rsif.2009.0374
- Fang, Y., Tolley, H. D., & Lee, M. L. (2010). Simple capillary flow porometer for characterization of capillary columns containing packed and monolithic beds. *Journal of Chromatography A*, 1217(41), 6405-6412.
- Fong, H., Chun, I., & Reneker, D. H. (1999). Beaded nanofibers formed during electrospinning. *Polymer*, 40(16), 4585-4592.
- Forouharshad, M., Saligheh, O., Arasteh, R., & Farsani, R. E. (2010). Manufacture and characterization of poly (butylene terephthalate) nanofibers by electrospinning. *Journal of Macromolecular Science, Part B*, 49(4), 833-842.
doi:10.1080/00222341003609377
- Frey, M. W., & Li, L. (2007). Electrospinning and porosity measurements of nylon-6/poly (ethylene oxide) blended non-wovens. *J.Eng.Fibers Fabrics*, 2, 31-37.
- Gibson, P., Schreuder-Gibson, H., & Rivin, D. (2001). Transport properties of porous membranes based on electrospun nanofibers. *Colloids and Surfaces A: Physicochemical and Engineering Aspects*, 187-188, 469-481.
- Han, H. R., Chung, S. E., & Park, C. H. (2013a). Shape memory and breathable waterproof properties of polyurethane nanowebs. *Textile Research Journal*, 83(1), 76-82.
- Huang, Z., Zhang, Y. Z., Ramakrishna, S., & Lim, C. T. (2004). Electrospinning and mechanical characterization of gelatin nanofibers. *Polymer*, 45(15), 5361-5368.
- Junkasem, J., Rujiravanit, R., & Supaphol, P. (2006). Fabrication of α -chitin whisker-reinforced poly(vinyl alcohol) nanocomposite nanofibres by electrospinning. *Nanotechnology*, 17(17), 4519-4528. doi:10.1088/0957-4484/17/17/039
- Khil, M. S., Kim, H. Y., Kim, M. S., Park, S. Y., & Lee, D. (2004). Nanofibrous mats of poly(trimethylene terephthalate) via electrospinning. *Polymer*, 45(1), 295-301.
- Koski, A., Yim, K., & Shivkumar, S. (2004). Effect of molecular weight on fibrous PVA produced by electrospinning. *Materials Letters*, 58(3-4), 493-497.

- Krifa, M., & Yuan, W. (2016). Morphology and pore size distribution of electrospun and centrifugal forcespun nylon 6 nanofiber membranes. *Textile Research Journal*, 86(12), 1294-1306. doi:10.1177/0040517515609258
- Kwok, D. Y., Gietzelt, T., Grundke, K., Jacobasch, H. -, & Neumann, A. W. (1997). Contact angle measurements and contact angle interpretation. 1. contact angle measurements by axisymmetric drop shape analysis and a goniometer sessile drop technique. *Langmuir*, 13(10), 2880-2894. doi:10.1021/la9608021
- Lee, S., & Obendorf, S. K. (2007). Use of electrospun nanofiber web for protective textile materials as barriers to liquid penetration. *Textile Research Journal*, 77(9), 696-702. doi:10.1177/0040517507080284
- Li, D., Frey, M. W., & Joo, Y. L. (2006). Characterization of nanofibrous membranes with capillary flow porometry. *Journal of Membrane Science*, 286(1-2), 104-114.
- LUONG, N. T. H. (2012). *Engineered Poly (L-Lactic Acid)-Based Nanofibers for Osteogenic Differentiation of Human Mesenchymal Stem Cells*,
- Matthews, J. A., Wnek, G. E., Simpson, D. G., & Bowlin, G. L. (2002). Electrospinning of collagen nanofibers. *Biomacromolecules*, 3(2), 232-238. doi:10.1021/bm015533u
- Moghadam, B. H., & Hasanzadeh, M. (2013). Predicting contact angle of electrospun PAN nanofiber mat using artificial neural network and response surface methodology. *Advances in Polymer Technology*, 32(4), n/a. doi:10.1002/adv.21365
- Ohgo, K., Zhao, C., Kobayashi, M., & Asakura, T. (2003). Preparation of non-woven nanofibers of bombyx mori silk, samia cynthia ricini silk and recombinant hybrid silk with electrospinning method. *Polymer*, 44(3), 841-846.
- Ojha, S. S., Afshari, M., Kotek, R., & Gorga, R. E. (2008). Morphology of electrospun nylon-6 nanofibers as a function of molecular weight and processing parameters. *Journal of Applied Polymer Science*, 108(1), 308-319. doi:10.1002/app.27655
- Park, S. H., Lee, S. M., Lim, H. S., Han, J. T., Lee, D. R., Shin, H. S., et al. (2010). Robust superhydrophobic mats based on electrospun crystalline nanofibers combined with a silane precursor. *ACS Applied Materials & Interfaces*, 2(3), 658.
- Pedicini, A., & Farris, R. J. (2003). Mechanical behavior of electrospun polyurethane. *Polymer*, 44(22), 6857-6862.

- Rutledge, G. C., & Fridrikh, S. V. (2007). Formation of fibers by electrospinning. *Advanced Drug Delivery Reviews*, 59(14), 1384-1391.
- Shchukin, E. D., Pertsov, A. V., Amelina, E. A., & Zelenev, A. S. (2001). I - surface phenomena and the structure of interfaces in one-component systems. *Studies in Interface Science*, 12, 1-63.
- Shenoy, S. L., Bates, W. D., Frisch, H. L., & Wnek, G. E. (2005). Role of chain entanglements on fiber formation during electrospinning of polymer solutions: Good solvent, non-specific polymer–polymer interaction limit. *Polymer*, 46(10), 3372-3384.
- Shirazi, M. J. A., Bazgir, S., Shirazi, M. M. A., & Ramakrishna, S. (2013). Coalescing filtration of oily wastewaters: Characterization and application of thermal treated, electrospun polystyrene filters. *Desalination and Water Treatment*, , 1-13.
doi:10.1080/19443994.2013.765364
- Wang, J., Kim, S. C., & Pui, D. Y. H. (2008). Investigation of the Figure of merit for filters with a single nanofiber layer on a substrate. *Journal of Aerosol Science*, 39(4), 323-334.
- Yao, J., Cees W M Bastiaansen, & Peijs, T. (2014). High strength and high modulus electrospun nanofibers. *Fibers*, 2(2), 158-186. doi:10.3390/fib2020158
- Yoon, B., & Lee, S. (2011). *Designing waterproof breathable materials based on electrospun nanofibers and assessing the performance characteristics*. Heidelberg: The Korean Fiber Society. doi:10.1007/s12221-011-0057-9
- Cengiz, F., & Jirsak, O. (2009). The effect of salt on the roller electrospinning of polyurethane nanofibers. - *Fibers and Polymers*, 10(2), 177.
- de Vasconcelos, C., Martins, R., Ferreira, M., Pereira, M., & Fonseca, J. (2002). Rheology of polyurethane solutions with different solvents. *Polymer International*, 51(1), 69-74.
- Deitzel, J. M., Kleinmeyer, J., Harris, D., & Beck Tan, N. C. (2001). The effect of processing variables on the morphology of electrospun nanofibers and textiles. *Polymer*, 42(1), 261-272.

- FungiLab, A. *Expert series rotational viscometer [instruction manual]*. . Unpublished manuscript.
- Hentschel, T., & Münstedt, H. (2001). Kinetics of the molar mass decrease in a polyurethane melt: A rheological study. *Polymer*, 42(7), 3195-3203.
- Nasouri, K., Kafrou, A., & Shoushtari, A. (2012). Investigation of polyacrylonitrile electrospun nanofibres morphology as a function of polymer concentration, viscosity and berry number.7(5)
- PSLC, P. *Dilute solution viscometry.*, 2016.
- Stenhouse, P., Valles, E., Kantor, S., & McKnight, W. (1989). Thermal and rheological properties of a liquid-crystalline polyurethane.22(3), 1467-1473.
- Tuzar, Z., & Beachell, H. C. (1971). Some notes on the behavior of polyurethane solutions in mixed solvents. *Journal of Polymer Science Part B: Polymer Letters*, 9(1), 37-41.
- Viscopedia. *Measuring principles.*, 2016
- Zhang, C., Yuan, X., Wu, L., Han, Y., & Sheng, J. (2005). Study on morphology of electrospun poly(vinyl alcohol) mats. *European Polymer Journal*, 41(3), 423-432.
- Lee, S., & Obendorf, S. K. (2007). Use of electrospun nanofiber web for protective textile materials as barriers to liquid penetration.77(9), 696-702.
- Yoom, B., & Lee, S. (2011). Designing waterproof breathable materials based on electrospun nanofibers and assessing the performance characteristics.12(1), 57-64.